ATLANTIC SURFCLAM LARVAL TRANSPORT, POPULATION CONNECTIVITY, AND PHYSICAL DRIVERS ON THE MIDDLE ATLANTIC BIGHT AND GEORGES BANK

By

XINZHONG ZHANG

A Dissertation submitted to the

Graduate School-New Brunswick

Rutgers, The State University of New Jersey

In partial fulfillment of the requirements

For the degree of

Doctor of Philosophy

Graduate Program in Oceanography

Written under the direction of

Dr. Dale B. Haidvogel

And approved by

_____

_____

_____

_____

New Brunswick, New Jersey

October, 2014

ABSTRACT OF THE DISSERTATION

ATLANTIC SURFCLAM LARVAL TRANSPORT, POPULATION CONNECTIVITY, AND PHYSICAL DRIVERS ON THE MIDDLE ATLANTIC BIGHT AND GEORGES BANK

By XINZHONG ZHANG

Dissertation Director:

Dr. Dale B. Haidvogel

The Atlantic surfclam, *Spisula solidissima*, is one of the most commercially important species along the Northeast U.S. coast. Similar to many other benthic invertebrates, surfclam life history includes a dispersive larval stage. Larval dispersal plays a key role in determining connectivity among geographically distinct populations, and is further influenced by physical dynamics and larval behavior. In this graduate work, a coupled modeling system combining a physical circulation model of the Middle Atlantic Bight (MAB), Georges Bank (GBK) and the Gulf of Maine (GoM), and an individual-based surfclam larval model has been implemented to study surfclam larval transport pathways, inter-population connectivity patterns, as well as the associated physical mechanisms.

Model results show a mean along-shore connectivity pattern from the northeast to the southwest among the surfclam populations. High-frequency (periods of 2~10 days) variation in larval along-shore drift is found to be due to along-shore surface wind stress variation, with the seasonal variation speculated to be driven mainly by changes in the

across-shelf density gradient. Surfclam across-shelf larval movement is also highly correlated with the along-shore surface wind stress as mediated by coastal upwelling and downwelling episodes. This correlation is further dependent on larval vertical distribution with respect to the thermocline, which is a direct result of the mutual interaction of the physical environment and larval behavior.

Water temperature is found to play a dominant role in larval settlement patterns. In the vertically integrated time-mean heat balance regulating water temperature on the MAB shelf, surface air-sea heat flux and horizontal heat advection are the two most important terms. Seasonal variation of water temperature is mainly controlled by the seasonally varying surface heat fluxes. Across-shore horizontal heat advection variations associated with different coastal across-shore circulation patterns contribute water temperature variations on shorter time scales from days to weeks. The long-term (e.g., decadal or longer) variation of water temperature is likely due to the variation of along-shore heat advection from the mean along-shore barotropic current acting on the mean along-shore temperature gradient, related to the large-scale coastal current system running from Labrador in the north to Cape Hatteras in the south.

Acknowledgements

Firstly, I would like to thank my advisor Dr. Dale B. Haidvogel, for his guidance, encouragement and support throughout my time at Rutgers. His brilliant critical thinking mind, enthusiasm devoted to the science, broach knowledge and detail-oriented professionalism really have inspired and taught me a lot. Being able to work with him in all of those years is really my great honor and I believe this experience will benefit me for my whole life. Without his continuous support and mentoring, this graduate work couldn't be completed.

I would also like to express sincere gratitude to my committee members, Dr. Daphne Munroe, Dr. John Wilkin and Dr. Dennis Mcgillicuddy for their constant support and help on my graduate work. Daphne gave me lots of encouragement and so many valuable advices on this surfclam study, from tiny little details to the big pictures, which are all very helpful for me as a non-biology student. John, as an excellent modeling expert, gave me lots of help on the modeling configuration for this graduate work. Dennis gave me many great suggestions on the Georges Bank study.

I would also give my thanks to Dr. Eric Powell for his great help in the surfclam study and introducing me opportunities to attend conferences and get exposed to broader scientific society. Another special thanks to Dr. Bob Chant for his care and help to me through all these years. I still remember his warmness when I firstly got interviewed as a prospective student years ago.

I also want to thank every current and previous members of the Ocean Modeling group at Rutgers, Julia Levin, Weifeng (Gordon) Zhang, Bin Zhang, David Robertson,

Hernan Arango, Maria Aristizabal, Frederic Castruccio, Enrique Curchitser, et al., for all their help and being involved in making this whole group such a wonderful one.

Also I wish thank every member in our surfclam project, Bonnie McCay, Roger Mann, John Klinck, et al., for their great help, feedback and encouragement as to my surfclam modeling participation.

I also want to thank my fellow graduate students in the Rutgers Oceanography program for the friendship and making it a pleasant stay at IMCS. Specifically, my officemate Alex López, and Aboozar Tabatabai, Sarah Lietzke in the ocean modeling suite all make my last years of PhD study in the closed-box office much more enjoyable.

Lastly, my tons of thanks go to my families, my parents in China who raised me, love me and taught me to be a right person, and another big family in the U.S, Rutgers Chinese student fellowship, which makes me feel as my beloved home in a foreign country.

Table of Contents

List of Tables

List of Figures

Figure 3.5 **Panel a:** Temporal variations of the mean along-shore surface wind stress (*wstr_al*, in $N*m^{-2}$, blue line) and across-shelf daily larval drifting distances (*d_cr*, in kms, green line) for larvae on the **New Jersey (NJ)** inshore shelf (depth < 20 m, Fig. 3.1). The x-axis indicates the actual dates in 2006 (note: these dates are not the release dates used in previously), the left y-axis in blue indicates the values of along-shore surface wind stress (in $N*m^{-2}$), and the right y-axis in green indicates the values of across-shelf daily larval drifting distances (in kms). The shaded region in either gray or blue indicates the period when the stratification index is > 0.2 (see panel b), with the gray portion indicating the period when the mean larval depth is shallower or close to the reversing depth, and blue portion indicating the period when the mean larval depth is deeper than the reversing depth. Yellow highlighted text labels the correlation coefficients between *d_cr* and *wstr_al* within each period. **Panel b**: Temporal variations of the mean larval depth (in meters, green line with colored stars), mean across-shelf current reversing depth (in meters, green line with colored dots) and mean water stratification index (in values between 0 and 1, blue dotted line) for larvae on the **New Jersey (NJ)** inshore shelf (depth < 20 m, Fig. 3.1). The x-axis indicates the actual dates in 2006, the left y-axis in blue color indicates the values of the water stratification index and the right y-axis in green indicates the values of both the reversing depth and larval depth. The colored dots along the mean reversing depth curve indicate the mean water temperatures (in ^{o}C) at those depths, scaled by the colorbar on the right (see the labels on the left of colorbar). The colored stars along the mean larval depth curve indicate the water temperature at those depths, also scaled by the colorbar on the right (see labels on the right of the colorbar). The gray and blue shading has the same meaning as panel a. 88

Figure 3.6 **Panel a:** Temporal variations of the mean along-shore surface wind stress (*wstr_al*, in $N*m^{-2}$, blue line) and across-shelf daily larval drifting distances (*d_cr*, in kms, green line) for larvae on the **South Virginia (SVA)** inshore shelf (depth < 20 m, Fig. 3.1). The x-axis indicates the actual dates in 2006 (note: these dates are not the release dates used previously), the left y-axis in blue indicates the values of along-shore surface wind stress (in $N*m^{-2}$), and the right y-axis in green indicates the values of across-shelf daily larval drifting distances (in kms). The shaded region in either gray or blue indicates the period when the stratification index is > 0.2 (see panel b), with the gray portion indicating the period when the mean larval depth is shallower or close to the reversing depth, and blue portion indicating the period when the mean larval depth is deeper than the reversing depth. Yellow highlighted text labels the correlation coefficients between *d_cr* and *wstr_al* within each period. **Panel b**: Temporal variations of the mean larval depth (in meters, green line with colored stars), mean across-shelf current reversing depth (in meters, green line with colored dots), and mean water stratification index (in values between 0 and 1, blue dotted line) for larvae on the **South Virginia (SVA)** inshore shelf (depth < 20 m, Fig. 3.1). The x-axis indicates the actual dates in 2006, the left y-axis in blue color indicates the values of the water stratification index, and the right y-axis in green indicates the values of both the reversing depth and larval depth. The colored dots along the mean reversing depth curve indicate the mean water temperatures (in ^{o}C) at those depths, scaled by the colorbar on the right (see the labels on the left of colorbar). The colored stars along the mean larval depth curve indicate the water temperature at those depths, also scaled by the colorbar on the right (see labels on the right of the colorbar). The gray and blue shading has the same meaning as panel a. 90

CHAPTER 1. INTRODUCTION

Many marine species, including fishes and invertebrates, have a pelagic larval stage in their life cycle, during which larvae are transported and grow in the ocean with the surrounding water current. Understanding the origins, trajectories and settlement patterns of larvae from different subpopulations of these species is essential for understanding population connectivity (Pineda et al., 2007), which plays an important role for these species in their local and metapopulation dynamics, genetic diversity, community dynamics and structure, and population resiliency to human exploitation (Hastings and Harrison, 1994; Botsford et al., 2001; Cowen et al., 2007).

Observational studies of larval transport are rare and are challenging to conduct, especially for species on the shelf with long larval duration and dispersal distances. Moreover, the combination of the large spatial and long temporal scales associated with the oceanic environment and processes related to biological larval behavior makes quantitative population connectivity studies difficult (Underwood and Keough, 2001; Werner et al., 2007). As such, numerical modeling techniques integrating both oceanic physical drivers and biological larval behavior have become more and more common in the study of marine population dynamics and physical environmental impacts (Werner et al., 1993; Lough et al., 2005; North et al., 2008; Savina and Menesguen, 2008; Xue et al., 2008; Ayata et al., 2009; Tian et al., 2009; Incze et al., 2010; Haase et al., 2012; Narváez et al., 2012a, b).

The Atlantic surfclam, *Spisula solidissima* (hereafter, surfclam), is a bivalve mollusc which lives on the continental shelf from shallow subtidal regions to depths of about 60 meters, inhabiting the waters from the southern Gulf of St. Lawrence to Cape Hatteras, North Carolina (Ropes, 1980; Cargnelli et al., 1999). It is one of the most

commercially important species along the Northeast U.S. coast. Total commercial landings of Atlantic surfclams in 2008 were approximately 28,000 metric tons (mt), with 22,000 mt from federal fisheries and the remainder from state fisheries (NEFSC, 2010).

The general distribution pattern of surfclams from the Northeast Fisheries Science Center (NEFSC) surveys indicates that the highest surfclam abundances occur along the New Jersey shelf (NJ), off the Delmarva Peninsula (DMV) and on Georges Bank (GBK). Similar to many other benthic invertebrates, surfclam life history includes a dispersive larval stage, followed by sessile juvenile and adult stages. Larval dispersal plays a key role in determining surfclam connectivity among geographically distinct populations, and is influenced by physical circulation and water properties.

The Middle Atlantic Bight (hereafter, MAB) refers to the U.S. east coast continental shelf region bounded by Cape Hatteras to the south and by Cape Cod and Nantucket Shoals to the northeast (Fig. 1.1) (Beardsley and Boicourt, 1981). The MAB is a biologically productive region, with several major rivers (e.g., Connecticut River, Hudson River, Delaware River, etc.) that deliver large volumes of fresh water. Most areas in the MAB are relatively shallow (<60 m). Seasonal variation in water-column stratification in the MAB is significant, with water and nutrients being vertically well mixed during fall and winter, and highly stratified from late spring to summer. These factors combine to induce spring blooms over a wide region and high rates of primary production each year (Schofield et al., 2008), consequently supporting highly productive MAB fisheries, such as the Atlantic sea scallop (*Placopecten magellanicus*), the Atlantic surfclam (*Spisula solidissima*), and the ocean quahog (*Arctica islandica*) that together constitute some of the largest fisheries in the U.S. (Council, 2005).

Recent surfclam stock assessments (NEFSC, 2010) show large variation in the surfclam population and also range redistribution which is potentially related to changes in the physical environment (Weinberg, 2005) . Studying the spatial and temporal variations in surfclam larval transport and the underlying physical mechanisms is essential for better understanding surfclam population dynamics, formulating improved management decisions for the surfclam fishery, and interpreting associated socio-ecological responses to climate change (McCay et al., 2011).

The general pattern of the time-mean shelf circulation in the MAB exhibits a consistent along-shelf southwestward flow, with depth-averaged barotropic mean velocities observed to be 3-7 cm/s (Beardsley and Boicourt, 1981). The study of the long-term climatology of the mean circulation over the MAB continental shelf shows that the mean equatorward along-shelf barotropic currents are nearly constant along isobaths and increase in speed with shelf water depth. In contrast, the mean across-shelf circulation is relatively weak, but the general vertical structure pattern is consistent (Lentz, 2008a).

Georges Bank (hereafter, GBK) refers to the large topographic high that bounds the Gulf of Maine (hereafter, GoM) and the U.S. northeast continental shelf break east of the Great South Channel, with depths ranging from less than 30 m near the center of the bank to over 300 m at the bank's edge facing the GoM (Fig. 1.1) (Backus, 1987). Tidal rectification and the GBK topography combine to create a year-round clockwise tidal front circulation around GBK on the order of 5-50 cm/s, aligned approximately with the 60 m isobath. The central GBK waters inside the 60 m isobath stay well mixed due to vigorous tidally induced vertical mixing, while surrounding waters become highly stratified during spring and summer (Csanady and Magnell, 1987). GBK is one of the

most physically energetic and biologically productive regions in the world, with annual phytoplankton primary production exceeding 450 g C m^{-2} yr^{-1} in the bank's central portion, historically supporting a lucrative fishery for the Atlantic cod, halibut, haddock, yellowtail flounder, and benthic fisheries like the sea scallop and surfclam (O'Reilly et al., 1987).

In this graduate work, a coupled modeling system combining a physical circulation model of the MAB, GBK and the GoM, with an individual-based surfclam larval model has been developed, validated and implemented in order to study the Atlantic surfclam, *Spisula solidissima*, its larval transport pathways and inter-population connectivity patterns, as well as the associated physical mechanisms. In the following, chapter 2 will introduce the coupled modeling system, show the mean connectivity pattern among different surfclam subpopulations, and give the general magnitude of larval drifting distances and the larval behavioral influences. Chapter 3 will examine variability in surfclam larval transport and settlement, relate these variations to underlying physical mechanisms, and compare the results with published observational studies. Chapter 4 will study the heat budget in the MAB, and examine the potential underlying physical mechanisms in causing the long-term and short-term temperature variations on MAB shelf. Finally, the results and conclusions will be summarized in Chapter 5.

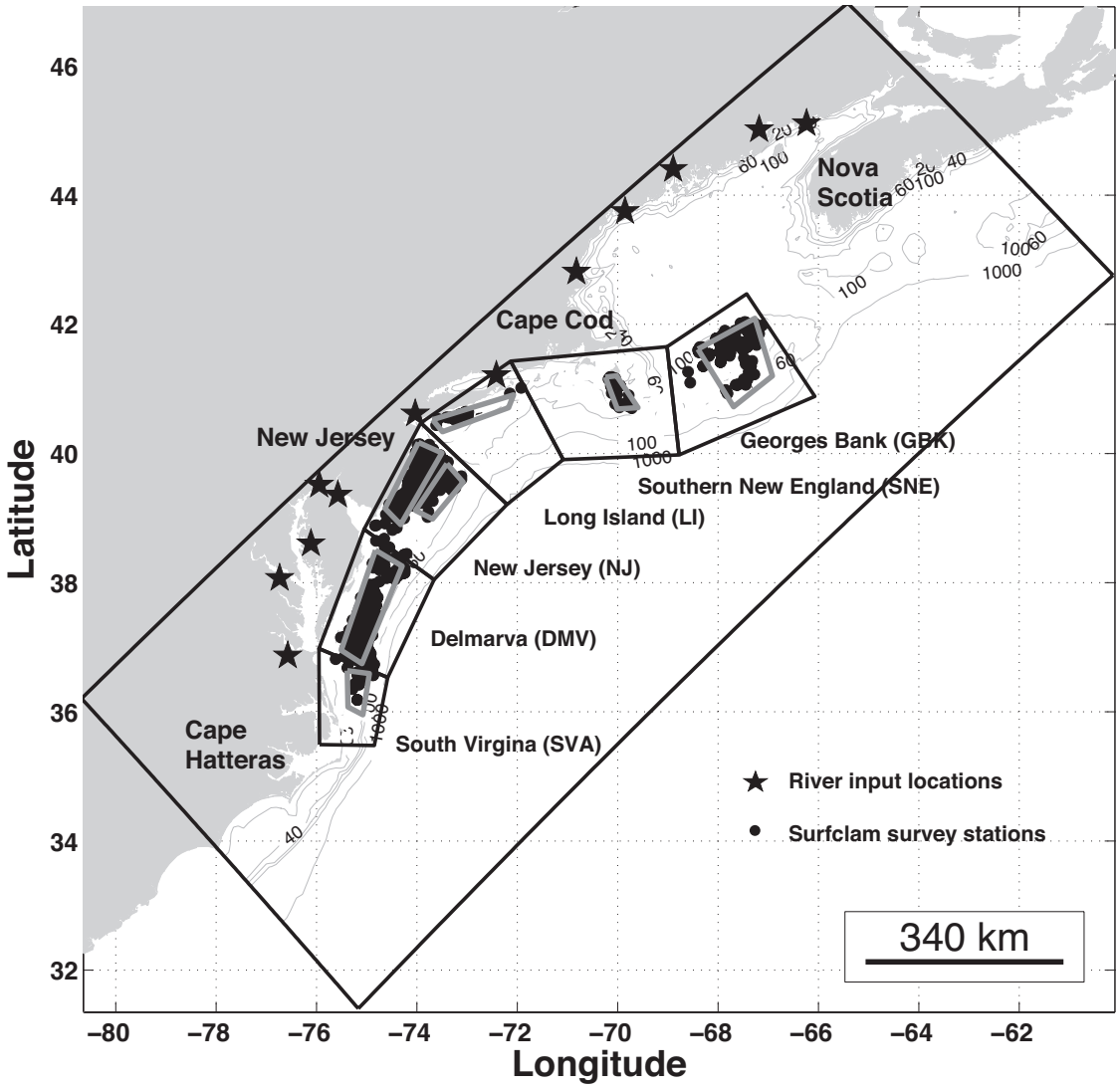

Figure 1.1 Model domain and distribution of surfclam populations within the Middle Atlantic Bight and Georges Bank. The model domain (shown as the large black rectangular box) is defined by 160 x 120 grid cells and includes 12 rivers. Black stars indicate river input locations. The grid resolution is approximately from 6 to 12 km (the resolution varies about 15% from south to north). Distribution of surfclams in the domain was based on the NEFSC survey data from 1982 to 2008 (NEFSC, 2010) and is shown by black dots representing those survey stations with surfclam density higher than 80 clams

per survey dredge tow. Black neighboring boxes along the coast represent conventionally used geographic regions for surfclam stock assessments (NEFSC, 2010); these are, from south to north: South Virginia/North Carolina (SVA), Delmarva (DMV), New Jersey (NJ), Long Island (LI), Southern New England (SNE) and Georges Bank (GBK). Gray boxes inside those black regions boxes denote regions of high surfclam density and are used as the larval release regions in the model (see section 2.3.2 in Chapter 2 for details). Isobaths of 20-, 40-, 60-, 100-, 1000 m are shown as gray solid lines.

CHAPTER 2. MODEL DEVELOPMENT, LARVAL DISPERSAL AND METAPOPULATION CONNECTIVITY

2.1 Introduction

Recent surfclam stock assessments (NEFSC, 2010) have shown that recruitment of surfclams into the fishable stock has been low in the southern portion of the range off DMV and to a lesser extent off NJ; commercial catch rates and stock biomass also have declined in recent years (1997 to 2005). In comparison, trends for large surfclam (>120mm shell length) abundance in the north are either increasing on GBK or variable along the Long Island (LI) and Southern New England (SNE) shelves. These trends in growth and recruitment, particularly off DMV and NJ, remain unexplained; however possibilities include environmental interactions causing poor juvenile survival and slow growth after settlement, high fishing pressure, or discontinuities in larval transport into those areas. Fishing has been suggested to be an unlikely driver of the current period of poor recruitment (NEFSC, 2010); larval transport and connectivity, however, remains an important and as yet understudied aspect of this dynamic.

Similar to many other benthic invertebrates, surfclam life history includes a dispersive larval stage, followed by sessile juvenile and adult stages. Larval dispersal plays a key role in determining connectivity among geographically distinct populations, and is influenced by physical circulation and water properties (Levin, 2006; Cowen and Sponaugle, 2009). Quantitative observation of larval concentration in the ocean is challenging (Underwood and Keough, 2001) and therefore is rarely performed except under conditions that are ideally suited for tracking and observation of marked larvae, e.g. Arnold et al. (2005). As a consequence, numerical modeling has become the method of choice (Peck and Hufnagl, 2012). Numerical modeling has the ability to couple hydrodynamic and larval behavioral models to simulate larval transport, dispersal and

growth (Werner et al., 1993; Lough et al., 2005; Savina and Menesguen, 2008; Ayata et al., 2009; Narváez et al., 2012a, b) and can therefore serve as a powerful tool for the study of larval dispersal and inter-population connectivity.

Numerical larval models have been in use for various invertebrate species and systems for many years (Leis et al., 2011), including applications examining larval transport on Georges Bank for sea scallops (Tian et al., 2009), the Gulf of Maine lobster (Incze and Naimie, 2000; Xue et al., 2008; Incze et al., 2010), and eastern oysters in Delaware Bay (Narváez et al., 2012a, b) and in Chesapeake Bay (North et al., 2008). Significant advances have been made in numerical modeling techniques; however, more detailed information concerning larval behavior and its interaction with the surrounding physical environment is necessary to further improve individual-based larval models (IBM) and thereby refine model simulations (Miller, 2007).

In this chapter, we introduce a coupled modeling system combining a physical circulation model and a biological individual-based model developed for Atlantic surfclam larvae. Specific research objectives focus on the development of the coupled modeling system and the determination of the main larval transport pathways and mean larval connectivity patterns for surfclam stocks in the MAB and GBK. These objectives are integral to management of the Atlantic surfclam fishery. Recent declines in surfclam abundance off Delmarva are thought to be the result of warming of Mid-Atlantic bottom waters in the late 1990s driving an ongoing range shift to the north and offshore (Weinberg et al., 2002; Kim and Powell, 2004; Weinberg, 2005). The failure of surfclams to repopulate southern and inshore waters remains unexplained, as recently observed bottom water temperatures would appear to be within surfclam physiological limits.

Thus, a better understanding of larval dispersal in this species may help explain ongoing changes in population abundance and provide increased predictive capability as to the potential of climate change to effect further impacts in this component of the MAB ecosystem.

In the following, Section 2.2 introduces both the physical circulation model and the surfclam larval individual-based model. Section 2.3 describes the model simulations and analyses conducted. Modeling results including model validation, larval transport and connectivity studies, estimates of larval drifting distances, and examination of behavioral effects, are shown in Section 2.4. Discussion of the modeling system and its results are presented in Section 2.5.

2.2 Model development

2.2.1 Physical circulation model

A coastal ocean model (hereafter called MABGOM) incorporating the Middle Atlantic Bight, Georges Bank, and the Gulf of Maine has been implemented using the Regional Ocean Modeling System (ROMS, http://www.myroms.org), a free-surface, terrain-following, primitive equation ocean model widely applied by the scientific community for various applications in both deep ocean and coastal settings, e.g., Budgell (2005); Zhang et al. (2009); Aristizabal and Chant (2013); Warner et al. (2005).

Resolution of the surface and bottom boundary layers is extremely important for coastal ocean modeling. Vertical stretching in the terrain-following coordinate system used in ROMS enables it to adopt high vertical resolution at the surface and bottom,

thereby improving the representation of the surface and bottom boundary layers. Details of the ROMS computational kernel can be found in Shchepetkin and McWilliams (1998, 2003, 2005). Our MABGOM model domain is bounded by Cape Hatteras, North Carolina in the southwest and Nova Scotia, Canada in the northeast, covering the whole U.S northeast continental shelf and also part of the Nova Scotia shelf (Fig. 1.1).

The atmospheric forcing applied in the model uses National Centers for Environmental Prediction (NCEP) hindcast data. However, when compared with observations measured from the Delaware Environmental Observing System (DEOS) and the Martha's Vineyard Coastal Observatory (MVCO), the NCEP incoming short-wave radiation was found to be consistently ~20% too high in the model domain from the year 2006 to 2009. Therefore, we applied a 20% reduction to the NCEP incoming short-wave radiation and used this corrected data to force the ROMS model, similar to the correction also done in Wang et al. (2012). The ADvanced CIRCulation model for ocean, coastal and estuarine waters (ADCIRC) (Reyns et al., 2006, 2007) is used to provide the tidal forcing at the boundaries of the ROMS domain, whilst observed riverine discharge and water temperature data from U.S. Geological Survey (USGS) are used to prescribe river inflow.

Following Chen and He (2010), we nested MABGOM within another global ocean circulation model, the HYbrid Coordinate Ocean Model/Navy Coupled Ocean Data Assimilation model, (HYCOM/NCODA) (Bleck, 2002), that provides ROMS MABGOM with boundary and initial conditions for temperature, salinity, and barotropic and baroclinic velocities. However, when comparing the HYCOM 4-year (2006-2009) mean temperature and salinity (T&S) with observed MABGOM climatological T&S data

(Fleming and Wilkin, 2010), a net bias in both T&S was identified in the HYCOM model data. In particular, HYCOM is approximately 2 to 3 degrees warmer over the entire MAB and GoM, and salinities in HYCOM on the MAB shelf and the Nova Scotia outer shelf are higher by 1 to over 10 (non-dimensional salinity units), especially in Chesapeake Bay, Delaware Bay, and other regions where freshwater inflow is high. The net bias in T&S also causes a bias in the density field, which in turn affects the mean along-shore and across-shelf pressure gradients and currents. We therefore apply corrections to the biased HYCOM model data. Based on observed T&S climatologies (Fleming and Wilkin, 2010), we calculate mean geostrophic transport and barotropic and baroclinic velocities along the model boundary, and use these to correct the HYCOM temporal mean bias, whilst still maintaining the original temporal and spatial variations due to seasonal cycles and various coastal physical processes. These corrected HYCOM boundary and initial conditions are applied to force and initialize the ROMS model.

2.2.2 Surfclam larval individual-based model (Scl-IBM)

The larval model is constructed of two parts, a larval growth sub-model and a larval behavior sub-model, following Dekshenieks et al. (1993) and Dekshenieks et al. (1996). Implementation of this model structure within ROMS has been used previously to study oyster larval connectivity in Delaware Bay (North et al., 2008; Leis et al., 2011; Narváez et al., 2012a, b). Basic clam variables are length (*Len*) in mm, age (*Age*) in days, number (*N*), and depth (*Z*) in meters. Environmental conditions are water temperature (*T*) in ^{o}C and larval food (*F*) in mg/liter. The independent variable is time (*t*) in days. The model is an individual-based model that calculates daily the size (*Len*) and depth (*Z*) for a

surfclam larva (Peck and Hufnagl, 2012). The variables used in the model are summarized in Table 2.1.

2.2.2.1 Growth sub-model

Larval growth data were obtained from laboratory studies (Hurley and Walker, 1996, 1997; Walker et al., 1998) on *Spisula solidissima* and the surfclam southern subspecies, *Spisula solidissima similis*, which is considered to be a separate but closely related species (Hare and Weinberg, 2005; Hare et al., 2010). Existing larval data for *S. solidissima* alone were insufficient for model parameterization; therefore laboratory data from both subspecies were used in model parameterization. Recent range extension of *S. s. similis* into Long Island Sound (Hare et al., 2010) suggests that the two subspecies have considerable latitudinal overlap.

In the model, clam length depends on growth rate (*Gr*), which is contingent on three factors: base growth rate (Gr_{Base}), which is a function of food (*F)* and *Age*, a correction factor (*CorT*) which depends on water temperature (*T*); and food quality (F_{Qual}):

$$Gr(F,Age,T,F_{Qual}) = \frac{dLen}{dt} = Gr_{Base}(F,Age) \times CorT(T) \times \qquad (2.1)$$

Larval growth experiments show that growth rate is relatively consistent at optimal standard hatchery feeding rates (Tahitian strain *Isochrysis galbana*, hereafter TIso ≥ 50,000 cells/ml). Data from Renaud et al. (2002) were used to convert cell numbers from experiments to “mg” food (model units). Using these values to solve the

above differential equation provides a linear relationship between length and age (Eq. 2.2), so that growth rate is constant ($Gr = Gr_0$) if food (F) is above a minimal concentration (Fs). Values of constants (Gr_0, Gr_1… L_0 etc) are shown in Table 2.2.

$$Len = Gr_0 \times Age + L_0 \tag{2.2}$$

Under conditions of starvation, surfclam larvae show limited growth that declines with age (Eq. 2.3):

$$Len = Gr_1 \times Age^{Gr_2} \tag{2.3}$$

yielding a growth rate of:

$$Gr_{Base} = \frac{dLen}{dt} = Gr_1 \times Gr_2 \times Age^{(Gr_2 - 1)} \tag{2.4}$$

If the food concentration is below Fs, but above zero, then the growth rate depends on both Age and F (Eq. 2.5, Fig. 2.1a):

$$Gr_{Base} = Gr_0 \times \frac{F}{Fs} + (Gr_1 \times Gr_2 \times Age^{(Gr_2 - 1)}) \times \frac{Fs - F}{Fs} \tag{2.5}$$

Temperature also affects growth rate. Larval growth data were available for three temperatures (15, 20 and 25 ^{o}C) (Hurley and Walker, 1997). High mortality of surfclam larvae at 0 ^{o}C and above 30 ^{o}C were also reported (Wright et al., 1983; Wright et al., 1984). Goldberg (1989) also noted optimal (maximal) larval growth of surfclams at 20-21 ^{o}C. Little information is known for larval growth rates at intermediate temperatures between these anchor points (0, 15, 20, 25, 30 ^{o}C).

Here in this study we assume linear interpolation to calculate larval growth rates at those intermediate temperatures, and linear extrapolation to presumed zero larval growth at 0 ^{o}C and above 30 ^{o}C, respectively. Thus, *CorT* is a piecewise fit to temperature effects on growth rate (Eq. 2.6, Fig. 2.1b).

$$\begin{aligned} CorT &= Gf_1 \ if \ T \le 10, \\ &= Gf_2 - (Gf_2 - Gf_1) \times \frac{15 - T}{15 - 10} \ if \ 10 < T \le 15 \\ &= Gf_3 - (Gf_3 - Gf_2) \times \frac{20 - T}{20 - 15} \ if \ 15 < T \le 20 \\ &= Gf_4 - (Gf_4 - Gf_3) \times \frac{25 - T}{25 - 20} \ if \ 20 < T \le 25 \\ &= Gf_5 - (Gf_5 - Gf_4) \times \frac{28 - T}{28 - 25} \ if \ 25 < T \le 28 \\ &= Gf_6 - (Gf_6 - Gf_5) \times \frac{30 - T}{30 - 28} \ if \ 28 < T \le 30 \\ &= Gf_6 \ if \ T > 30 \end{aligned} \tag{2.6}$$

Surfclam larvae are thermally sensitive; survival is high at 25 ^{o}C, but declines rapidly at 30 ^{o}C (Wright et al., 1983; Roosenburg et al., 1984). Temperatures encountered by larvae in the model domain range approximately from 5-30 ^{o}C; therefore, temperature as a mortality agent was not included in the model.

Lastly, we impose a food quality correction of 1.2, i.e. $F_{Qual} = 1.2$, to increase growth rates enough for settlement to occur in about 25 days at temperatures near 20 ^{o}C and a food supply of 1 mg/liter, which is more realistic for growth under optimal food conditions (unpublished data) than is a 30-day period that occurs without the correction ($F_{Qual} = 1.0$). This assumes that diets used in reported hatchery experiments on which these rates are based (Tiso) are good, but not optimal diets. Salinity affects larval growth

(Hurley and Walker, 1997), but not at salinities encountered on the continental shelf; hence, salinity effects on growth were not included in the model. Growth is debited by the percent time sinking because sinking larvae do not feed.

2.2.2.2 Behavioral sub-model

The horizontal swimming speed of larvae is low in comparison with water current speeds, whereas vertical swimming speed is often comparable to vertical water movement, and can influence overall larval transport and dispersal (Werner et al., 1993; North et al., 2008). Larval behavior data were obtained from Mann et al. (1991) who provide upward and downward swimming speeds and sinking speeds as a function of larval length. In addition, Ma et al. (2006a) and Shanks and Brink (2005) provide information on the vertical distribution of larvae on the continental shelf. Observations show that small larvae tend to orient to water near 20 ^{o}C and avoid temperatures greater than 22-23 ^{o}C or less than 12 ^{o}C, and as larvae get larger (nearer to metamorphosis and settlement), they tend to be found deeper in the water column. Larval swimming behavior was implemented on the assumption that swimming time up and down is a direct function of temperature, but that the swimming and sinking speeds themselves are not temperature-dependent.

The vertical speed and direction of movement of the larvae depend on the sinking rate (*Sk*), the swimming speed which is a function of length, and the fraction of time spent swimming upward (*Usf)* or downward *(1-Usf)*, which is a function of temperature.

Larvae do not swim constantly; therefore the fraction of time swimming (*Stf*) is set at 92.5%. Combining all of these elements, the net vertical speed is:

$$\frac{dZ}{dt} = -Sk(Len) \times (1 - Stf) + Stf \times [Uss(Len) \times Usf(T) - Dss(Len) \times (1 - Usf(T))] \quad (2.7)$$

Sinking rate is a function of weight, which is a power function of length, so the sinking rate is:

$$Sk(Len) = S_0 \times Len^{S_1} \quad (2.8)$$

The upward (*Uss*) and downward (*Dss*) swimming speeds are quadratic functions of length (Mann et al., 1991):

$$Uss(Len) = \max(U_0 + U_1 \times Len + U_2 \times Len^2,\ 0) \quad (2.9)$$

and

$$Dss(Len) = \max(D_0 + D_1 \times Len + D_2 \times Len^2,\ 0) \quad (2.10)$$

We assume that larvae respond to ambient temperature, not the vertical gradient in temperature. Thus, the fraction of swimming time spent swimming upwards depends on the ambient temperature (Fig. 2.1c, d):

$$Usf(T) = 0.5\left[1 - \tanh\left(\frac{T - St_0}{St_1}\right)\right] \quad (2.11)$$

Initial larval size is set equal to egg diameter (58 μm) (Walker and OBeirn, 1996; Cargnelli et al., 1999). Larvae settle and metamorphose at approximately 260 μm shell length (Fay et al., 1983; Mann et al., 1991; Cargnelli et al., 1999). In the model,

settlement occurs at first bottom contact upon reaching this settlement size. The three time-dependent equations are solved with a third-order Adams-Bashforth scheme. The model was verified against data in Ma et al. (2006b) with reference also to Shanks and Brink (2005) and the observed size at settlement. The only tuning required was the percent time swimming, the food quality factor, and the relationship of temperature to swimming speed, where a hyperbolic-tangent relationship was imposed to permit larvae to achieve the observed water column distributions given the observed temperature gradients (Fig. 2.1c, d).

2.3 Model simulations and analysis

2.3.1 Physical circulation

The ROMS MABGOM model was run for years 2006 to 2009. For this study, temperature and coastal currents are the most important physical circulation features (see Section 2.2). Therefore, the mean circulation field and the mean surface and bottom temperature fields from the model output were analyzed and validated by comparison with available observational data. In this study region, the Gulf Stream is an important dynamic feature, as its mean path and variation can cause large variations in the MAB shelf water properties (Churchill et al., 1993). Therefore, the simulated and observed mean Gulf Stream paths have also been compared.

2.3.2 Larval release strategies

The surfclam larval model was coupled with the physical circulation model for the years 2006 to 2009. A similarly coupled shellfish larval submodel, an oyster larval model, is currently available to the public as a new capability within ROMS, and more details about the coupling method can be found in Narváez et al. (2012a, 2012b)

Surfclam spawning ranges from late spring (late May or June) until fall (Ropes, 1968; Jones, 1981; Fay et al., 1983; Cargnelli et al., 1999). Accordingly, simulated larvae were released throughout the spawning season at 5-day intervals from May 21st until October 16th, generating a total of 30 release times in each year. Larval release locations are defined in the model following the observed surfclam population distribution pattern (Fig. 1.1). A map of surfclam abundance from 1982-2008 NEFSC surfclam stock surveys (NEFSC, 2010) shows the 7 major geographic regions with large surfclam stocks (blue boxes in Fig. 1.1), namely from south to north: South Virginia/North Carolina (SVA), Delmarva (DMV), New Jersey inshore (NJ_in), New Jersey offshore (NJ_off), Long Island (LI), Southern New England (SNE) and Georges Bank (GBK). The New Jersey region was divided into offshore and inshore components in this study to permit investigation of the offshore shift in range identified by Weinberg (2005).

The numbers of larvae released from within each of these regions was calculated by multiplying the average clam density (numbers/tow) in each region by its area. This assumes that the number of larvae released within each region is proportional to the local adult clam density. The derived population numbers for region (SVA, DMV, NJ_in, NJ_off, LI, SNE and GBK) are 400, 2000, 1800, 300, 400, 400 and 1500, respectively. These numbers of surfclam larvae are then approximately evenly released within each

box simultaneously at midnight of the selected release dates. The release depth was the bottom-most grid cell. Therefore, a total of 204,000 larvae (6,800 per release) were released each year, covering the spawning season and all the major surfclam spawning regions on the Northeast U.S. shelf.

In addition to the physical fields that the circulation model provided for the surfclam larval model, we also set the food concentration (*F,* in mg/liter). Reliable field estimates for larval food are unavailable (Munroe et al., 2013); therefore, food concentration was set to be an optimal constant value (1 mg/liter), on the assumption that surfclam larvae never lack food in the water. Thus, times to settlement for these simulations are minimal given the temperatures to which the simulated larvae were exposed.

2.3.3 Larval transport, connectivity, and behavioral sensitivity

Metamorphosis for surfclams occurs from 19 to 35 days depending on temperature during larval growth (Fay et al., 1983). Given our assumption that food supply is not limited for the simulated larvae, we further assume that the maximum duration of the larval stage for successfully recruiting larvae is 35 days. Additionally, nearly all adult surfclams are found shallower than 60 m (NEFSC, 2010) (Fig. 1.1). Thus, in the model we define successful larvae as those that i) reach settlement size (260 μm) within 35 days of release and ii) do so within potential settlement habitat (shallower than the 60 m isobath).

The along-shore and across-shelf drift for each larva were calculated by comparing the release position and the point of final settlement, or the place where the larva was at the end of 35 days if it had not yet successfully settled. The mean drifting pattern among all the larvae released at the same time from the same region was calculated and used to determine the average larval connectivity pattern for all 4 years. The connections among the different geographically distributed subpopulations are illustrated with a connectivity matrix. The connectivity matrix is computed between each of the 6 along-shelf regions (black boxes in Fig. 1.1), showing the percentage of larvae released from one region that arrive and settle into the same region or one of the other regions.

To test the importance of larval behavior, both vertical swimming and sinking, on transport and connectivity, additional simulations were performed for year 2006: a) with only larval vertical swimming, b) with only larval vertical sinking, and c) with neither (purely passive). In the "swim only" simulation (a), the larval sinking behavior was turned off and larvae were assumed to be swimming continuously in the vertical direction, while in the "sink only" simulation (b), the larval swimming behavior was turned off but larvae were still allowed to grow and to sink at the rate dependent on larval size. In the "purely passive" simulation (c), larvae are only transported as passive neutrally-buoyant particles without swimming and sinking behaviors, but can still grow and reach settlement size. These passive particles are both transported by the simulated 3D currents, but also mixed vertically by a random walk motion scaled by the intensity of parameterized turbulent mixing. The resulting mean larval drifting distances in these simulations were calculated in the same way as previously described, and were compared

with the results of the initial 2006 simulation with both larval swimming and sinking behaviors in the model.

2.4 Results

2.4.1 Model validation

2.4.1.1 Physical circulation model

Daily values of temperature, salinity, sea surface height, and barotropic and baroclinic current velocities are obtained from a 4-year ROMS MABGOM simulation. The 4-year average of sea surface temperature (at 1 m depth) and barotropic current fields were calculated from the model output (Fig. 2.2a). The path of the Gulf Stream (GS) can be detected readily by the mean sea surface temperature (SST) 21 °C isotherm. Comparison of the GS path between the model (green line) and observation (blue line) shows good agreement where the GS flows into and out of the model domain (Fig. 2.2a, b).

The mean barotropic currents on the MAB shelf and GBK southern flank in the model flow generally southwestward along the coast, with both magnitude and direction consistent with the long-term mean climatological observations (Lentz, 2008a) (Fig. 2.2a). On the southern flank of GBK, simulated mean barotropic currents reach close to 0.09 m/s, while along the NJ and DMV shelf break they also approach 0.1 m/s. The inner shelf mean southwestward flow is slower than the shelf break current, at around 0.03~0.04 m/s. The model barotropic zonal and meridional current biases are approximately 0.0003 m/s and 0.0061 m/s respectively (model - climatology), which indicates good consistency (p-

value < $1x10^{-10}$). The physical circulation model is thus found to capture the main pattern of the MAB shelf current system.

Model output for the 4-year mean SST from year 2006 to 2009 is compared to satellite observations in Fig. 2.2a,b. This comparison shows reasonable agreement for both the Gulf Stream region and the MAB shelf. The simulated surface and bottom temperatures during late spring to early fall in 2006-2009 are compared with Northeastern Fishery Science Center (NEFSC) observations (NEFSC Oceanography Branch CTD Data Reports, 2006-2009) in Fig. 2.2c,d. Model temperature biases (model-observation) at the surface and bottom are about 0.15 ^{o}C (RMS=1.32 ^{o}C) and -0.32 ^{o}C (RMS=2.03 ^{o}C), respectively. In general, this comparison shows acceptable consistency between model results and observation, assuring that the model reproduces the main MAB shelf water surface and bottom temperature distributions with accuracy sufficient for the requirements of the Scl-IBM.

Sporadic and sparse dots with relatively larger temperature differences (around ± 5 ^{o}C) between model results and observations are also detected (Fig. 2.2c, d), especially close to the shelf break regions where Gulf Stream meanders might cause large temporal and spatial variations. This might be attributed to the difficulty that numerical models traditionally have in capturing the exact variability of Gulf Stream meanders due to the dynamic complexities and high nonlinearities involved (Miller and Lee, 1995).

2.4.1.2 Larval model validation

In the coupled modeling system, larval trajectories allow us to observe larval transport and horizontal and vertical distributions. Observational data of the distribution of surfclam larvae in the ocean are rare, making it difficult to validate the larval model in a fashion similar to that used for the physical model. However, detailed observations of larval distributions along an across-shelf section at the New Jersey LEO-15 observatory (Long-term Ecosystem Observatory, Fig. 2.3) during upwelling and downwelling periods do provide sufficient detail for qualitative validation (Ma et al., 2006a), and thus were used to compare modeled larval distributions for the same location within the model domain. Observations show that during upwelling, surfclam larvae tend to concentrate near the thermocline, while during downwelling they concentrate at the intersection of the thermocline and the bottom (Figure 4 in Ma et al., 2006a). Modeled larval distributions followed the same pattern during upwelling and downwelling (Fig. 2.3), indicating that the coupled modeling system is faithfully reproducing surfclam larval behavior and water-column vertical distribution.

2.4.2 Larval transport and population connectivity

As an example, we follow the horizontal and vertical transport trajectory (Fig. 2.4a, c) and growth history (Fig. 2.4b) for an individual larva released along the southern New Jersey shelf on Aug. 1st, 2006. This larva spends about 35 days in the water column. At day 35, it reaches settlement size (260 μm) and settles to the bottom. In the horizontal, this larva was transported southwestward along the shore following the coastal current and eventually settled close to the mouth of Chesapeake Bay.

In the vertical, this larva quickly swims upward after release and spends most of the larval stage close to the thermocline, near the 20~21 ^{o}C isotherm (Fig. 2.4c), the preferred temperature range for surfclam larval growth. Some abrupt larval vertical movement related to strong turbulence events are obvious when the larva drifts close to the Delaware Bay mouth (Fig. 2.4c). Close correlation between the variation in larval transport and the surrounding coastal current pattern indicates a strong influence of the physical environment on the larval position and performance.

Focusing on the entire population of larvae shows that average larval transport is to the southwest. The mean larval transport and connectivity pattern in MAB and GBK can be generalized as shown in Figure 2.6. In this example taken from the August 1st, 2006 release (Fig. 2.5a, b), almost all the larvae released in the model domain are transported southwestward along-shore, except for some released from DMV and SVA that are entrained into the Gulf Stream and transported northeastward into the open ocean where they can be expected to die (Fig. 2.5b). Connectivity is highest between adjacent management regions. In each region, most recruiting larvae either originate from their release region (self-recruits) or from the neighboring region upstream. For example, in the August 1st, 2006 release, most larvae released in LI were finally transported into the NJ region, while most larvae released in NJ were transported into the DMV region, and so on. The mean subpopulation connectivity matrix (Fig. 2.7) summarizes this finding.

Two different 4-year-mean connectivity matrices were calculated for larval transport after 35 days post-release. The first matrix shows the overall pattern of larval supply, which is defined as the portion of larvae transported from one region to another (Fig. 2.7a). The second matrix indicates the pattern of larval settlement, defined as the

portion of larvae from one region that were both transported and successfully settled in another (Fig. 2.7b). The connectivity pattern is similar in both matrices, but with different magnitudes. Diagonal trends in both matrices are obvious, indicating good larval retention within each geographic region and significant self-settlement. The off-diagonal values in the lower half are relatively larger than the analogous values in the upper half, confirming that larvae are generally transported from upstream (north and east) regions into downstream (south and west) regions, forming a southwestward connection pattern. Thus, pairs of adjacent geographic regions typically show substantial connectivity, as revealed by the values in cells below the diagonal in the matrix, and often these larvae provide more settlement potential than those derived locally. For instance, on average, 43.4% of all larvae released in NJ are transported into DMV while 45.6% remain on the NJ shelf (Fig. 2.7a), and 20.2% of all larvae released in NJ reach settlement size in DMV whereas 19.7% reach settlement size on the NJ shelf (Fig. 2.7b). Compared to the MAB geographic regions, GBK is relatively more isolated, with little larval transport to other regions and very few immigrants from other regions.

2.4.3 Larval drifting distances and behavior effects

On average, surfclam larvae drifted 119 km (±94 km st. dev.) southwestward along-shore, and 5 km (±17 km st. dev.) inshore (perpendicular to the coast). Large variations of both along-shore and across-shelf larval drifting distances exist among larvae released from different regions (Fig. 2.8a, b). In the along-shore direction, larvae released in DMV experienced the longest southwestward drift, while those released from

GBK experienced the shortest along-shore drifting distance, which is intuitively understandable because of the clockwise gyre on the bank that reduces along-shore drift.

In the across-shelf direction, larvae released from the SVA, DMV, and NJ regions experienced onshore drifting with median distances over 10 km, while larvae released in LI and SNE experienced predominantly offshore drifting with median distances of 1.5 km and 6 km respectively, and the GBK larvae experienced almost no across-shelf drifting on average. In addition, statistical tests show significant across-region differences in the temporal variances of larval drifting distances in both along-shore and across-shore directions. For the along-shore larval drifting distance, larvae released from NJ, LI, and SNE experienced about 1.5 to 2 times larger temporal variances than those released from SVA, DMV, and GBK (Fig. 2.8a). For the across-shore larval drifting distance, larvae released from GBK experienced about 3 to 5 times larger temporal variances than those released elsewhere (Fig. 2.8b).

The results of simulations to examine the sensitivity of larval trajectories to larval behavior indicate that both larval swimming and sinking behavior significantly influence larval along-shore drifting (Fig. 2.8c). On average, larval swimming behavior increases the along-shore southwestward drifting distances by about 56 km ($F = 45923$, $n=244341$, p-value $< 1x10^{-10}$), whereas larval sinking behavior decreases the along-shore drifting distances by about 26 km ($F = 8929$, $n=246293$, p-value $< 1x10^{-10}$). In the standard model configuration with both swimming and sinking behaviors (Fig. 2.8c, magenta color), the combined effects of both behaviors increase the mean larval drifting distance by about 30 km ($F =6220$, $n=121219$, p-value $< 1x10^{-10}$) compared to the distance achieved by purely passive transport (Fig. 2.8c, cyan color). In addition, statistical tests show that both larval

swimming and sinking behaviors affect the temporal variances of larval along-shore drifting distances in a significant way, with larval swimming behavior increasing the temporal variance and the sinking behavior decreasing the variance (Fig. 2.8c).

2.5 Discussion

2.5.1 Larval transport and connectivity

The model results indicate a mean upstream-downstream (northeastward-southwestward) surfclam larval transport and connectivity pattern, which is mainly driven by the mean shelf current flowing southwestward (Fig. 2.2a). For most surfclam geographic regions, larval supply comes from larvae retained in the region and released from the region immediately upstream. Thus, variability in the number of larvae released from an upstream region can be expected to be a significant factor in determining the number of larvae settling in the adjoining downstream region.

Another factor influencing the contribution of larval supply from the local and upstream regions is temporal variability, both seasonally and inter-annually, in larval transport (see the 3rd chapter in this thesis for the intra-annual variability, and appendix B for the inter-annual variability). Here, we have considered the average larval transport patterns over the entire spawning season and over 4 years from 2006 to 2009; however our observations, and those of others (Xue et al., 2008; Tian et al., 2009; Narváez et al., 2012a), indicate that physical and environmental changes can cause strong temporal variability in larval supply.

A great deal of individual variation also exists among larval release times within a given region and between regions (Fig. 2.8a, b). For example, larvae released from SVA, DMV, and GBK experienced smaller temporal variability in the along-shore drifting distances than those released from NJ, LI, and SNE (Fig. 2.8a), potentially related to the fact that larvae released from SVA and DMV generally stay deeper in the water column and experience less along-shore current variations (see the 3rd chapter in this thesis), and that the GBK around-bank circulation retains most larvae on the bank. The same factor on GBK is the likely cause of the larger variance in the across-shore larval drifting distances for larvae released on GBK. This variability is the topic of additional research using this coupled modeling system (see the 3rd chapter in this thesis), and also suggests the need to further examine in detail how the physical environment impacts larval growth, transport and population connectivity.

In this study, the larval settlement connectivity matrix (Fig. 2.7b) shows a continuous, although variable, surfclam larval input into the SVA, DMV, and NJ regions, either through the retention of larvae spawned in that region or the transport of larvae from regions upstream (particularly the immediately upstream region). Assuming this pattern based on the 2006 to 2009 simulation is unchanged from 1980's and 1990's, this result suggests that insufficient larval supply and settlement is an unlikely cause for the failure of the surfclam population to recover after the decline in DMV and NJ observed from 1997 to 2005 because larvae would have likely been supplied from upstream populations that had not coincidentally declined. Factors such as poor juvenile survival and slow growth after larval settlement are therefore more likely explanations, e.g. Quijon et al. (2007).

The connectivity matrix shows low larval settlement among those released from SNE into SNE itself and LI, about 0.3% in total on average in 4 years (Fig. 2.7b). In the example of the August 1st, 2006 release, few larvae released from SNE settled successfully (Fig. 2.5). This might not reflect reality. O'Connor et al. (2007) suggest that larval survival is lower at colder temperatures for most marine planktonic larvae because slower growth rates at lower temperatures extended the planktonic larval duration. In this surfclam model, the decline in the fraction of larvae reaching settlement size by 35 days at higher latitudes such as SNE and GBK is due less to the failure of larvae to be available in these regions as it is to failure of larvae to reach settlement size in 35 days. This effect results directly from the lower temperatures of surface waters at higher latitudes that slow growth rates of the simulated larvae.

Our larval model assumes that larval mortality rates are sufficiently high that few larvae will survive much longer than 35 days. If larval mortality rates are lower than routinely assumed, see for example, Rumrill (1990); Johnson and Shanks (2003) Shanks et al. (2003) Short et al. (2013) permitting considerable larval survival beyond 35 days, settlement rates would be higher than indicated in the connectivity matrices presented in Figure 2.7b. A similar argument also applies to those larvae released from NJ offshore, as model results show few larvae settling from those larvae released from NJ offshore and the bottom temperature at NJ offshore is colder than inshore (Castelao et al., 2008).

The model shows little connection between the GBK surfclam subpopulation and others to the west and south (Fig. 2.5, 2.7b). Georges Bank (GBK) is becoming an increasingly important region for the surfclam fishery after it was reopened after a lengthy closure since 1989 due to the occurrence of Paralytic Shellfish Poisoning (PSP)

(NEFSC, 2010). However, our modeling results suggest that the GBK surfclam fishery reopening might only have limited influence on the MAB subpopulations as a spawning stock to support regions downstream. In terms of human fishing, the shift of fishery efforts onto the bank could be important in easing the fishing pressure on NJ and DMV and help populations there to recover.

2.5.2 Larval drifting distances and behavioral effects

On average, simulated surfclam larvae drifted over one hundred kilometers southwestward along the shelf (Table 2.3). In a meta-analysis of correlation between larval duration and observed drifting distances, Shanks (2009) demonstrated that nearly half of the observed variability in drift distance can be explained by pelagic larval duration. The drift distances for surfclams estimated by this model are comparable to model estimates of drifting distances of sea scallop larvae on Georges Bank (Tian et al., 2009) and lobster larvae in the Gulf of Maine (Incze et al., 2010). These three species inhabit the continental shelf, and all have larval life spans near one month.

In contrast, model estimates of larval drifting distances for oysters in east coast estuaries are found to be 80 to 90% shorter, in the range of only 10-30 km (North et al., 2008; Haase et al., 2012; Narváez et al., 2012a), even though their larval durations are comparable to the continental shelf species (e.g.,(Dekshenieks et al., 1993)). In a comparison of observed dispersal distances for sympatric species from the U.S. Pacific Coast, López et al. (2012) similarly found that oyster larva planktonic duration was twice that of mussels, yet the dispersal distances were half as far. Thus, besides pelagic larval

duration, other potential factors contributing to the larval drifting distance vary between these taxa, such as differential larval behavior and properties of the physical environment that they inhabit. Species that live in estuaries often develop complex behaviors such as vertical migrations with daily or lunar periodicity, that allow them to be carried preferentially in water masses that keep them near or return them to natal habitats, thereby reducing overall drift distances (Tilburg et al., 2010; Miller and Morgan, 2013). Salinity gradients are also important (Dekshenieks et al., 1996) whereas they exert little influence on the shelf. Additionally, estuarine water is typically more mixed and the current more variable causing larvae to experience less drifting, whereas on the shelf the physical environment is less variable so that drifting larvae are carried greater distances.

In general, model estimates of passive larval drift tend to predict longer than observed distances of travel (Shanks, 2009), supporting the current paradigm that larvae are retained at a greater rate than would be expected based simply on physical transport (Levin, 2006; Cowen and Sponaugle, 2009; López et al., 2012). This paradigm derives from comparisons between model predictions using both passive models and those including behavior, and observations of dispersal distances (Shanks, 2009). Results of sensitivity simulations performed in this modeling study show that surfclam larval vertical swimming behavior increases the mean larval drifting distances by permitting larvae to access stronger horizontal surface currents. In contrast, larval sinking behavior permits larvae to sink deeper into the water column and experience slower bottom currents and shorter drifting distances (see Figure 3.5 and 3.6 in Chapter 3 for more details).

The combined effects of both vertical swimming and sinking increased larval drifting distances by around 25%, contrary to the general trend in which larval behavior decreases drifting distances for many other species (Shanks, 2009; López et al., 2012). This difference might be attributable to different mechanisms controlling larval behavior that were not included here. In this study, larval behavior is based only on water temperature, while more complex behaviors can be generated by interaction with the background currents, salinity, turbulence, light, gravity and pressure that could create greater larval retention and shorter dispersal distances (Largier, 2003; Shanks, 2009; Miller and Morgan, 2013).

Longer drifting distances may be valuable to a widely distributed open shelf species such as the surfclam. Whether the longer dispersal distances we predict with the addition of larval behavior to the model is truly a reflection of realistic conditions or not, it is noteworthy in that it is an unexpected and contradictory result when compared to most studies. Surfclam larval behavior in this study also causes differences in the temporal variances of larval along-shore drifting distances, with vertical sinking behavior decreasing the variance and swimming behavior increasing the variance (Fig. 2.8c). This is associated with the different turbulence scales near the surface and bottom of the water column, as larval sinking exposes larvae to deeper water with less turbulence and larval swimming places larvae closer to surface water with stronger turbulence (see the 3rd chapter in this thesis).

In terms of the 'larval drift paradox', species with larvae that move uni-directionally downstream will tend to go extinct from the upstream edge of their distribution (Gaines et al., 2003; Shanks and Eckert, 2005; Byers and Pringle, 2006). If

the model sensitivity prediction observed here is reflective of empirical trends, then for surfclams, increased downstream larval drift distances would further exacerbate this effect. Shanks and Eckert (2005) suggest the paradox can be solved by spreading spawning over times during which predominant currents move in different directions (e.g., seasonally shifting north versus south currents). The influence of seasonal variability of spawning on larval connectivity in surfclams is not addressed in this paper, but is the focus of a companion contribution (see the 3rd chapter in this thesis). In the case of surfclams, and other sympatric species with comparable larval duration (e.g., ocean quahogs and sea scallops), the paradox may be avoided because a gyre is present at the upstream end of the distribution in the Georges Bank region that facilitates self-recruitment to that 'upstream' extent of the population and thus maintains that upstream distribution, thereby preventing localized extinction at that upstream end of the population.

2.5.3 Coupled modeling system

In this study, a physical circulation model based on the Regional Ocean Modeling System (ROMS) was coupled with the surfclam larval individual based model to simulate surfclam larval transport. A few other larval transport modeling studies for benthic species along the U.S. northeast coast are also summarized and compared in Table 2.3, including those for the sea scallop (Tian et al., 2009), lobster (Incze and Naimie, 2000; Xue et al., 2008), and oyster (North et al., 2008; Haase et al., 2012; Narváez et al., 2012a, b). Comparison and evaluation of different physical circulation models is beyond the scope of this study (see for example, Leis et al. (2011)). However, the differences in

coupling methods, in particular “in-line” or “off-line”, and inclusion of different larval behaviors merit further discussion here.

In this study, the physical circulation model was coupled with the surfclam larval model using an “in-line” method, which enables both models to be run simultaneously. Another typically used coupling method is “off-line”, wherein both models are run separately. Both “in-line” and “off-line” coupling methods have their strengths and limitations, and no systematic comparison study has as yet been conducted.

For “in-line” coupling, the biological model and the physical circulation model are run together for every time step (4 minutes in this study). Smaller spatial-scale and shorter time-scale physical processes such as tidal effects, sub-grid turbulence, etc., can be better resolved, which might potentially affect larval transport greatly, depending on the specific conditions of the physical environment simulated. The compensating drawback of “in-line” coupling is its additional computational cost, especially when a large number of larvae are released in the model.

In “off-line” coupling, the hydrodynamic model output is stored and later interpolated and provided to a separate larval tracking model. This method is more computationally efficient and more convenient for sensitivity tests of larval behavior, release locations, diffusivity, etc., without the need to redo the hydrodynamic model calculation each time. However, the archived physical model output is often not stored in small enough time intervals so that the information provided to the larval tracking model might fail to resolve important small spatial-scale or short time-scale physical processes. The MAB and GBK are relatively more dynamic regions, especially the Southern New

England shelf and the GBK where tidal effects are strong (Csanady and Magnell, 1987; He and Wilkin, 2006). Thus the "in-line" coupling method applied in this modeling system is likely to better resolve larval trajectories in these dynamic regions.

Besides larval growth required for surfclam larval settlement, both swimming and sinking behaviors were included in the larval model. Vertical behavior is found to be significant in determining surfclam larval drifting distances (Fig. 2.8) and mean connectivity patterns (not shown), further confirming the importance of including behavior in the larval model. Generally larval growth and vertical swimming are the primary components of most larval models, although the relative importance of each differs in determining larval drifting distance, larval settlement success, larval transport patterns, etc. (Xue et al., 2008; Kim et al., 2010; Narváez et al., 2012a, b).

Larval growth is itself intimately meshed with the larval vertical sinking rate and swimming speed, as each of these is a function of larval size and larval size is used as the criterion for larval settlement. Larval vertical swimming and sinking behaviors generally combine with background vertical advection and turbulent mixing to determine the position of the larvae in the water column, thereby determining the exposure of larvae to different temperature fields and water current velocities, and ultimately resulting in differential drifting distances (North et al., 2008; Tian et al., 2009).

A sensitivity study focused on larval swimming behavior for two oyster species (*Crassostrea virginica* and *C. ariakensis*) in Chesapeake Bay demonstrated significant impacts on larval transport by influencing dispersal distances, transport success, and connectivity among different subpopulations (North et al., 2008). However, in some

systems, the background vertical advection and turbulent vertical mixing might be strong enough to de-emphasize larval behavior effects. Such is the case for eastern oysters (*Crassostrea virginica*) in Mobile Bay, Alabama, and in Delaware Bay, New Jersey/Delaware (Kim et al., 2010; Narváez et al., 2012a, b). Off northeastern U.S in this study, surfclam larval behaviors interact with different underlying physical mechanisms to make a significant impact on their transport and to regional connectivity. More details of larval transport variations and larval behavior effects are presented in the 3rd chapter in this thesis.

Habitat selection at larval settlement is another important component in larval models, especially for those species with high sensitivity to different substrates for larval settlement. In a study on sea scallops (*Placopecten magellanicus*) on GBK, this behavior was applied in the larval model in the form of varying settlement probabilities for different bottom substrates (Tian et al., 2009). In an oyster (*Ostrea chilensis*) larval transport study in Tasman Bay, a threshold of habitat quality and larval searching behavior were implemented in the larval model, so that the "landed" larvae could still return to the water column if the bottom substrate was not suitable and did not meet the quality threshold (Broekhuizen et al., 2011). For the Atlantic surfclam in this study, suitable habitat ranges from the Gulf of Maine south to Cape Hatteras of North Carolina, covering almost half of the MAB shelf and GBK in depths of 8-66 m. There is no obvious variation of surfclam habitat within these regions, except that those regions deeper than 60 m are not considered suitable habitat for surfclams, and we assume 100% mortality once they settle into those regions.

2.6 Model limitations

The Gulf Stream is one important current system known to have a significant impact on the MAB/GBK shelf water and its circulation properties, particularly through the formation of meanders and eddies (Churchill et al., 1993; Gawarkiewicz et al., 2001; Rasmussen et al., 2005; Chen et al., 2014). One warm-core ring (WCR) off the Gulf Stream penetrating onto the MAB/GBK shelf might affect water properties substantially with a duration lasting as long as several months. Accurately simulating the variability of the Gulf Stream, including the development of its meanders and warm-core rings has proven to be difficult, without further aid from more advanced modeling techniques such as data assimilation (Chen et al., 2014), etc. In our modeling system, although the main characteristics of the mean shelf current system are adequately captured by the circulation model, the full range of temporal and spatial variability might not be, especially along the shelf break where Gulf Stream meanders have a large impact (Fig. 2.2c, d). We cannot estimate the degree to which inaccuracies in the position and behavior of the Gulf Stream may affect surfclam larval trajectories, although we believe this influence is likely to be minor to the long-term mean pattern of larval transport and connectivity, for example the 4-year means examined in this study.

Food concentration in the model is set at an optimal constant value, because we have insufficient information from field observations to provide an accurate and reliable time- and space-varying estimate to the model, e.g., Munroe et al. (2013). Once we have enough data to be able to construct a food climatology dataset for the model, improvements in model performance can be expected, but sensitivity results with modified food quality values indicate that the main larval transport and connectivity

pattern is unchanged. This is largely due to saturation of larval feeding rate at relatively low planktonic algal densities. Apart from the assumed mortality due to unsuccessful settlement before 35 days or due to settlement into inappropriate water depths, planktonic daily mortality was not included in the current model. Sensitivity analyses using modified planktonic mortality (see appendix A) likewise demonstrated that the main transport and connectivity patterns remain unchanged, but the magnitude of dispersal drops with increasing planktonic mortality. More observational data of surfclam larval concentration or an estimate of surfclam connectivity from genetic studies would be extremely valuable for better model validation and evaluation.

Table 2.1 List of surfclam larval individual-based model variables

Symbol	Name	Units
t	Time	day
Z	Larval depth	meters
T	Water temperature	^{o}C
F	Food concentration	mg/liter
Age	Larval age	day
Len	Larval length	mm
Gr	Larval growth rate	mm/d
Gr_{Base}	Base growth rate	mm/d
$CorT$	Temperature effect on growth	
Sk	Sink rate	m/d
Uss	Upward swim speed	mm/s
Usf	Time fraction swimming upward	
Dss	Downward swim speed	mm/s

Table 2.2 List of surfclam larval individual-based model constants

Symbol	Values	Symbol	Values
F_{Qual}	1.2	Fs	1.0
L_0	58	Stf	0.920
Gr_0	8.165	S_0	2.220×10^{-4}
Gr_1	71.810	S_1	1.744
Gr_2	0.0907	U_0	-0.381
Gf_1	0	U_1	9.262×10^{-3}
Gf_2	0.144	U_2	-2.692×10^{-5}
Gf_3	1	D_0	-0.561
Gf_4	1	D_1	1.749×10^{-2}
Gf_5	0.144	D_2	-6.538×10^{-5}
Gf_6	0	St_0	21
		St_1	0.900

Table 2.3 Summary of recently published larval transport model studies for benthic species along the U.S northeast coast.

Species	Study Region(s)	Physical circulation model	Larval behavior	Model coupling method [a]	Pelagic duration	Larval drifting distances	References
Atlantic surfclam (*Spisula solidissima)*	Georges Bank, Middle Atlantic Bight	Regional Ocean Modeling System (ROMS, www.myroms.org)	1. Growing, 2. Vertical swimming and sinking	In-line	~19-35 days	~119 km (mean along-shore)	This study
Sea scallop (*Placopecten magellanicus*)	Georges Bank, Middle Atlantic Bight	Finite-Volume Coastal Ocean Model (Chen et al., 2001)	1. Vertical swimming 2. Habitat selection by settlement probability	Off-line	~40-50 days	As long as hundreds of kilometers	Tian et al., 2009
Lobster (*Homarus amerianus*)	Gulf of Maine	Dartmouth Circulation Model (Lynch et al., 1996; Lynch et al., 1997)	1.Growing 2.Constant larval depth	Off-line	~18-38 days	~19–280 km	Incze and Naimie, 2000
	Gulf of Maine	Princeton Ocean Model (Mellor, 2003)	1. Growing 2. Ontogenetic changes in vertical distribution	Off-line	~22–44 days	--	Xue et al., 2008
Eastern oyster (*Crassostrea virginica*)	Delaware Bay	Regional Ocean Modeling System (ROMS, www.myroms.org)	1. Growing, 2. Vertical swimming and sinking	In-line	<30 days	Mostly 0-20 km	Narváez et al., 2012b
	Chesapeake Bay	Regional Ocean Modeling System (ROMS, www.myroms.org)	1. Vertical swimming	Off-line	~14-21 days	~9.0 km (median distance)	North et al., 2008
	Pamlico Sound, North Carolina	Advanced CIRCulation model (Reyns et al., 2006, 2007)	None, with larvae constrained at constant depth	Off-line	~14-25 days	~0.3-35.8 km	Haase et al., 2012

- Model coupling method: "Inline" indicates that the physical model and biological model are embedded such that both models are running simultaneously, while "Offline" indicates separate computations, usually with the physical model run first, then providing the necessary circulation fields to the biological model.

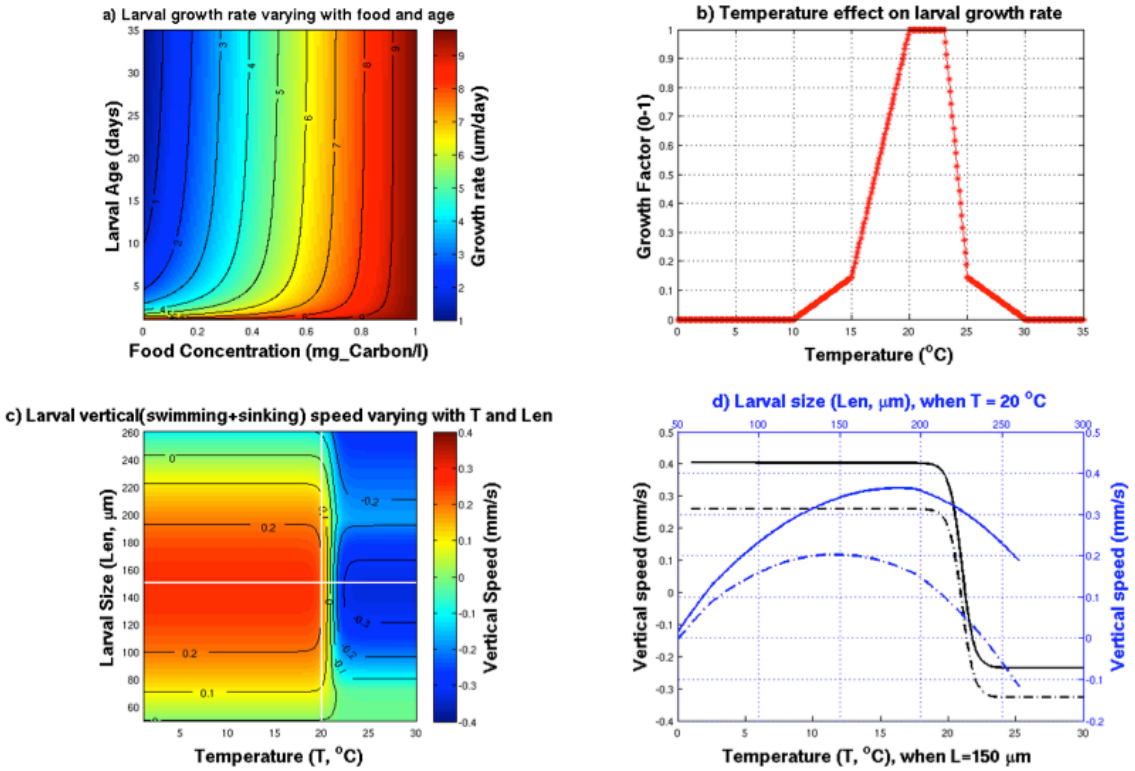

Figure 2.1 **Panel a-b:** Variation in modeled larval growth. Panel (a) shows the variability in modeled larval growth rate with food concentration and larval age. The temperature-dependent growth correction factor (*CorT*) is shown in Panel (b); **Panel c-d:** Variation in modeled larval vertical motion. Panel (c) shows the variability in larval vertical motion (swimming + sinking behavior) with temperature and larval size. Panel (d) shows the variability in vertical speed with both swimming+sinking (dashed lines) or swimming only (solid lines) under conditions of varying temperature for larvae of length = 150 µm (lower x-axis, black lines), or under varying larval size at temperature = 20 ^{o}C (upper x-axis, blue lines).

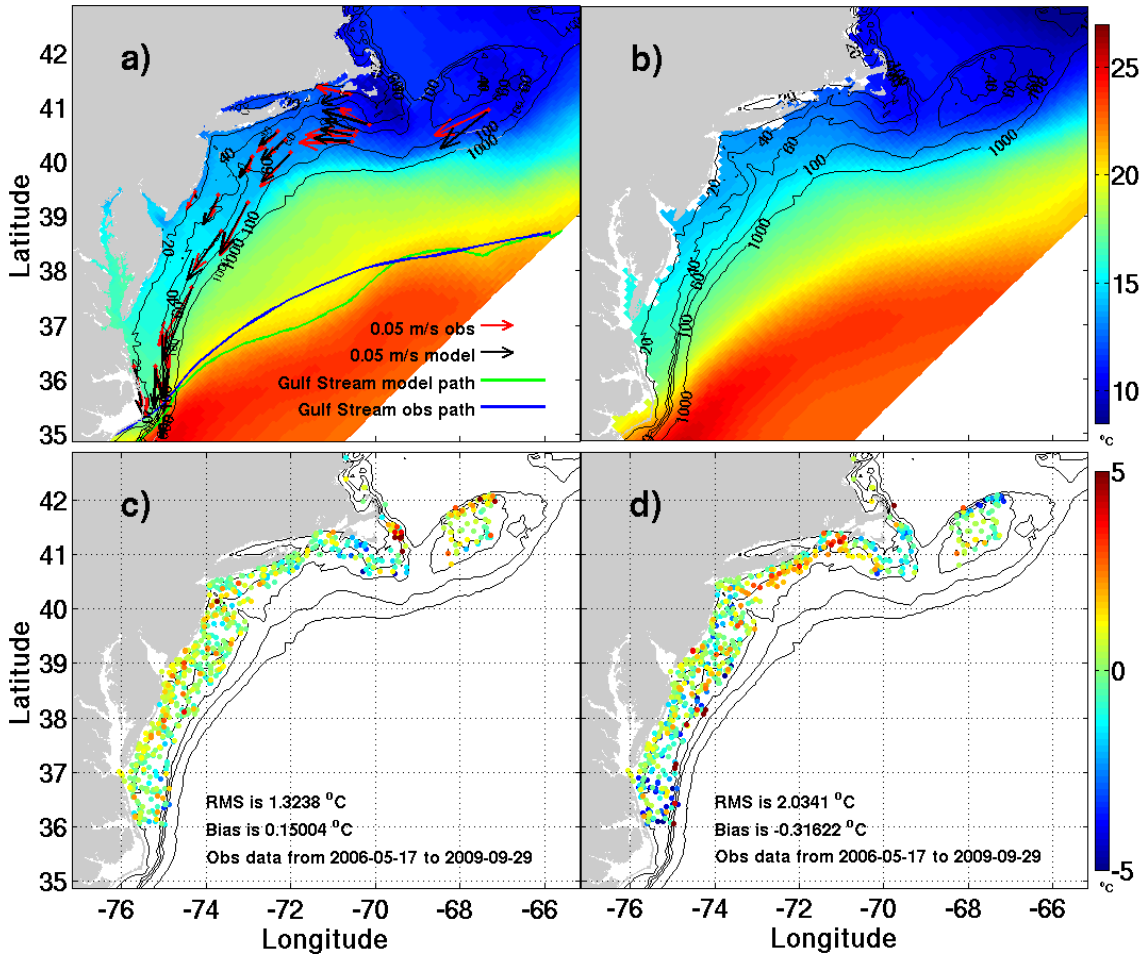

Figure 2.2 **Panel a-b:** Comparison of modeled 4-year mean SST at 1-m depth (Panel a) and satellite observed 4-year mean SST (Panel b) (Reynolds et al., 2007) from year 2006 to 2009, as indicated by the colorbar on right. In Panel a, the green line indicates the 21 °C SST isotherm from the mean simulated SST (used here as a proxy of the modeled Gulf Stream location), and the blue line shows the 21 °C SST isotherm based on mean observed SST over the same period (Reynolds et al., 2007). The comparison between the 4-year mean barotropic currents (black arrows) from model output and the long-term mean climatological barotropic currents (red arrows) (Lentz, 2008a) is also shown in Panel a. **Panel c-d:** Comparisons of surface (Panel c) and bottom (Panel d) temperature

between model output and NEFSC observational data during late-spring to early-fall from 2006 to 2009. Colorbar on the right shows the temperature differences (model - observation in ^{o}C), at each survey station on the corresponding survey date. In all panels, the 20-, 40-, 60-, 100-, 1000-m isobaths are also shown as black lines.

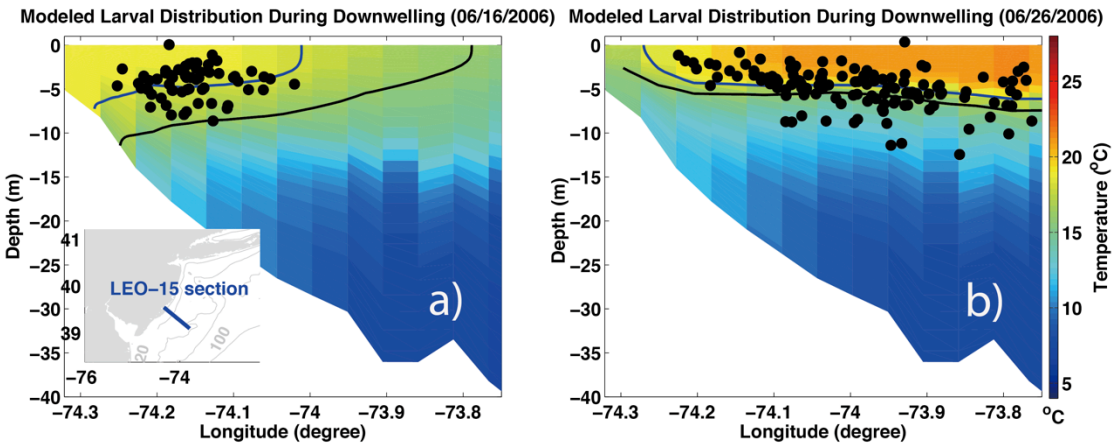

Figure 2.3 Modeled surfclam larval distribution along the New Jersey LEO-15 across-shelf section during downwelling (June 16th 2006, panel a) and upwelling periods (June 26th 2006, panel b) in 2006, with each dot representing each larva in the water. The 16 °C (lower black line) and 18 °C (upper black line) isotherms are shown to indicate the approximate thermocline positions. The bottom left inset of panel a shows the location of the LEO-15 transect (blue line) off NJ shelf.

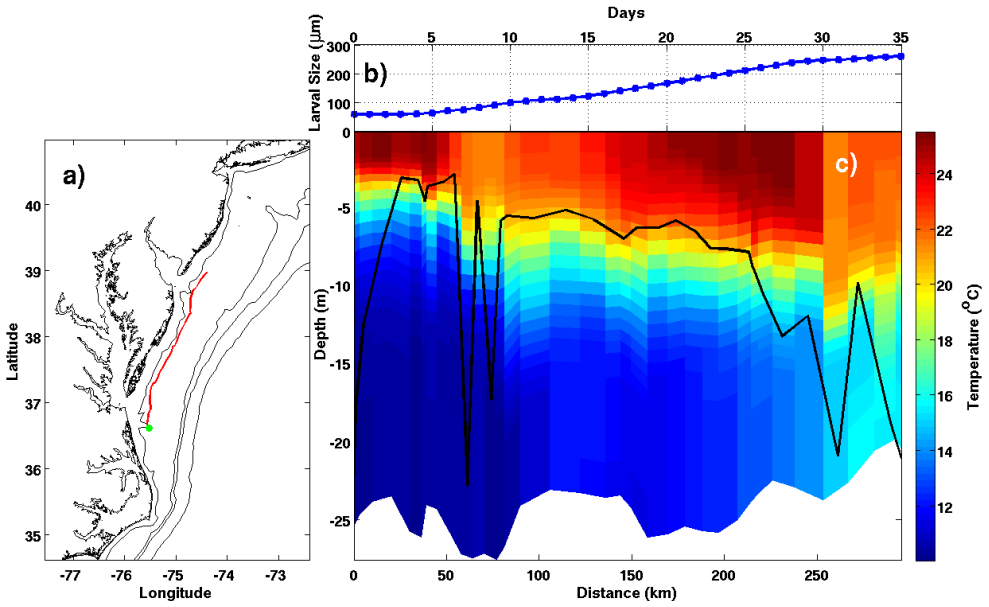

Figure 2.4 Horizontal (panel a) and vertical (panel c) larval trajectories of an individual larva released along the southern New Jersey shelf on August 1, 2006. In Panel a, the green dot represents the final larval settlement position. Isobaths of 20-, 40-, 60-, 100-, 1000 m are shown in black solid lines. In Panel c, the colorbar indicates the background water temperature. Panel b shows the size of the larva as it grows over time.

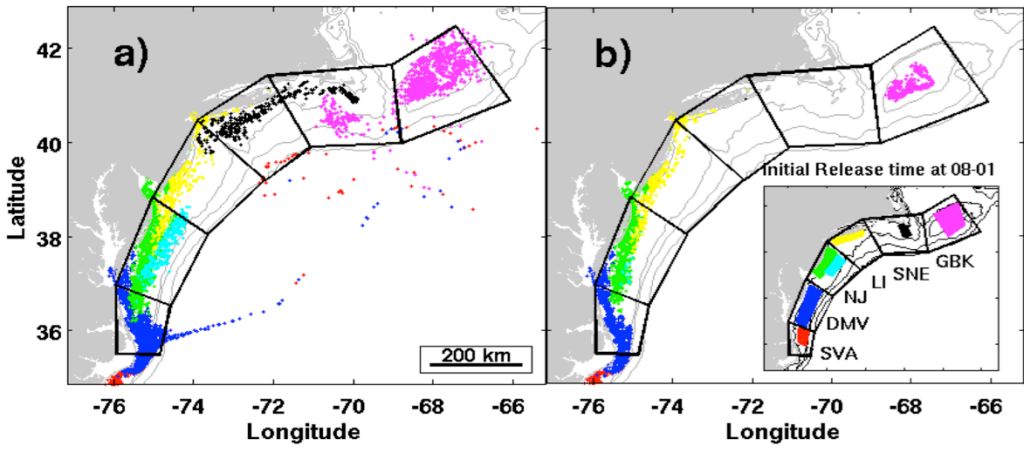

Figure 2.5 Larval distribution on September 5, 2006, 35 days after larval release on August 1. Panel a shows the distribution of all larvae from the initial release, including those that settled successfully and those that did not. Panel b shows the distribution of only those larvae able to successfully settle within the 35-day limit. Each dot represents one larva and colors indicate initial release locations as follows: GBK-pink, SNE-black, LI-yellow, NJ inshore-green, NJ offshore-light blue, DMV-blue, SVA-red. Lower right inset in panel b shows the initial distribution of the larvae at the time of release.

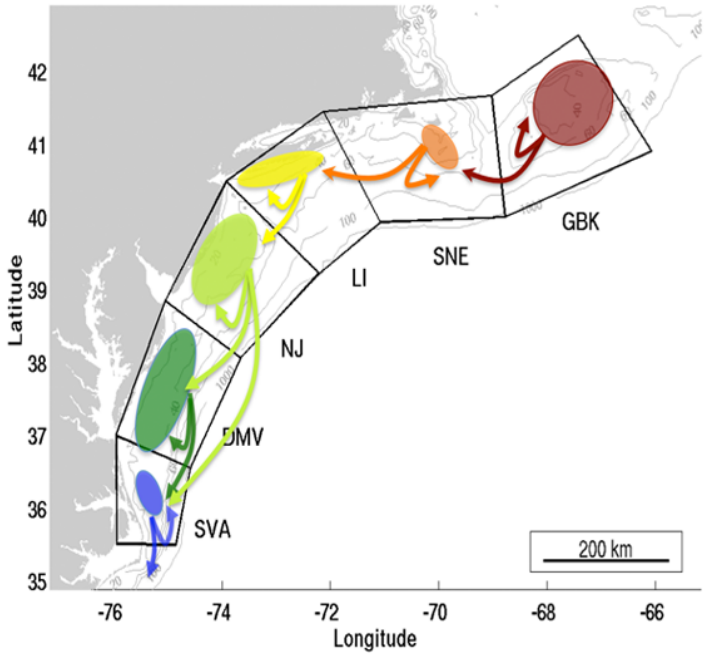

Figure 2.6 Generalized mean connectivity pattern between the MAB and GBK surfclam subpopulations based on the model output for all releases in 2006 to 2009.

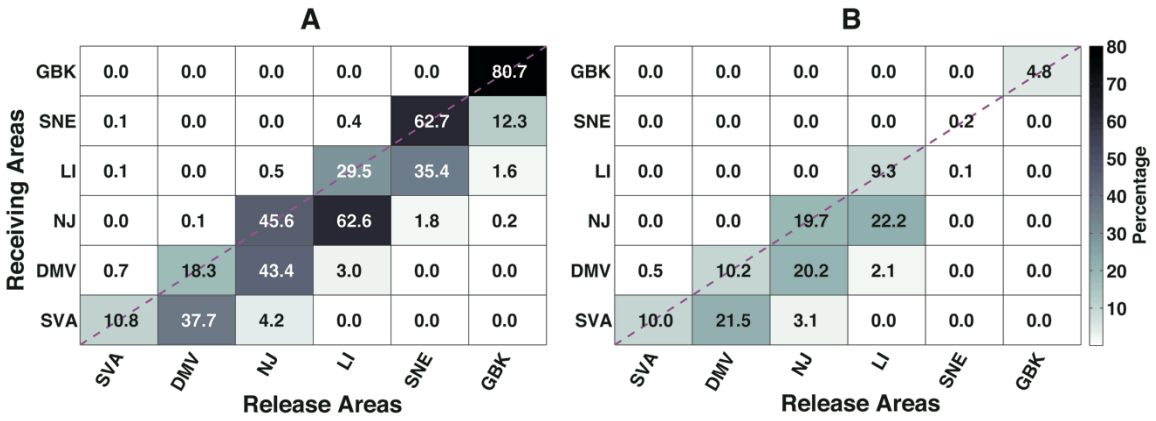

Figure 2.7 Four-year (2006-2009) mean modeled connectivity matrix among the 6 main surfclam geographic regions: SVA, DMV, NJ, LI, SNE and GBK, showing the percentage of larvae released in one region (x axis, see Figure 1.1 for their locations) that are transported (larval supply, panel A) or successfully settled (larval settlement, panel B) into the same or another region (y axis, see Figure 1.1 for their locations). The exact percentage values are indicated by both the colorbar and the text in each cell.

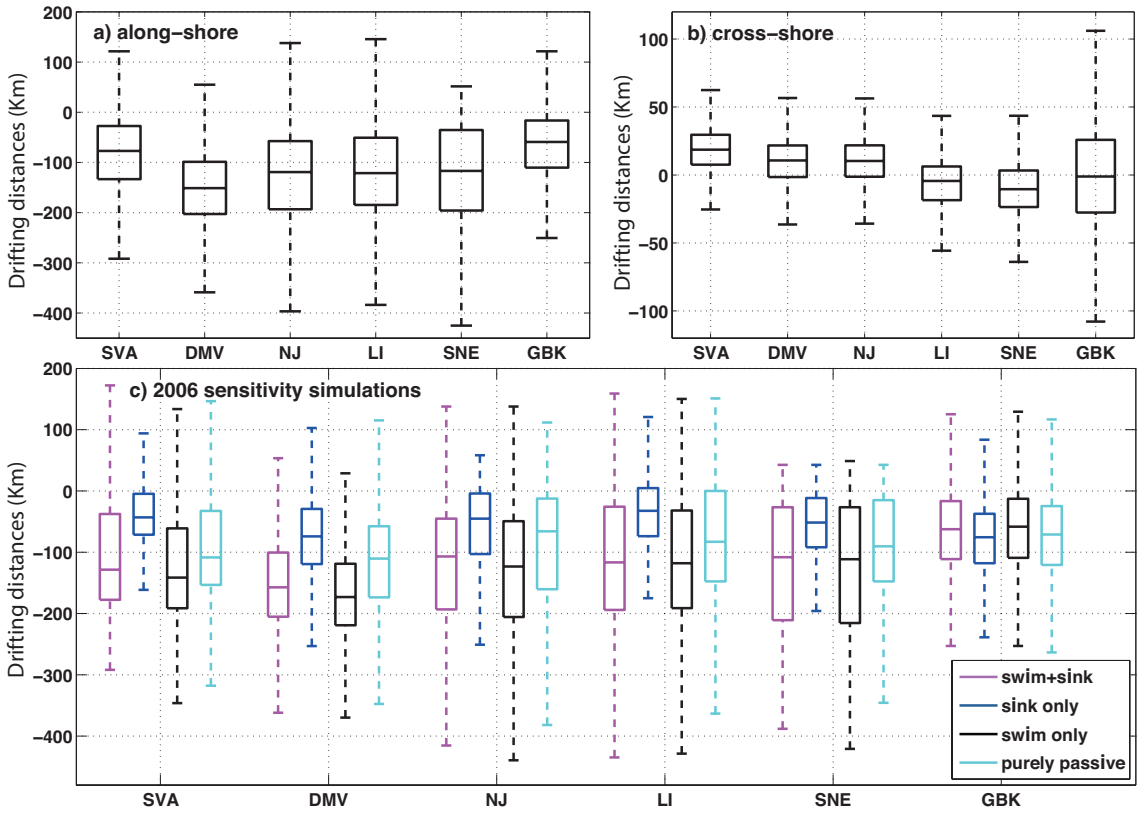

Figure 2.8 Panel a-b: Box-plots of larval drifting distances (units: kms; y-axis) in the along-shore (panel a) and across-shelf (panel b) directions for all released larvae from regions of SVA, DMV, NJ, LI, SNE and GBK (x-axis) in 2006 to 2009. Along the y-axis, positive values indicate southwestward along-shore drifting, or onshore across-shelf drifting; negative values indicate the opposite direction. Panel c: Box-plots of larval drifting distances (units: kms; y axis) in the along-shore direction for all released larvae from regions of SVA, DMV, NJ, LI, SNE and GBK (x axis) in 2006, with both swimming and sinking behaviors (magenta: swim + sink, the standard model setup), only sinking behavior (blue: sink only), only vertical swimming behavior (black: swim only), and neither (cyan: purely passive).

CHAPTER 3. PHYSICAL MECHANISMS UNDERLYING LARVAL TRANSPORT AND SETTLEMENT VARIATIONS

3.1 Introduction

Larval transport is the horizontal displacement of larvae from one point to another within a certain time interval (Pineda et al., 2007). At least since Thorson (1966), larval transport and settlement have been considered to be primary determinants of adult population size, although Ólafsson et al. (1994) stressed the importance of post-settlement processes in determining the ultimate influence of larval supply. Nevertheless, post-settlement processes are of no consequence without larval supply and thus connectivity among different geographically distributed subpopulations leading to source and sink dynamics (Swearer et al., 2002; Condie et al., 2005; Munroe et al., 2012) becomes an important component of the dynamics of the metapopulation.

Knowledge of governing processes and mechanisms affecting larval transport and settlement is fundamental in understanding the population structure of marine sessile invertebrates, and more broadly to predict the effects of global climate change on benthic marine ecosystems (GLOBEC, 1991; Gawarkiewicz et al., 2007). Processes on a broad range of temporal and spatial scales can impact coastal currents and thereby larval transport. For nearshore systems, a variety of region-specific processes such as along-shelf cold/warm currents (Hickey, 1979; Leaman et al., 1989), coastal upwelling/downwelling (Garland and Zimmer, 2002; Garland et al., 2002; Shanks et al., 2002; Shanks et al., 2003; Ma and Grassle, 2004; Ma, 2005; Ma et al., 2006a), shelf break fronts (Marra et al., 1990; Munk et al., 1995), tidal induced mixing fronts (Smith and Morse, 1985), seasonal changes in shelf stratification (Aikman and Posmentier, 1985), and transport of “cold pool” bottom water (Houghton et al., 1982) may influence, and potentially dominate, the dynamics of larval transport. Unlike water parcels which

only flow passively with the surrounding currents, marine larvae generally have some degree of behavior (Hill, 1991; Dekshenieks et al., 1996; Pfeiffer-Hoyt and McManus, 2005), such as swimming, growth, ontogenetic changes in sinking rate, and selection of substrates before settlement, which are observed for many invertebrates to be essential factors in determining the dynamics of larval transport and spatial variations in settlement (Werner et al., 1993; Lough et al., 2005).

The Atlantic surfclam (hereafter surfclam), *Spisula solidissima*, is a bivalve mollusc with a life history that includes a planktotrophic larval dispersal stage and a sessile juvenile/adult stage. Surfclam adults inhabit waters from Cape Hatteras, North Carolina to the southern Gulf of St. Lawrence, in a depth range from shallow subtidal regions to around the 60 m isobath (Ropes, 1980; Cargnelli et al., 1999), depending on bottom water temperature (Kim and Powell, 2004; Weinberg, 2005). Most of the surfclam stock exists today on the Middle Atlantic Bight (MAB) shelf and Georges Bank (GBK) (Fig. 1.1), where it supports a high-value commercial fishery (NEFSC, 2010). Studying the spatial and temporal variations in surfclam larval transport and the underlying physical mechanisms is essential for better understanding surfclam population dynamics, formulating improved management decisions for the surfclam fishery, and interpreting associated socio-ecological responses to climate change (McCay et al., 2011).

The MAB is the primary focus for this study that examines variations in surfclam larval transport and settlement. The MAB is a shallow and wide continental shelf bounded by Cape Hatteras in the south and Cape Cod in the north (Fig. 1.1). The MAB exhibits a mean depth-independent along-shore current of 5-10 cm s^{-1} equatorward with a nearly constant flow along isobaths, and a mean but relatively weak across-shelf

circulation (Beardsley and Boicourt, 1981; Lentz, 2008a). Large variations in the flow, both in the along-shore and across-shelf directions, exist and are well documented (Shearman and Lentz, 2003; Kohut et al., 2004; Ullman and Codiga, 2004; Gong et al., 2010). Various factors potentially contribute to these variations, including wind stress (Kohut et al., 2004; Dzwonkowski et al., 2009; Gong et al., 2010), topography (Harris et al., 2003; Gong et al., 2010), seasonal stratification (Shearman and Lentz, 2003; Dzwonkowski et al., 2009), and river plumes (Fong and Geyer, 2002; Zhang et al., 2009).

Surfclam larvae, like most larvae in the ocean, are mainly transported passively in the horizontal plane, being subject to the influences of these factors affecting the flow. In addition, surfclam larval behavior such as vertical swimming and growth also influence the horizontal trajectories. By active movement, larvae are able to modulate the water properties they experience and thus their growth history (see the 2nd chapter in this thesis). One objective of this study is to identify the primary mechanisms controlling the dispersal patterns of surfclam larvae in the MAB.

Observational studies of surfclam larval transport within the MAB are few. Ma et al. (2004; 2005; 2006a) examined larval vertical distribution along LEO-15, a cross-shelf transect off Tuckerton, New Jersey (NJ), during summer upwelling and downwelling episodes. Studies by Garland and Zimmer (2002), Garland et al. (2002), Shanks et al. (2002), and Shanks et al. (2003) examined the vertical dispersion and across-shelf transport of various species including the surfclam across the shelf off of the Outer Banks of North Carolina (NC), also under upwelling and downwelling periods. These studies, however, show different vertical patterns and across-shelf transport on the NJ and NC shelves for surfclam larvae. At LEO-15 in July of 1997 and 1998, surfclam larvae were

observed to be concentrated more inshore, near the intersection of the thermocline and the bottom during downwelling, and more offshore, close to or above the thermocline during well-developed upwelling. Larval concentrations were observed to be correlated positively with water temperature at this time, indicating that larvae were more likely to be transported by the water above the pycnocline.

Off NC in August of 1994, surfclam larvae were mostly found below the pycnocline in the bottom layer, with larval concentrations correlating negatively with water temperature. During upwelling, larvae were transported onshore by advection of subpycnocline waters, while during downwelling larvae were transported offshore. Ma (2005) speculated that these differences in larval vertical distribution and across-shelf transport between the NJ and SVA shelves might be due to the difference in larval sources, whether inshore or offshore, and spawning time, as a seasonal change in larval vertical distribution might be expected.

In this study, the vertical distribution and across-shelf transport patterns of surfclam larvae will be examined for different regions of the MAB using a coupled physical and biological model, to determine if observed patterns can be reproduced and to determine the underlying mechanisms generating these patterns. In the following, section 3.2 introduces the simulations of the coupled physical circulation and surfclam larval model, methods of processing model output in examining the intra-annual variation of larval transport and settlement within Mid-Atlantic Bight and also the underlying physical mechanisms causing those variations. Section 3.3 presents the results of the intra-annual variations in surfclam larval transport, settlement and along-shore and across-shelf daily drifting distance. Discussions of the results and effects of underlying

physical mechanisms and larval behavior are presented in section 3.4. Section 3.5 gives a brief summary.

3.2 Methods

3.2.1 Coupled physical circulation and surfclam larval model simulations

A physical circulation model based on the Regional Ocean Modeling System (ROMS) and a surfclam larval individual-based model have been developed, coupled, and validated (see the 2nd chapter in this thesis). The domain for the physical circulation model covers the entire Middle Atlantic Bight, Georges Bank, and the Gulf of Maine, including regions with high surfclam abundances (Fig. 1.1). The model was forced by real-time solar radiation, wind, river discharge, and tides. The boundary conditions are provided by output from a larger-scale circulation model with verified corrections. The physical model was run for 4 years from 2006 to 2009, and the main features of the shelf circulation and temperature distribution from the model output were analyzed and validated.

The surfclam larval model has two main components: larval growth and vertical swimming behavior. Larvae grow in size after release, with the growth rate expressed as a function of water temperature, larval age, and food concentration. Larvae become competent to settle at 260 μm and settle when they reach the bottom. No daily mortality is applied; however model sensitivity to daily larval mortality was assessed and the results of this analysis can be found in appendix A. Larvae drift passively in the horizontal by means of the surrounding water currents. In contrast, vertical movement of

larvae is the sum of sub-grid vertical mixing implemented as a vertical random walk and swimming behavior exhibited by the larvae, with the speed and direction being functions of water temperature and larval size. The parameters inside the larval model were obtained and calibrated from laboratory experiments. More detailed descriptions of both models are provided in Chapter 2.

For each year in this study, 2006-2009, surfclam larvae are released from regions with high surfclam abundances identified using the 1982-2008 NEFSC surfclam stock surveys (NEFSC, 2010). From south to north these are: South Virginia/North Carolina (SVA), Delmarva (DMV), New Jersey inshore (NJ_in), New Jersey offshore (NJ_off), Long Island (LI), Southern New England (SNE), and Georges Bank (GBK) (Fig. 1.1). The number of larvae released in each region is proportional to both the historically observed surfclam density and the regional area. As a result, 400, 2000, 1800, 300, 400, 400 and 1500 larvae were released within the SVA, DMV, NJ_in, NJ_off, LI, SNE, and GBK regions, respectively.

The spawning time of surfclams generally ranges from late spring (late May or June) until fall (Ropes, 1968; Jones, 1981; Fay et al., 1983; Cargnelli et al., 1999), so the release times for surfclam larvae in the model were chosen to be from May 21st until October 16th at 5-day intervals throughout the spawning season. Surfclam larvae are approximately evenly released from each region simultaneously at midnight of the selected release dates. The release depth was the bottom-most grid cell. In total, 30 releases and 204,000 larvae (6,800 per release) were generated each year of simulation, covering the entire spawning season and also the main surfclam spawning areas along the U.S northeastern shelf.

The coupled physical circulation and surfclam larval model was also run for year 2006 to examine intra-annual variations in larval transport and settlement. Year 2006 was taken as a representative year based on the previous chapter (as well as appendix B which considers interannual variations in larval distributions).

3.2.2 Larval transport and settlement variations

Surfclam metamorphosis generally occurs from 19 to 35 days after spawning depending on water temperature during larval growth (Fay et al., 1983). Comprehensive information on food supply is not available for the MAB; hence the model was run under the assumption that food supply did not limit larval growth. Larvae are variously affected by periods of suboptimal food, e.g., Powell et al. (2002), Moran and Manahan (2004), and Przeslawski and Webb (2009), and this can influence survival and location of settlement because larval growth frequently may be food-limited (Olson and Olson, 1989; Bos et al., 2006; Gireesh and Gopinathan, 2008). Thus, our simulations represent the results for optimal conditions in the MAB. The maximum duration of the larval stage for successfully recruiting larvae is set at 35 days; that is, few larvae are assumed to survive at anticipated planktonic mortality rates (Rumrill, 1998) beyond 35 days if not successfully settled by that time.

The total along-shore and across-shelf drifting distances, average temperature experienced by larvae (ATEL), and the determination of whether the larva has successfully settled in 35 days or not was recorded for each larva. The total along-shore and across-shelf drifting distances were computed by comparing the final larval

settlement position or the position at the end of 35 days with the initial larval release position, with reference to the approximate along-shore line as indicated in Figure 3.1. The along-shore drift is the length of the projected curve of larval trajectory on the along-shore reference line, while the across-shelf drift is the net displacement distance perpendicular to the along-shore line from the initial release position to the final position.

The average temperature experienced by each larva (ATEL) is calculated as the time mean of the temperatures that the larva experiences during the entire larval stage. The final determination of whether the larva successfully settled requires that two conditions are satisfied: first, that the larva reaches settlement size and intersects the bottom within 35 days, and second, that the larva location of settlement is shallower than 60 m. For each release from each region, the ratio of successful settlements with respect to the total number of larvae released was calculated and defined as the settlement rate. The mean ATEL and total along-shore and across-shelf larval drifting distances among all larvae released from each region at each time were also computed, excluding only those that eventually drift into regions with water depths exceeding 100 m. Variations in outcome as determined by these variables are examined both intra-annually among all releases in 2006 and spatially among all releases from different regions.

The spatial variability of the four variables--ATEL, settlement rate, and total along-shore and across-shelf drifting distance--were also investigated for surfclam larvae released from different depths. In this case, the entire shelf from the coast to the 60 m isobath was partitioned into slices of 1-m-depth interval in the across-shelf direction and these variables are examined for larvae released from each 1 m depth interval in each region.

3.2.3 Physical mechanisms underlying larval transport variations

To examine the physical mechanisms causing variations in larval transport, larval daily movement and its relationship to the background physical environment were calculated in both the along-shore and across-shore directions. Larval daily drifting distance is calculated by examining the net change in position within each day, which accumulates during the larval stage to form the larval total transport. The mean along-shore and across-shelf daily drifting distances were computed among larvae inside each of three regions (NJ, DMV, and SVA; see Figure 3.1) on each day, regardless of where and when they were released.

This computing method is different from that applied in calculating the larval total drifting distance. In this analysis, the immediate position and daily drift within each day is utilized, whereas in the previous method, the larval release location/time and larval total drift are calculated over the entire planktonic life span (up to 35 days) for each larva. For example, the mean daily along-shore drift on August 1st, 2006 off NJ is calculated as the mean among all larvae inside the NJ release area on that specific day, regardless of where and when those larvae were released, while the mean larval total along-shore drift for the larvae released on August 1st, 2006 refers to the mean among all larvae released from the NJ shelf on that chosen release date, regardless of their present location. Note that the SVA region chosen here approximates the North Carolina (NC) shelf region from observational studies (Garland and Zimmer, 2002; Garland et al., 2002; Shanks et al., 2002; Shanks et al., 2003).

The daily mean surface wind stress is computed as the mean of the surface wind stresses above the waters of larvae inside each region on each day, and compared to the simulated larval daily trajectories. The approximate along-shore line, as indicated in Figure 3.1, is used as the reference direction for the calculation of along-shore and across-shelf daily larval drifting distances and wind stresses. The relationship between the mean along-shore larval daily drifting distances (*d_al*) and the mean along-shore surface wind stress (*wstr_al*) was investigated for three regions: NJ, DMV and SVA. To examine the difference between this relationship between the inshore and offshore larvae, the entire shelf was further separated into the inner shelf (depth < 30m) and the outer shelf (depth > 30m) and the same calculations made. The relationship between the mean larval daily across-shelf drifting distances (*d_cr*) and the mean along-shore surface wind stress (*wstr_al*) was also examined for all three regions. However, only those inshore larvae in regions shallower than 20 m are included, to be compatible with the available surfclam larval observations from the inner NJ and NC shelves (Shanks et al., 2002; Shanks et al., 2003; Ma et al., 2006a).

Besides the wind effect (*wstr_al*), the vertical location of the larvae relative to the depth in the water column where the across-shelf current reverses directions (hereafter called the reversing depth) is investigated. For each larva, whether the larva is above or below the reversing depth was determined. A stratification index was calculated as the ratio of the temperature difference between surface and bottom with respect to the water depth. The more strongly stratified period, when the stratification index is greater than 0.2, is used for examination of the relationship between *d_cr* and *wstr_al*.

3.3 Results

3.3.1 Intra-annual variation in larval transport and settlement

Larvae released from different source populations at different times experience different ATEL (average temperature experienced by larvae) and larval settlement rates. The ATEL is larger for releases from July until early October (Fig. 3.2a-1), and for releases from the southern two regions of DMV and SVA (Fig. 3.2a-3). Larval releases from LI during mid-July to late-September experience relatively higher settlement rates than other release times. Larvae released from NJ are more successful slightly later in the year, from early August to late-September, and larvae from DMV later still, from early-September to early-October (Fig. 3.2b-2). Comparing regions, on average, larvae released from LI, NJ, and DMV experience higher settlement rates than the others (Fig. 3.2b-3), whereas comparing time periods, larvae released from late-July to late-September have higher settlement rates (Fig. 3.2b-1). Across-shelf variations of ATEL and settlement rates are also evident (Fig. 3.3a-f). Generally, larvae released from regions shallower than 40 m experience larger ATEL and larval settlement rates than those released farther offshore (Fig. 3.3a-c, d-f).

The spatial and temporal pattern of larval settlement rate (Fig. 3.2b-2, Fig. 3.3d-f) was similar to that of ATEL (Fig. 3.2a-2, Fig. 3.3a-c). Larval releases with relatively larger ATEL experience higher settlement rates. The black lines on panels in Figure 3.2a-2, 3.2b-2 and Figure 3.3a-f enclose those larval releases experiencing ATEL higher than 18 ^{o}C, and most of those releases also experience larger settlement rates (Fig. 3.2b-2, Fig. 3.3d-f). About 97.7% of those releases with settlement rates larger than 60% are found to

experience ATEL larger than 18 ^{o}C. The relationship between ATEL and settlement rate is correlated, but is not necessarily deterministic as some releases show ATEL greater than 18 ^{o}C, yet have low settlement success mostly due to settlement in inappropriate regions. For those larval releases from DMV and SVA with a high ATEL but low settlement rates, for example, most of the "unsuccessful" larvae were entrained into the Gulf Stream and were transported out of suitable habitat into the open ocean and thus settled in waters too deep for survival.

Along-shore and across-shelf total drifting distances also vary both spatially and temporally in 2006. Along-shore larval drift is typically in the southwestward direction (Fig. 3.2c-2). Larvae released during August on average experience relatively longer southwestward drift, around 200 km (Fig. 3.2c-1), than those released at other times, whereas releases from NJ, DMV, and SVA drift farther than those from other regions, with an average drift of 120~150 km (Fig. 3.2c-3). The longest along-shore southwestward drift, at around 220 km, was observed for releases during August from LI, NJ, DMV, and SVA (Fig. 3.2c-2). Comparing larval releases from inshore and offshore regions, the larvae released offshore tend to drift farther in the along-shore direction than those released onshore (Fig. 3.3g-i).

Larvae released from NJ, DMV, and SVA experience net total inshore transport on most release dates, whereas those released from LI, SNE and GBK generally experience net total offshore transport (Fig. 3.3d-2, d-3). The net larval onshore drifting distances are generally larger for releases during July and August than for releases at other times (Fig. 3.2d-1), with the maximum value close to 40 km for some releases from NJ, DMV, and SVA (Fig. 3.2d-2). No significant difference was found in the across-shelf larval drifting

distances between the inshore and offshore larval releases on shelves of LI, NJ, and DMV (Fig. 3.3j-l).

3.3.2 Along-shore larval daily drifting distance variation

Temporal variations in the mean along-shore daily drifting distances (*d_al*) and along-shore surface wind stresses (*wstr_al*) on the NJ shelf are highly correlated ($r = 0.60$, Fig. 3.4a, Table 3.1). A linear regression model (M1) between *d_al* and *wstr_al* was applied and the model fit (*d_al_m1*) explains 35.7% of the total variance in the daily drifting distances, *d_al*. A plot of the residuals of this linear model (*res* = *d_al* – *d_al_m1*) shows a noticeable seasonal signal (Fig. 3.4b, gray line). The least-squares best fit to *res* using results of a seasonal model (M2) shows a significant seasonal cycle with a 147.4-d period and a 4.21 km amplitude (Fig. 3.4b, black line; Table 3.1). The minimum value in the seasonal signal appears in mid-August corresponding to the longest southwestward drift, and the maximum occurs at the end of October corresponding to the least southwestward, or in some cases a northeastward, drift (Fig. 3.4a, b). The simulated seasonal signal (*d_al_m2*) explained about 28.2% of the total variance of the daily drifting distances, *d_al* (Table 3.1). Together, the linear regression model (M1) and the seasonal model (M2) contribute 63.9% of the total variance of the mean along-shore larval daily drifting distances (*d_al*).

The same analysis, using the linear regression model (M1) and the seasonal model (M2), was applied to larvae on the DMV and SVA shelves (Table 3.1). On both the DMV and SVA shelves, the surface along-shore wind stress (*wstr_al*) and the along-shore

larval daily drift (*d_al*) were highly correlated (r = 0.65 and 0.61 respectively). The linear regression models (M1) between *d_al* and *wstr_al* explain 41.9% and 37.3% of the variance of *d_al* for larvae within DMV and SVA shelves respectively. The least-squares best fit of a seasonal model to the linear regression model residuals shows a significant (p-value =5.77×10^{-7}) seasonal signal with a period of 159.2 days on the DMV shelf, with a variance contribution of 10.1% to the total *d_al* variance. Together, models M1 and M2 contribute 52.0%. On the SVA shelf, however, the seasonal signal within the linear model residuals is not significant.

For larvae inshore of 30 m and offshore of 30 m respectively, high correlations between the surface along-shore wind stress (*wstr_al*) and along-shore larval daily drift (*d_al*) are found for the NJ, DMV, and SVA regions. After the wind-induced components in the residuals of *d_al* are removed, seasonal signals are significant for both inshore and offshore larvae on both the NJ and DMV shelves, but with a phase difference from inshore to offshore. For example, inshore NJ larvae experience the maximum southwestward drifting at around August 6th whereas it is around August 24th for the offshore larvae (Fig. 3.4c). A statistically significant (p-value =7.82×10^{-5}) forward phase shift in the seasonal signal occurs for the offshore larvae relative to those inshore. A similar trend in forward phase shift from inshore to offshore larvae is also found on the DMV shelf (not shown).

3.3.3 Variation in across-shelf larval daily drifting distance

The mean along-shore surface wind stress (*wstr_al*) and the mean across-shelf larval daily drifting distance (*d_cr*) for NJ inshore larvae (depth<20m) are plotted in Figure 3.5a. The correlation between these two variables varies in time between negative and positive. A positive correlation indicates that the northward (southward) along-shore surface wind stress corresponds to inshore (offshore) larval daily drifting, whereas a negative correlation indicates that the northward (southward) along-shore surface wind stress corresponds to offshore (inshore) across-shelf larval daily drifting.

Larval vertical distribution in the water column during more stratified times, whether concentrated in the upper layer or bottom layer, is a critical factor in determining the correlation between *d_cr* and *wstr_al*. We use the water depth where the across-shelf current reverses directions (the reversing depth) as the depth separating the water column into top and bottom layers. During periods with a stratification index greater than 0.2, roughly June 16th to September 1st on the NJ shelf (Fig. 3.5, shaded period in both gray and blue) or June 11th to September 6th on the SVA shelf (Fig. 3.6, shaded period in both gray and blue), the correlation between *d_cr* and *wstr_al* is mostly negative when larvae are close to or above the reversing depth, whereas the correlation becomes positive when larvae are below the reversing depth.

For example, on the NJ shelf from June 16th until the end of July (Fig. 3.5, gray-shaded region) the mean larval depth is mostly close to or above the across-shelf current reversing depth and the correlation between *d_cr* and *wstr_al* is negative ($r = -0.64$), whereas in August (Fig. 3.5, blue-shaded region) the mean larval depth is largely below

the reversing depth and the correlation becomes positive (*r = 0.60*). On the SVA shelf from around June 11th to the end of June (Fig. 3.6, gray-shaded region) when the mean larval depth is mostly above or close to the reversing depth, the correlation between *d_cr* and *wstr_al* is negative (*r = -0.25*), whereas later in the year from July to September 7th (Fig. 3.6, blue-shaded region) when the mean larval depth is below the reversing depth, the correlation becomes positive (*r = 0.71*).

Results (*d_cr_M3*) of the linear regression model between *d_cr* and *wstr_al* (M3), with the larval vertical concentration included as a dummy variable (L_i), during the stratified season explains about 53%, 52% and 38% of the variance of the original data of *d_cr* for larvae on the NJ, DMV, and SVA shelves respectively, all with levels of high statistical significance (Table 3.2). The model shows that *d_cr* correlates negatively with *wstr_al* when larvae are in the upper layer (L_i=1) and positively with *wstr_al* when larvae are in the bottom layer (L_i=-1, Table 3.2), further confirming the importance of larval vertical distribution on larval across-shelf transport.

3.4 Discussion

3.4.1 Larval transport, settlement, and regional connectivity

A mean downstream connectivity pattern from the northeast to the southwest exists for surfclams living in the MAB and GBK (see the 2nd chapter in this thesis), yet large variations in the connectivity pattern are also observed, potentially associated with various factors such as larval spawning time and location, larval transport dynamics, planktonic life span, and location of settlement (Edwards et al., 2007). Knowledge of

connectivity is crucial for better understanding and predicting ecosystem responses to changing environment conditions (GLOBEC, 1991; Gawarkiewicz et al., 2007).

In this study, the number of released (spawned) larvae, their distribution at release, and the criteria for successful settlement are set to be invariant. Thus, variations in connectivity mainly originate from variations in larval transport and planktonic life span. As described above, larval life span is an inverse function of larval growth rate, which is mainly determined by the water temperature that the larvae experience. The combined effect of larval transport and life span determines the total larval drift from spawning to final settlement (Pineda et al., 2007), which is equivalent to the connectivity distance between release regions.

During summer, relatively longer larval along-shore drift and higher settlement rates associated with higher average temperatures experienced by the larvae (ATEL) indicate broader and more effective connections from source regions to regions downstream. In comparison, larval spawns from late spring to early summer experience relatively shorter along-shore drift and lower settlement rates due to lower ATEL, indicating lower connectivity and an increased waste of spawn at that time. Inshore releases (< 30 m) from LI, NJ, and DMV during September to early October experience higher settlement rates and shorter along-shore drift, implying increased self-recruitment for those releases. Relatively high settlement rates for releases from LI and NJ during summer and early fall indicate the importance of both regions as the larval supply sources to local and downstream regions.

High ATEL is found to be a necessary yet not sufficient condition for a high settlement rate. For example, larval releases from DMV in summer or from SVA during summer and early fall experience low settlement rates, although with high ATEL, due to the assumed high mortality of those larvae entrained into the Gulf Stream and transported into the open ocean. Studies by Hare and Cowen (1996) and Hare et al. (2002) identified a possible return path for those larvae transported into the open ocean back to the shelf via the penetration of Gulf Stream warm core rings onto the shelf. This transport mechanism, however, does not affect the surfclam connectivity pattern as almost no surfclam larvae are observed in the model to be able to get back onto the shelf shallower than 60 m within 35 days after release if they are transported off the shelf.

Results in this study show large variations in larval transport and settlement rates closely associated with environmental changes, which further cause large variations in surfclam population connectivity. For better understanding, predicting, and managing surfclam populations in response to the potential effect of climate change, the governing processes and mechanisms causing such variations in larval transport and settlement need to be distinguished.

3.4.2 Larval along-shore movement

The horizontal swimming speed of surfclam larvae is low in comparison with the horizontal velocity of the water currents; thus in the model larvae are assumed to drift passively in the horizontal direction (see the 2nd chapter in this thesis). In principle, those factors that affect the MAB horizontal current flow can be expected to affect the

horizontal movement of surfclam larvae. Observations of the along-shore current on the MAB shelf (Lentz, 2008b) show high correlation between the along-shore current and the surface wind stress at all observation sites spanning the inner, middle, and outer shelf of the MAB and southern GBK. Seasonal variation of the along-shore current was found to be mainly driven by the across-shelf density gradient, as the direction of most significant seasonal wind variation is approximately perpendicular to the direction of the wind stress that drives the along-shore current. In this study, the results show that larval along-shore movement in NJ, DMV, and SVA is highly correlated with the surface along-shore wind stress, which mostly introduces high frequency variations (periods of 2~10 days) in the along-shore daily movement of the larvae.

While the wind-induced component of larval along-shore movement does not show obvious seasonal variations in itself, significant seasonal signals are found in the residuals after the wind-induced components are removed from the larval along-shore movement for larvae in NJ and DMV. These significant seasonal signals are speculated to be associated with the variation in the across-shelf density gradient. During late summer on the NJ shelf, the pycnocline deepens. As a consequence, the more nearshore bottom waters warm up first, while the more offshore bottom waters remain colder due to along-shore "cold" pool advection (Fig. 3.7a; also (Houghton et al., 1982; Castelao et al., 2008)).

Combined with the across-shelf salinity gradient, the fresher warmer nearshore water and the saltier colder offshore water produce a large across-shelf density gradient and therefore a strong along-shore current (Lentz, 2008a). Later in the fall when the water column is well mixed on the shelf (Fig. 3.7d), the across-shelf density gradient lessens

(Gong et al., 2010). In this study, the maximum (minimum) southwestward larval drift over the seasonal cycle occurs in mid and late August (late October and early November) respectively on the NJ and DMV shelves (Fig. 3.4b for NJ; DMV not plotted), consistent with the approximate timing of a larger (smaller) across-shelf density gradient and along-shore current. This mechanism also explains the pattern of larval along-shore total transport for larvae released from the LI, NJ, and DMV inshore (<30 m) shelves. That is, those larvae released during September experience a much shorter southwestward drift compared with those released at earlier times, due to the weaker across-shelf density gradient when the water column is well mixed. These results indicate that although variation in the along-shore larval transport is dominantly a function of the wind stress, its seasonal modulation is mainly driven by the across-shelf variation in the density gradient.

The model results also show a forward phase shift of the seasonal signal from inshore (<30 m) to offshore (30~60 m) on both the NJ and DMV shelves. Lentz (2008b) found a steady phase increase with water depth of the seasonal variation of the along-shore current offshore of Cape Cod, consistent with the seasonal variation in the across-shelf temperature gradient associated with the "cold pool" development and break-down. On the NJ and DMV shelves, as the wind stress increases from summer to fall, stronger mixing causes the coastal well-mixed warmer region to expand gradually from inshore to offshore, pushing the position of the mixing front and the maximum across-shelf density gradient offshore (Fig. 3.7). Thus the inshore waters experience the maximum across-shelf density gradient and the strongest along-shore current relatively earlier than for

offshore waters, generating a forward phase shift as found in the seasonal signal of the along-shore larval drifting.

This mechanism also explains the larval total along-shore transport pattern for larvae released from NJ (Fig. 3.3). That is, the larvae released inshore begin to experience longer total along-shore drifting at an earlier time than those released offshore, as those larvae are mostly transported along the NJ or DMV shelves. This phase difference between the inshore and offshore larvae in the seasonal signal of their along-shore transport also suggests the importance of across-shelf movement of larvae permitting larvae to experience different along-shore current conditions and thus different along-shore transport and connectivity patterns.

No significant seasonal signal was found for SVA in the residuals of larval along-shore drifting distances after the wind-driven component was removed. One possibility is that the wind-driven along-shore current in SVA already has a significant seasonal variation, as the direction of the wind component that drives the along-shore current was observed to be close to the direction of the largest variation in seasonal wind and thus this wind component drives significant seasonal variation to the along-shore flow (Lentz, 2008b). In this study, the wind-induced larval along-shore drifting distances themselves have significant seasonal variations, and the removal of wind contribution from the original data also removes or reduces the seasonal signal in the residuals of larval along-shore drifting. The across-shelf density gradient off the SVA shelf also influences the along-shore current and the degree of larval along-shore drifting, but is not the main factor causing seasonal variations.

3.4.3 Larval across-shelf movement

On the MAB shelf during the stratified season, a wind-driven across-shelf circulation pattern consistent with coastal upwelling/downwelling episodes is well documented; that is, the upwelling- (downwelling-) favorable wind causes surface layer offshore (onshore) transport and bottom layer onshore (offshore) transport (Lentz, 2001; Kohut et al., 2004; Dzwonkowski et al., 2009; Gong et al., 2010). Surfclam larvae are transported passively in the horizontal direction, thus their across-shelf transport is expected to follow the across-shelf circulation. Larval vertical swimming behavior, however, is critical in determining the larval across-shelf transport pattern by modifying the larval vertical distribution relative to the reversing layer, thus exposing larvae to different across-shelf current patterns. When larvae are concentrated in the surface (bottom) layer, an upwelling-favorable wind generally causes larval offshore (onshore) movement and downwelling-favorable wind causes onshore (offshore) transport.

Larval vertical swimming behavior, as defined in the model, is mainly dependent on the water temperature and larval size (see the 2nd chapter in this thesis). Larvae tend to swim in the vertical to get close to their most suitable temperature range of ~20-21 ^{o}C, but a countervailing sinking rate also increases with increased larval size. These two factors, however, are not completely independent as the water temperature experienced by larvae also determines growth rate and hence larval size.

Here the main focus is on the effects of water temperature. The water temperature at the reversing depth where the across-shelf current reverses direction is assumed to be

the lower limit of surface water temperature, and is used as the criterion for defining surface layer temperature. The regression of the depth difference (larval depth minus the reversing depth) with the water temperature at the reversing depth shows an inverse linear relationship between these two variables for all larvae at all times within the MAB shelf (Fig. 3.8). This mean trend indicates that as the surface water temperature increases, larvae tend to be deeper in the water column relative to the reversing depth, and *vice versa*.

This regression provides a critical value of water temperature (Table 3.2), defined as the value corresponding to the zero depth difference in the regression, such that when the water temperature at the reversing depth is greater than the critical value, larvae will concentrate below the reversing depth in the bottom layer, and *vice versa.* It is worth noting, however, that water temperature not only affects larval vertical distribution in a direct way, but also in an indirect way by influencing first larval growth and hence size, and then the larval vertical position. Therefore, the relationship between larval vertical distribution and water temperature revealed by these simulations is not purely linear, and the critical value obtained here from the linear regression analysis is only a statistical estimate, not a deterministic forcing factor.

Observational studies of the vertical distribution of surfclam larvae and their across-shelf transport show different patterns between the SVA shelf (Garland and Zimmer, 2002; Garland et al., 2002; Shanks et al., 2002; Shanks et al., 2003) and the NJ shelf (Ma and Grassle, 2004; Ma, 2005; Ma et al., 2006a). Off NJ, across the LEO-15 transect in July of 1997 and 1998, surfclam larvae were observed to mainly concentrate above the thermocline and to follow the surface layer horizontal water movement, while

off SVA in August of 1994 larvae were observed to mainly concentrate below the thermocline and follow the bottom layer horizontal water movement.

Model results for 2006 produce the same patterns as observed for larvae on both the NJ and SVA shelves in the same months (Fig. 3.5, 3.6). One possible mechanism in causing such differences in vertical distribution and across-shelf movement is the water temperature at the reversing depth. Model results show that the mean water temperature at the reversing depth on the NJ shelf in July of 2006 was around 17 ^{o}C, a value lower than the critical value of water temperature of 19.0 ^{o}C (Table 3.2), and accordingly larvae were mostly found close to or above the reversing depth and observed to follow the surface layer across-shelf water movement.

Off SVA in August of 2006, the mean water temperature at the reversing depth was around 22 ^{o}C, higher than the critical value, and as a result larvae were mostly found below the reversing depth and observed to follow the bottom layer across-shelf flow. In the observational studies, the thermocline temperature on the NJ shelf in mid-July of 1998 was around 16 ^{o}C (Ma et al., 2006a), lower than the critical value, and larvae congregated in the surface layer, whereas the temperature of the thermocline off SVA in late August of 1994 was around 18.5~22 ^{o}C (Austin, 1999; Garland et al., 2002; Shanks et al., 2002; Shanks et al., 2003), close to or higher than the critical value, and larvae were observed to congregate in the bottom layer.

Thus, the cause of the difference in the vertical distribution of surfclam larvae and their across-shelf transport pattern between larvae off NJ and SVA is likely differences in water temperature at the reversing depth. The critical value is 19 ^{o}C from the modeling

results instead of 21 ^{o}C as described in the larval model in chapter 2. This is the result from the combined effects of larval swimming and sinking behaviors. Larval swimming behavior is defined to be able to enable larvae to swim close to 21 ^{o}C, their most suitable temperature, but larval sinking behavior decreases the mean larval depth so that 19 ^{o}C becomes the critical value.

Analysis of model results show that about 60.7%, 69.4% and 77.2% of surfclam larvae released off NJ, DMV, and SVA shelves respectively are below the reversing depth when the water column is stratified. In the summer months (June-August) when upwelling-favorable winds generally dominate, larvae on the NJ, DMV, and SVA shelves mostly experience onshore transport. This also explains the previous finding that, for larvae released from NJ, which are mainly transported along the NJ and DMV shelves, and larvae released from DMV, which are mainly transported along the DMV and SVA shelves, a total larval transport in the onshore direction is more prevalent (Fig. 3.3k, l).

3.5 Summary

In this study, a physical circulation model covering the Middle Atlantic Bight, Georges Bank and Gulf of Maine was coupled to a surfclam larval model to investigate variations in larval transport and settlement in 2006, and also to investigate the primary physical mechanisms causing such variations. Model results show that the highest larval settlement rate occurs when larvae are released during July to early October, corresponding to higher average temperatures experienced by the larvae (ATEL).

Larval along-shore transport exhibits a mean downstream pattern following the mean coastal current from the northeast to the southwest, with the maximum southwestward transport occurring for the August releases. Most high-frequency (periods of 2~10 days) variations in along-shore larval transport were associated with changes in the along-shore surface wind stress, whereas the seasonal variation seems to be mainly driven by changes in the across-shelf density gradient. A forward phase shift in the seasonal signal was observed to occur from inshore to offshore larvae, with the offshore larvae experiencing maximum southwestward along-shore drift later than the inshore larvae by around 20 days. This result indicates the importance of larval across-shelf movement in affecting the larval along-shore transport and connectivity pattern.

In the across-shelf direction, larvae released from the New Jersey, Delmarva and South Virginia shelves mostly experience onshore transport during the summer months when upwelling-favorable winds dominate. This is consistent with another finding that most surfclam larvae are found in the bottom layer most of time during the summer-stratified season, following the onshore water movement generated by upwelling-favorable wind forcing. Two mutually dependent factors, water temperature and larval size, affect the larval vertical distribution through their influence on larval vertical swimming and sinking behaviors. Statistical estimates based on all larvae released within the Middle Atlantic Bight shelf during the stratified season show a critical value of water temperature at 19.0 ^{o}C, such that when the water temperature at the thermocline is above this critical value, surfclam larvae tend to escape the warm surface layer to concentrate below the thermocline and follow the bottom layer across-shelf movement, and *vice versa*.

These results are consistent with observations of larvae on the New Jersey (NJ) and South Virginia (SVA) shelves in their vertical distribution and across-shelf movement patterns. This critical value theory of water temperature also successfully explains the observed difference in larval vertical distribution and across-shelf movement patterns between larvae observed on the NJ shelf in July of 1997 and 1998, where surfclam larvae were found close to or above the thermocline in the vertical and follow the surface layer across-shelf movement, and on the SVA shelf in August of 1994, where surfclam larvae were observed to be mostly below the thermocline and therefore to follow the bottom layer across-shelf movement.

This confirms the importance of water temperature not only in determining surfclam larval settlement rate but also in affecting their vertical distribution, across-shelf transport, and also along-shore transport. All these results provide an important insight into the general mechanism of how physical environmental factors interact with the biological behavior to influence larval transport, population connectivity, and population dynamics, while also providing a mechanism by which climate variability and change may significantly impact benthic species and coastal ecosystems.

Table 3.1 Linear regression and seasonal models of along-shore larval daily drifting distances

Regions	Linear regression model (M1) [a]					Seasonal model (M2) [b]			
	Correlation coefficient [c]	Model parameters ± 95% confidence intervals		$\frac{Var(M1)}{Var(d\_al)}$	p-value	Model parameters ± 95% confidence intervals		$\frac{Var(M2)}{Var(d\_al)}$	p-value
		Intercept (*B1*)	Coefficient (*B2*)			Amplitude (*A*, in km)	Period (*T*, in days)		
NJ shelf	0.60	-4.45 ± 0.70	95.39 ± 19.74	0.357	$<10^{-10}$	4.21 ± 0.74	147.4 ± 12.45	0.282	$<10^{-10}$
DMV shelf	0.65	-6.36 ± 0.93	143.40 ± 25.74	0.419	$<10^{-10}$	3.50 ± 1.17	159.2 ± 32.93	0.101	5.77×10^{-7}
NC shelf	0.61	-6.29 ± 1.03	130.07 ± 25.63	0.373	$<10^{-10}$	1.81 ± 0.88	174.7 ± 50.25	0.036	0.1007

a) Linear regression models (M1: ***d_al_m1 = B1 + B2 * wstr_al***) between along-shore larval daily drifting distances (*d_al*) and along-shore surface wind stress (*wstr_al*) for larvae in different regions,

b) Seasonal models (M2: ***d_al_m2 = A*sin(2*pi/T * t)***) of the linear regression model residuals (*res = d_al – d_al_m1*) with time (*t*, in days), using the least-squares best fit.

c) Correlation between the along-shore larval daily drifting distances and the along-shore wind stress in different regions.

d) Variables included: *wstr_al*, along-shore wind stress; *d_al_m1*, along-shore larval daily drifting distances simulated by linear regression models; *d_al_m2*, along-shore larval daily drifting distances simulated by seasonal models; *T*, seasonal cycle period; *t*, days in the year.

Table 3.2 The 2-layer linear regression model (M3) of across-shelf larval daily drifting distances with the mean along-shore surface wind stress

Regions	Model expressions (M3) [a]	$Var\_ratio = \frac{Var(M3)}{Var(d\_cr)}$	p-value	Critical water temperature [b] (^oC)
NJ shelf	$d\_cr\_M3 = 0.44 - 35.60*wstr\_al - 38.68 * L_i * wstr\_al$	0.53	$<1x10^{-10}$	
DMV shelf	$d\_cr\_M3 = -0.11 + 5.36*wstr\_al - 28.42 * L_i * wstr\_al$	0.52	$<1x10^{-10}$	19.0
SVA shelf	$d\_cr\_M3 = -0.31 + 2.66*wstr\_al - 40.89 * L_i * wstr\_al$	0.38	$<1x10^{-10}$	

a) The 2-layer linear regression model (M3) between the mean across-shelf larval daily drifting distances (*d_cr*) and the mean along-shore surface wind stress (*wstr_al*) for larvae in inshore waters (depth < 20 m) on different shelf regions. The linear regression model equations have different coefficient values. L_i is the dummy variable indicating whether larvae are located in the upper layer or bottom layer. L_i = 1 when larvae are in the upper layer, or the larval depth is shallower than the across-shelf current reversing depth, while L_i = -1 when larvae are in the bottom layer, or the larval depth is deeper than the across-shelf current revering depth;

b) The water temperature at the across-shelf current reversing depth.

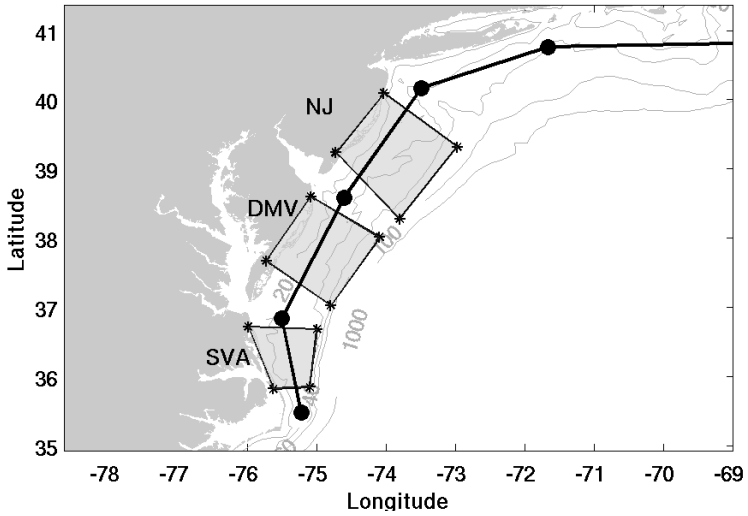

Figure 3.1 Map of the arbitrarily chosen NJ, DMV, and SVA shelf regions (as shaded) for the analysis of variation in the along-shore and across-shelf larval daily movement. These regions cover the corresponding shelves from the coast to at least 60-m isobath. The black-dot-line indicates the approximate along-shore direction, which is used as the reference line relative to which the along-shore and across-shelf daily drifting distances and along-shore and across-shelf wind stresses are calculated. The 20-, 40-, 60-, 100- and 1000-m isobaths are shown in gray lines.

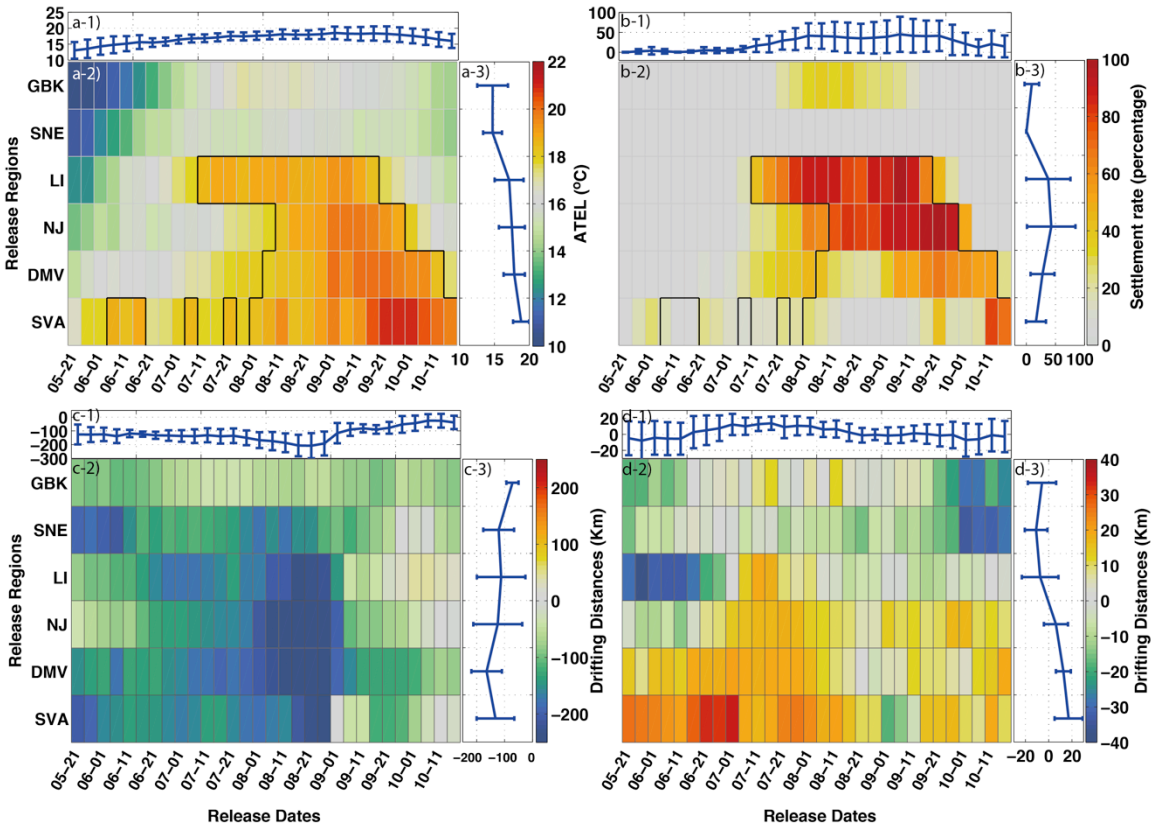

Figure 3.2 Intra-annual and spatial variations of ATEL (in ^{o}C, Panel a-2), larval settlement rate (in percentage, Panel b-2), along-shore larval drifting distances (in kms, positive values indicate along-shore southwestward drifting, Panel c-2) and across-shelf larval drifting distances (in kms, positive values indicate onshore drifting, Panel d-2) for larvae released from different regions at different times in 2006. Inside those panels, the x-axis indicates different release times, the y-axis indicates different release regions, and the colorbar on the right indicates the values of each variable. The black lines in panels a-2 and b-2 enclose those larval releases with ATEL higher than 18 ^{o}C. Inside panels of a-1, b-1, c-1 and d-1, the curves show the mean of each variable among releases from all regions at each release time (+/- standard deviation), while inside panels of a-3, b-3, c-3 and d-3, the curves show the mean among releases at all times from each region (+/- standard deviation).

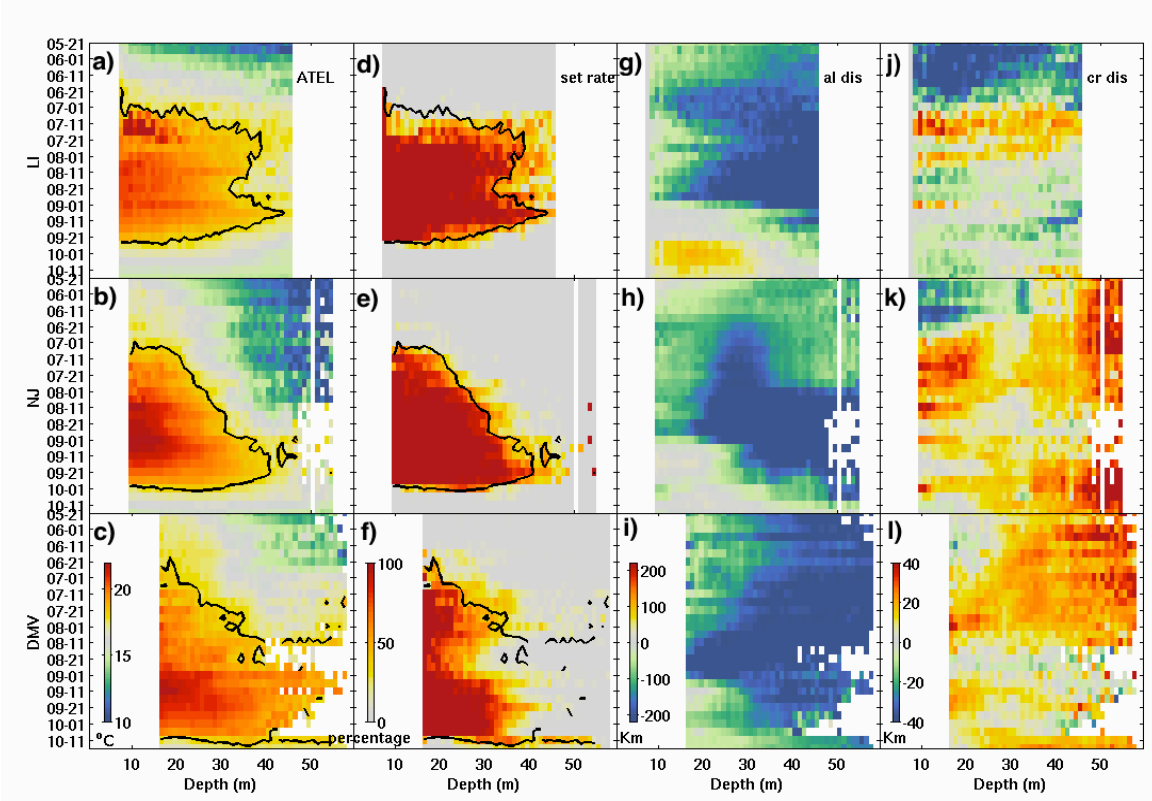

Figure 3.3 Intra-annual and across-shelf variations of ATEL (in ^{o}C, panel a, b, c), larval settlement rate (in percentage, panel d, e, f), mean along-shore larval drifting distances (in kms, positive values indicate along-shore southwestward drifting, panel g, h, i) and mean across-shelf larval drifting distances (in kms, positive values indicate onshore drifting, panel j, k, l) for larvae released in 2006 from different depths in regions of LI (panel a, d, g, j), NJ (panel b, e, h, k), and DMV (panel c, f, i, l). The x-axis shows the across-shelf depth ranges for each 1-m interval, and the y-axis shows the different release times from May 21st to October 16th in 2006. The black lines in the left two columns of panels (panel a-f) indicate the 18 ^{o}C ATEL contour line, enclosing those larval releases with ATEL higher than 18 ^{o}C.

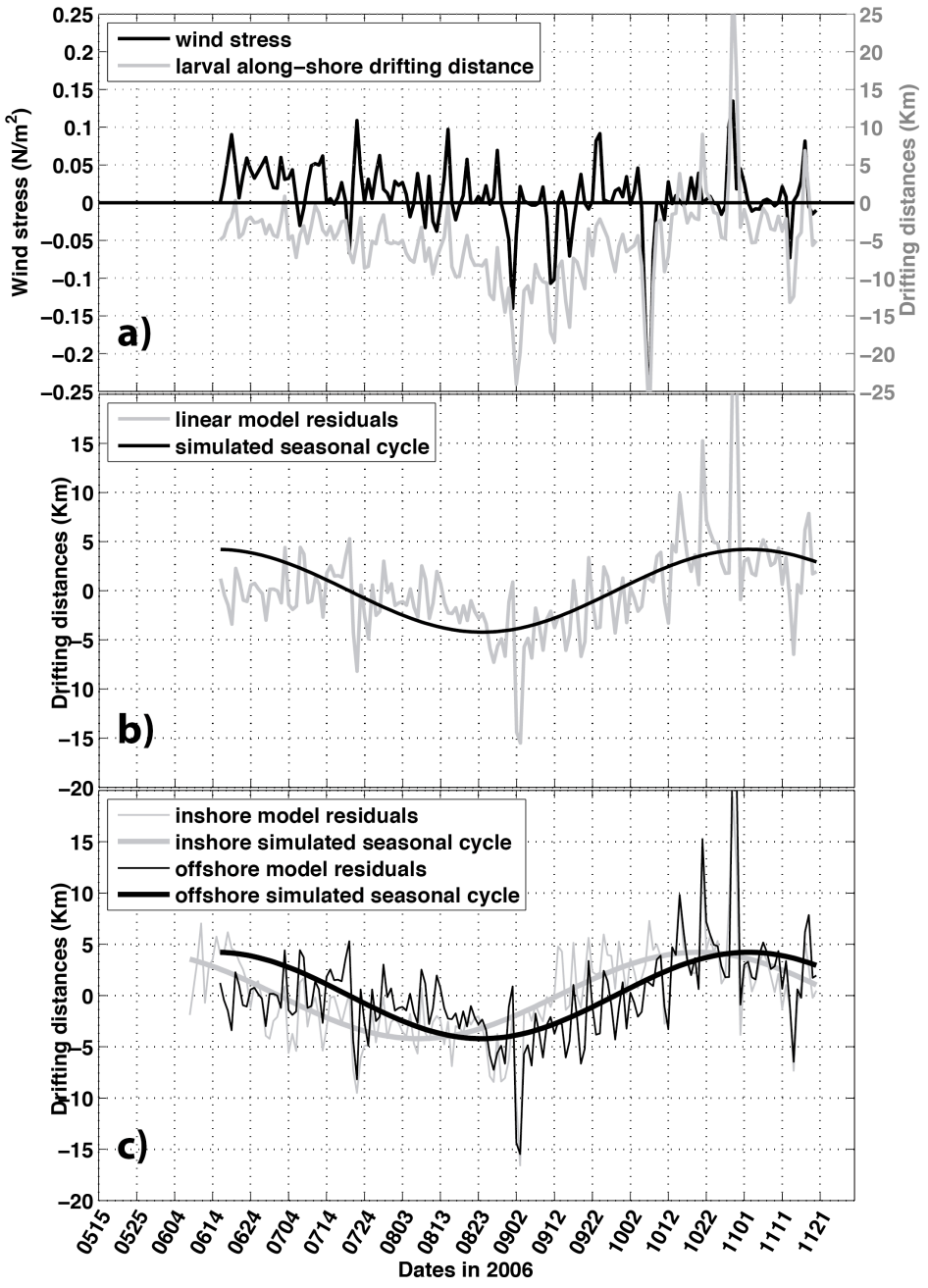

Figure 3.4 **Panel a:** Plots of temporal variations of the along-shore surface wind stress (*wstr_al*, in black line) and along-shore larval drifting distances (*d_al*, in gray line) for larvae off NJ. **Panel b:** Plots of the linear model residuals with the wind-induced component removed (*res*, in gray line) and the simulated seasonal cycle signal (*d_al_m2*, in black line), for larvae off NJ. **Panel c:** Similar to panel c, the linear model residuals (*r*,

in thin lines) and the simulated seasonal cycle signal (*d_al_m2*, in thick lines), respectively for inshore NJ larvae (0~30 m, in gray lines) and offshore NJ larvae (30~60 m, in black lines).

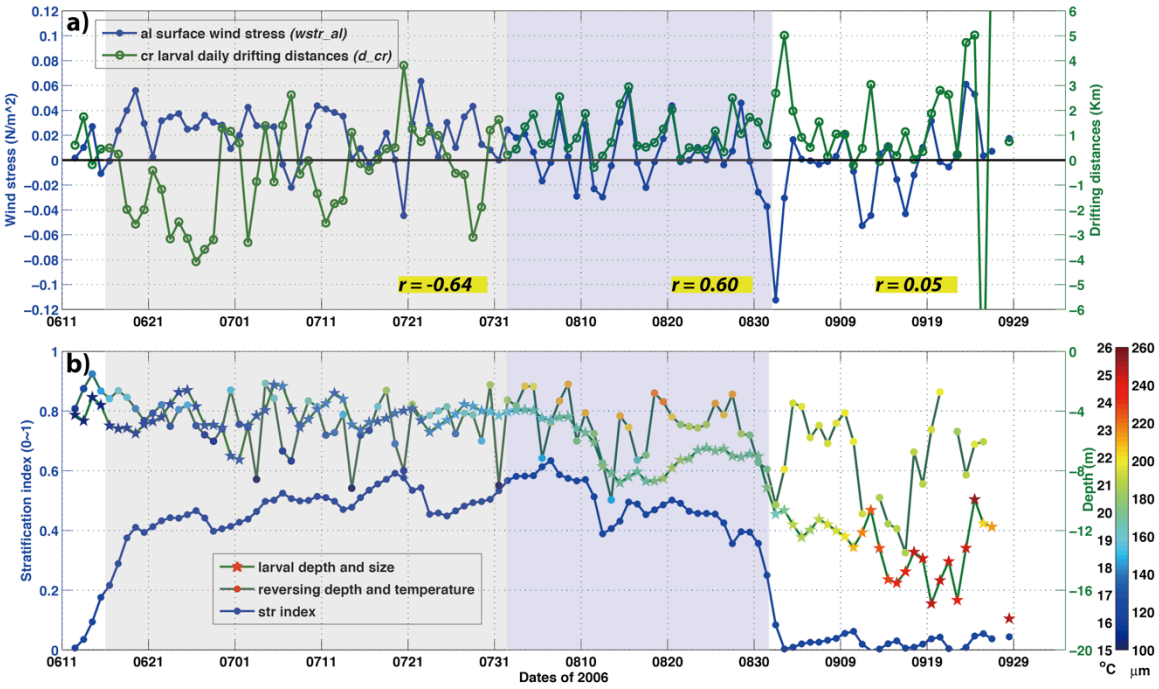

Figure 3.5 **Panel a:** Temporal variations of the mean along-shore surface wind stress (*wstr_al*, in N*m^{-2}, blue line) and across-shelf daily larval drifting distances (*d_cr*, in kms, green line) for larvae on the **New Jersey (NJ)** inshore shelf (depth < 20 m, Fig. 3.1). The x-axis indicates the actual dates in 2006 (note: these dates are not the release dates used in previously), the left y-axis in blue indicates the values of along-shore surface wind stress (in N*m^{-2}), and the right y-axis in green indicates the values of across-shelf daily larval drifting distances (in kms). The shaded region in either gray or blue indicates the period when the stratification index is > 0.2 (see panel b), with the gray portion indicating the period when the mean larval depth is shallower or close to the reversing depth, and blue portion indicating the period when the mean larval depth is deeper than the reversing depth. Yellow highlighted text labels the correlation coefficients between *d_cr* and *wstr_al* within each period. **Panel b**: Temporal variations of the mean larval depth (in meters, green line with colored stars), mean across-shelf current reversing depth (in meters, green line with colored dots) and mean water stratification index (in values

between 0 and 1, blue dotted line) for larvae on the **New Jersey (NJ)** inshore shelf (depth < 20 m, Fig. 3.1). The x-axis indicates the actual dates in 2006, the left y-axis in blue color indicates the values of the water stratification index and the right y-axis in green indicates the values of both the reversing depth and larval depth. The colored dots along the mean reversing depth curve indicate the mean water temperatures (in ^{o}C) at those depths, scaled by the colorbar on the right (see the labels on the left of colorbar). The colored stars along the mean larval depth curve indicate the water temperature at those depths, also scaled by the colorbar on the right (see labels on the right of the colorbar). The gray and blue shading has the same meaning as panel a.

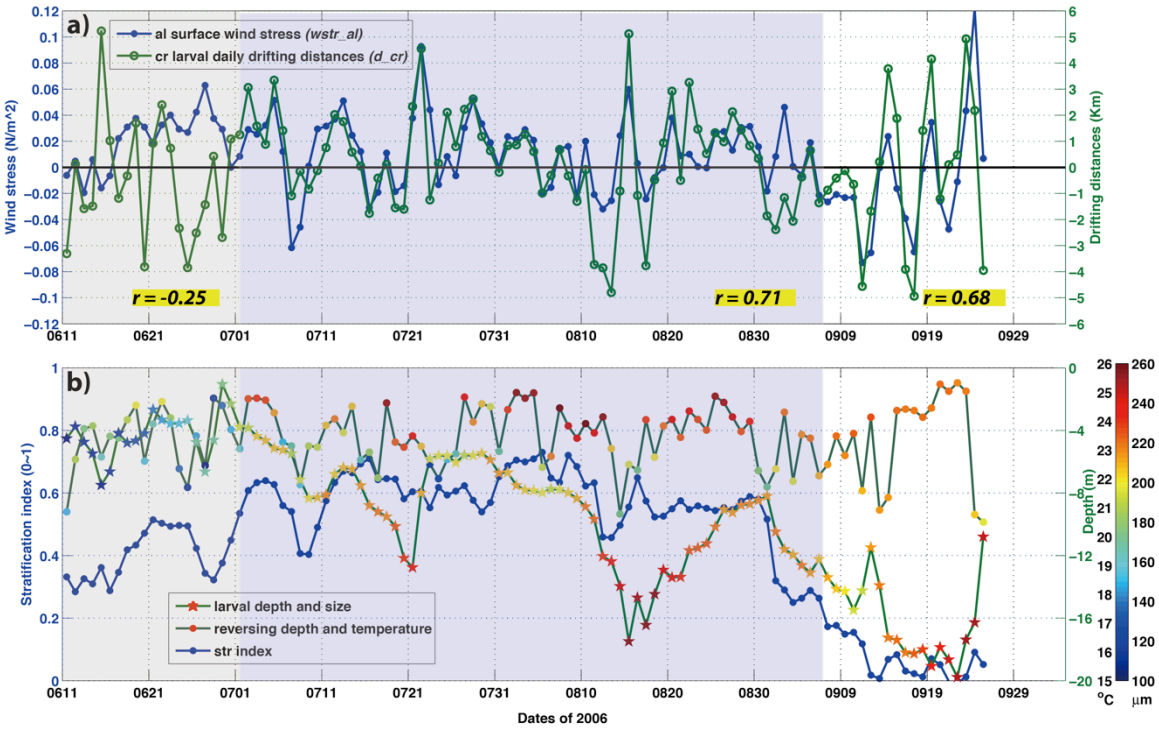

Figure 3.6 **Panel a:** Temporal variations of the mean along-shore surface wind stress (*wstr_al*, in N*m^{-2}, blue line) and across-shelf daily larval drifting distances (*d_cr*, in kms, green line) for larvae on the **South Virginia (SVA)** inshore shelf (depth < 20 m, Fig. 3.1). The x-axis indicates the actual dates in 2006 (note: these dates are not the release dates used previously), the left y-axis in blue indicates the values of along-shore surface wind stress (in N*m^{-2}), and the right y-axis in green indicates the values of across-shelf daily larval drifting distances (in kms). The shaded region in either gray or blue indicates the period when the stratification index is > 0.2 (see panel b), with the gray portion indicating the period when the mean larval depth is shallower or close to the reversing depth, and blue portion indicating the period when the mean larval depth is deeper than the reversing depth. Yellow highlighted text labels the correlation coefficients between *d_cr* and *wstr_al* within each period. **Panel b**: Temporal variations of the mean larval depth (in meters, green line with colored stars), mean across-shelf current reversing depth

(in meters, green line with colored dots), and mean water stratification index (in values between 0 and 1, blue dotted line) for larvae on the **South Virginia (SVA)** inshore shelf (depth < 20 m, Fig. 3.1). The x-axis indicates the actual dates in 2006, the left y-axis in blue color indicates the values of the water stratification index, and the right y-axis in green indicates the values of both the reversing depth and larval depth. The colored dots along the mean reversing depth curve indicate the mean water temperatures (in ^{o}C) at those depths, scaled by the colorbar on the right (see the labels on the left of colorbar). The colored stars along the mean larval depth curve indicate the water temperature at those depths, also scaled by the colorbar on the right (see labels on the right of the colorbar). The gray and blue shading has the same meaning as panel a.

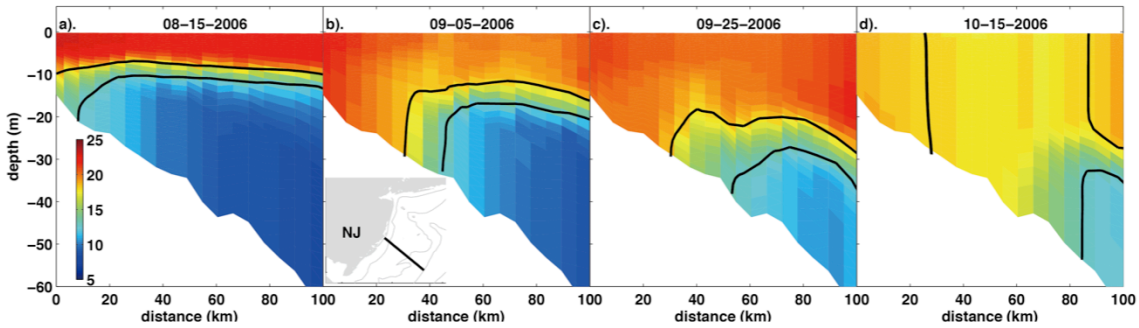

Figure 3.7 The offshore progression of the mixing front on the NJ shelf from Aug. 15th (panel a) to Sep. 5th (panel b), Sep. 25th (panel c) and Oct. 15th (panel d) in 2006. The across-shelf temperature is indicated by the colorbar down the left corner of panel a. X-axis indicates the across-shelf distances in kms from the coast. Y-axis indicates the water depth in meters. The black lines inside each panel indicate the 18 ^{o}C (above one) and 13 ^{o}C (below one) isotherm lines. The black line in the inset panel, bottom left of panel b, shows the locations of the NJ across-shelf transect shown in this figure.

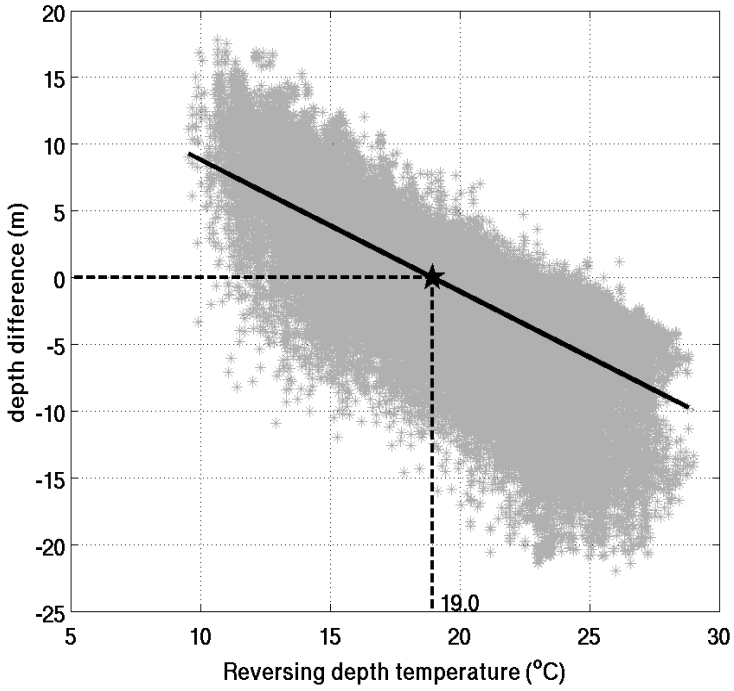

Figure 3.8 Depth difference (larval depth minus the across-shelf current reversing depth, in m, y-axis) versus water temperature at the reversing depth (in ^{o}C, x-axis) for larvae within MAB (NJ, DMV, and SVA). The black line indicates the linear regression between these two variables. Positive values along the y-axis indicate that the larvae are above the reversing depth in the upper layer, while negative values indicate that the larvae are below in the bottom layer. The black star indicates the point of depth difference being zero, and the corresponding water temperature at reversing depth (critical water temperature), as also shown in Table 3.2.

CHAPTER 4. MEAN AND SEASONAL HEAT BUDGET IN THE MIDDLE ATLANTIC BIGHT AND ASSOCIATED PHYSICAL MECHANISMS

4.1 Introduction

The Middle Atlantic Bight (MAB) refers to the continental shelf off the northeastern United States coast bounded by Cape Hatteras, North Carolina to the south and Cape Cod, Massachusetts to the north, and ranging from the coast to around the 100 m isobath shelf break (Beardsley and Boicourt, 1981). It is a biologically productive region, being habitat for many species from invertebrates to marine fish (Council, 2005). In the previous two chapters, we introduced the Atlantic surfclam, *Spisula solidiss*ima, and showed that variations in the MAB physical environment play an important role in affecting its larval transport and connectivity.

Among the physical environmental drivers, shelf water temperature and its variation have been shown in many studies to influence the local ecosystem and marine species in the MAB (Szedlmayer et al., 1992; Rose, 2005; Manderson, 2008; Nye et al., 2009) (also see the 2nd chapter in this thesis). The shelf water temperature in the MAB displays large seasonal variation (Bigelow, 1933) and also a long-term warming trend over the past 100 years (Shearman and Lentz, 2010). Generally, the surface air-sea net heat flux is thought to be the dominant factor in determining the water temperature variation, with solar heat input warming the ocean in spring and summer, and latent and sensible heat losses cooling the water column during fall and winter (Austin, 1999; Austin and Lentz, 1999; Lentz et al., 2003; Lentz, 2010; Lentz et al., 2010).

The long-term mean surface heat flux over the MAB shelf is positive with a magnitude of about 10 W m^{-2}, indicating a net warming effect to the shelf water (Beardsley and Boicourt, 1981; Joyce, 1987). However, the observed long-term shelf water temperature increase is much less than that indicated by the surface heat flux net

warming. Thus there has to be some lateral process in the ocean to cool down the water column and balance the heat budget (Lentz, 2010).

Observational studies show that in the MAB the near-surface water temperature responds primarily to the seasonal cycle of surface heating/cooling, while the deep waters are primarily influenced by advection of cold waters from the cold pool in the north during spring/summer and by vertical mixing during fall (Houghton et al., 1982; Castelao et al., 2008). Shearman and Lentz (2010) found that the along-shore transport mechanism associated with the mean coastal current system running from Labrador in the north to Cape Hatteras in the south is the main factor controlling the MAB long-term (>100 years) temperature changes, not the local air-sea heat exchange. All of these studies support the conclusion that horizontal heat advection also plays a role in water temperature variations in the MAB.

Lentz (2010) investigated the contribution of along-isobath heat advection resulting from the mean, barotropic along-isobath flow acting on the mean, depth-averaged along-isobath temperature gradient, and found that it balanced the mean surface heat flux estimated from a 50-yr National Center for Environmental Prediction (NCEP) reanalysis product, but was too large to balance the mean surface heat flux estimated from the Objectively Analyzed Air-Sea Fluxes (OAFlux) product spanning 1984-2004. The latter result suggests a potential across-shore heat flux convergence to complete the heat balance.

Across-shore heat advection is known to be one important source of cooling/warming through the coastal upwelling/downwelling mechanism, transporting

warm surface water offshore/inshore, and cold bottom water inshore/offshore (Lentz, 1987; Dever and Lentz, 1994; Austin, 1999; Fewings and Lentz, 2011). However, there is also another source of across-shore heat advection, which is due to the mean, barotropic across-isobath flow acting on the mean, depth-averaged across-isobath temperature gradient. This component of the heat budget has rarely been examined before.

The main objectives of this study are, first, to determine which term(s) in the heat budget control the MAB water temperature variation, and, second, to examine the underlying physical mechanisms over various time scales from days and weeks to years. Lastly, the along-shore and across-shore components of the horizontal heat advection will be examined and their relative contributions to the total heat budget compared.

In the following, section 4.2 will introduce the implementation of the physical circulation model, including the methods used in computing different heat budget terms and in separating horizontal heat advection into both its along-shore and across-shore components. Section 4.3 will show the results of the mean and seasonal variations of the different budget terms, and examine their relative importance. Summary and discussion of results will be given in sections 4.4 and 4.5.

4.2 Methods

4.2.1 Model configuration

As introduced in Chapter 2, a physical circulation model (hereafter called MABGOM) incorporating the Middle Atlantic Bight, Georges Bank and the Gulf of Maine has been implemented based on the Regional Ocean Modeling System (ROMS,

www.myroms.org). ROMS is a free-surface, terrain-following, primitive equation ocean model widely used by the scientific community for various both coastal and deep ocean applications (Budgell, 2005; Warner et al., 2005; Zhang et al., 2009; Aristizabal and Chant, 2013). In this study, the model domain encompasses the U.S northeastern coast, bounded by Cape Hatteras, NC to the southwest and Nova Scotia, Canada to the northeast, covering shelves of South Virginia (SVA), Delmarva (DMV), New Jersey (NJ), Long Island (LI), South New England (SNE) and Georges Bank (GBK) (Fig. 1.1). The resulting computational grid has a horizontal resolution of 8~12 km and 36 layers in the vertical.

Following Chen and He (2010), MABGOM was forced on its lateral open boundaries by another global ocean circulation model HYCOM/NCODA (Bleck, 2002), which provides boundary and initial conditions for temperature, salinity, barotropic and baroclinic velocities. Net biases in temperature and salinity were found in the HYCOM mean field inside MABGOM when compared with the long-term mean climatology temperature/salinity data (Fleming and Wilkin, 2010), and corrected HYCOM boundary data were used to force MABGOM (see the 2nd chapter in this thesis for more details). Chapman (1985) and Flather (1976) open boundary conditions are applied on the model boundaries for sea level elevation and the barotropic component of velocity respectively. Sea level elevation was forced by tidal harmonic variability (seven components: K1, O1, Q1, M2, S2, N2, K2) extracted from a regional advanced circulation model for oceanic, coastal and estuarine waters (ADCIRC) simulation (Mukai et al., 2002).

Surface atmospheric forcing was applied via bulk formulas (Fairall et al., 2003), using ocean boundary layer winds, temperature, humidity, and air pressure from National

Centers for Environmental Prediction (NCEP) hindcast data, and ROMS sea surface temperature and currents to compute air-sea momentum and heat (sensible, latent and longwave) fluxes. A 20% positive bias in 2006 to 2009 incoming shore-wave radiation from NCEP data was found when compared with observation data (Wang et al., 2012) (see also the 2nd chapter in this thesis). Thus corrected NCEP incoming shortwave radiation with 20% reduction was used to force the model. River discharge forcing was applied through 12 rivers flowing into the model domain, with data obtained from the U.S. Geological Survey (USGS). A four-year simulation from 2006 to 2009 was conducted in association with the previous surfclam larval transport study, outputting the daily oceanic state (temperature, salinity, sea surface heights, currents, etc.) and diagnostic heat budget terms (see section 4.2.2).

4.2.2 Heat budget calculation

The ROMS model is developed based on the primitive fluid equations, conserving mass and tracers (e.g. temperature and salt) for each model grid box. ROMS on-line software computes and outputs various diagnostic terms for each grid box, including momentum balance terms, heat/salt budget terms, etc. In this study, we take advantage of this ROMS functionality to calculate the heat budget terms at each grid box in the model domain.

The heat balance equation for the whole vertical column in each grid box is indicated by equation 4.1. The 1st term represents the net heat content rate of change for the whole water column (dT/dt), the 2nd term the vertically integrated horizontal

advection (*temp_hadv*), the 3rd term the vertically integrated horizontal diffusion (*temp_hdiff*), and the 4th term the net surface heat transfer between ocean and atmosphere (*Q_net*), all in the units of $W \cdot m^{-2}$. In our model simulation, the daily averaged heat budget terms are computed and stored for year 2006 through 2009.

$$\underset{[1]}{\int_{-h}^{zeta} \frac{\partial T}{\partial t} dz} = \underset{[2]}{\int_{-h}^{zeta} -\nabla \cdot (\vec{v}T) dz} + \underset{[3]}{\int_{-h}^{zeta} A_h \cdot \nabla^2 T dz} + \underset{[4]}{Q_{net}} \tag{4.1}$$

To study the mean state of the heat balance, the four-year mean heat budget terms for each grid box were calculated and their relative magnitudes were compared. Similarly, to study the seasonal variation of these heat budget terms, their seasonal means were calculated for each season over all four years, e.g. the spring mean is the mean taken over four springs in four years.

To study the spatial variation of different heat budget terms in the along-shore and across-shore directions, the 20-m isobath along the MAB shelf, and two across-shore lines off NJ and DMV respectively were chosen (Fig. 4.1), where the four-year mean and seasonal means of different heat budget terms are computed.

4.2.3 Along/Across-shore horizontal heat advection

To examine the relative importance of the along-shore and across-shore components of horizontal heat advection, the horizontal heat advection term (2nd term in equation 4.1, *temp_hadv*) was separated into components in the along-shore and across-shore directions. Here on the NJ and DMV shelves, we define the across-shore direction

to be along the chosen across-shore sections (purple lines in Fig. 4.1), while the along-shore direction is defined to be perpendicular to the across-shore profile. A new along-shore/across-shore coordinate system was established, with along-shore northeastward (x positive) and across-shore towards the shore (y positive). The separation of horizontal heat advection is shown in equation (4.2), with the 2nd term representing along-shore heat advection (*al*) and 3rd term the across-shore (*ac*).

$$\underset{[1]}{\int_{-h}^{zeta} -\nabla\cdot(\vec{v}T)dz} = \underset{[2]}{\int_{-h}^{zeta} -\frac{\partial(uT)}{\partial x}dz} + \underset{[3]}{\int_{-h}^{zeta} -\frac{\partial(vT)}{\partial y}dz} \tag{4.2}$$

Defining

$$\langle\bullet\rangle = \frac{1}{zeta+h}\int_{-h}^{zeta} \bullet\, dz \tag{4.3}$$

to be the vertical averaging operator for the whole water column in each grid box, then, we write:

$$\begin{aligned} T &= \langle T\rangle + \tilde{T} \\ u &= \langle u\rangle + \tilde{u} \\ v &= \langle v\rangle + \tilde{v} \end{aligned} \tag{4.4}$$

where $\tilde{T}$, $\tilde{U}$, $\tilde{V}$ indicate the depth-varying part of the temperature, along-shore and across-shore velocity respectively.

Inserting (4.4) into (4.2), we get:

$$\int_{-h}^{zeta} -\nabla\cdot(\vec{v}T)dz = \langle T\rangle * \int_{-h}^{zeta} -\nabla\cdot(\vec{v})dz + \int_{-h}^{zeta} -\langle u\rangle \frac{\partial\langle T\rangle}{\partial x}dz + \int_{-h}^{zeta} -\frac{\partial(\tilde{u}\tilde{T})}{\partial x}dz + \int_{-h}^{zeta} -\langle v\rangle \frac{\partial\langle T\rangle}{\partial y}dz + \int_{-h}^{zeta} -\frac{\partial(\tilde{v}\tilde{T})}{\partial y}dz \quad (4.5)$$

al_heat_bar al_heat_var ac_heat_bar ac_heat_var

Inside (4.5), the $\langle T\rangle * \int_{-h}^{zeta} -\nabla\cdot(\vec{v})dz$ term indicates the horizontal heat advection due to the horizontal volume convergence/divergence. Also,

$$\frac{d(zeta)}{dt} = \int_{-h}^{zeta} -\nabla\cdot(\vec{v})dz \quad (4.6)$$

Over a long time period, the magnitude of the mean surface height change rate is small and close to zero, as is $\int_{-h}^{zeta} -\nabla\cdot(\vec{v})dz$. Thus the long-time averaged $\langle T\rangle * \int_{-h}^{zeta} -\nabla\cdot(\vec{v})dz$ in (4.5) is also close to zero.

In this study, we examine the other terms:

$$\begin{aligned} al &= al\_heat\_bar + al\_heat\_var \\ ac &= ac\_heat\_bar + ac\_heat\_var \end{aligned} \quad (4.7)$$

where *al* and *ac* indicate corresponding along-shore and across-shore heat advection, defined as:

$$
\begin{aligned}
al\_heat\_bar &= \int_{-h}^{zeta} -\langle u\rangle \frac{\partial\langle T\rangle}{\partial x} dz = -\langle u\rangle \frac{\partial\langle T\rangle}{\partial x}(zeta+h), \\
al\_heat\_var &= \int_{-h}^{zeta} -\frac{\partial(\tilde{u}\tilde{T})}{\partial x} dz, \\
ac\_heat\_bar &= \int_{-h}^{zeta} -\langle v\rangle \frac{\partial\langle T\rangle}{\partial y} dz = -\langle v\rangle \frac{\partial\langle T\rangle}{\partial y}(zeta+h), \\
ac\_heat\_var &= \int_{-h}^{zeta} -\frac{\partial(\tilde{v}\tilde{T})}{\partial y} dz,
\end{aligned}
\tag{4.8}
$$

Here al_heat_bar and ac_heat_bar indicate the along-shore and across-shore horizontal heat advection due to horizontal depth-averaged current acting on the horizontal depth-averaged temperature gradient (hereafter referred to as "barotropic"), while al_heat_var and ac_heat_var indicate the along-shore and across-shore parts due to depth-varying currents acting on the depth-varying temperature ("baroclinic"). Their means and seasonal variation will be examined on the NJ and DMV shelves.

4.3 Results

4.3.1 Mean heat balance

4.3.1.1 Spatial variation

On average within 4 years (2006-2009), for the whole water column integrated from the surface to the bottom, the net surface heat input (*Q_net*) generally balances the horizontal heat advection (*temp_hadv*) on the shelf (Fig. 4.2a, b). Horizontal diffusion (*temp_hdiff*) is only significant around the shelf break and the edge of Georges Bank where the bathymetric change is sharp (Fig. 4.2c). The vertically integrated vertical advection ($\int -\nabla_v \cdot (vT) dz$) and vertical diffusion ($\int A_v \cdot \nabla_v^2 (T) dz$) do not input or output

heat to the water column as a whole (not shown here), although they do play important roles in the vertical heat transfer within the water column. The net heat change (*dT/dt*) in the water column during the four years (2006-2009) is small (<10 $W \cdot m^{-2}$), equivalent to small net water temperature changes within these four years (Fig. 4.2d). The regions of DMV, SNE and GBK have the largest magnitudes of *Q_net* and *temp_hadv*, but still nearly zero net *dT/dt* after balancing with each other.

Along the 20 m isobath in the along-shore direction (Fig. 4.3), the long-term mean of the net surface heat input (*Q_net*) and the horizontal heat advection (*temp_hadv*) generally balance each other. Their magnitudes are larger in the SNE and SVA regions compared with those at other regions (DMV, NJ, LI). In comparison, the horizontal diffusion (*temp_hdiff*) term along the 20-m isobath is much smaller in magnitude in all regions.

The difference between the NJ inshore and offshore regions in the four-year mean heat budget terms is not evident (Fig. 4.4, upper panel), with net surface heat input balancing horizontal heat advection, and horizontal heat diffusion much smaller in magnitude. The same also applies on the Delmarva shelf (Fig. 4.4, lower panel), except that the horizontal heat diffusion has a larger magnitude in the offshore region close to 50m~60m isobaths where the bathymetry changes are sharp.

4.3.1.2 Horizontal advection components

Following the method introduced in section 4.2.3, the horizontal heat advection term was separated into its along-shore (*al*) and the across-shore (*ac*) components. On

both the NJ and DMV shelves, the four-year mean state shows that the along-shore heat advection (*al*) is negative (red curves in Fig. 4.5) while the across-shore part (*ac*) is positive (blue curves in Fig. 4.5). Adding them together, the sum is largely negative (green curves in Fig. 4.5), indicating that horizontal heat advection is cooling the water column. However, the broad shaded regions in Figure 4.5 for both along-shore (red-shaded) and across-shore (blue-shaded) heat advection indicate large temporal variance; thus their means are not statistically different from zero. On both the NJ and DMV shelves, the magnitudes of both mean *al* and *ac* at inshore regions are smaller than those at offshore regions, as are their variances.

Further splitting the horizontal along-shore and across-shore heat advection into the barotropic and baroclinic parts, as described in section 4.2.3, their relative contributions may be examined. The four-year mean state (Fig. 4.6) shows that the along-shore barotropic part (*al_heat_bar*, $-\int \langle u \rangle * \partial \langle T \rangle / \partial x \, dz$) is negative and the across-shore barotropic part (*ac_heat_bar*, $-\int \langle v \rangle * \partial \langle T \rangle / \partial y \, dz$) is positive for both NJ and DMV shelves, while the along-shore baroclinic part (*al_heat_var*, $-\int \partial(\tilde{u}\tilde{T}) / \partial x dz$) is mostly positive or close to zero and the across-shore baroclinic part (*ac_heat_var*, $-\int \partial(\tilde{v}\tilde{T}) / \partial y dz$) mostly negative on both shelves.

Comparing with the previous findings of the along-shore and across-shore heat advections (*al* = *al_heat_bar* + *al_heat_var*, *ac* = *ac_heat_bar* + *ac_heat_var*), we further conclude that the along-shore barotropic part term is dominant among the along-shore terms and outweighs *al_heat_var* to make the four-year mean *al* negative, while the

ac_heat_bar term dominates and outweighs *al_heat_var* to make *ac* positive. On both the NJ and DMV shelves, the magnitudes of *al_heat_bar* and *ac_heat_bar* at offshore regions are larger than those at inshore regions, indicating larger influences of horizontal barotropic currents acting on the depth-averaged temperature gradient at offshore regions.

4.3.2 Seasonal variation

The MAB and GBK water columns warm in both spring and summer, mostly due to the contribution of increased net heat flux from the atmosphere into the ocean (Fig. 4.7). During fall and winter, the cooling effects mainly due to the net heat flux from ocean into the air are dominant. The depth-integrated *temp_hadv* is largely negative in all seasons, indicating a net cooling effect due to horizontal advection. This cooling effect is stronger during spring and summer and weaker during fall and winter. In all four seasons, the warming or cooling of the water column is consistent with the sign of the net surface heat flux, whether it is in the direction into the ocean or out of the ocean, with the horizontal advection cooling effect only modifying the warming or cooling magnitude (Fig. 4.8).

During all four seasons along the 20 m isobath (Fig. 4.8), the negative *temp_hadv* decreases its magnitude from south to the north until SNE where it reverses to become more negative. Q_net decreases in value from south to the north until LI, and then increases going into SNE. The horizontal heat diffusion term is small during all four seasons (<10 $W \cdot m^{-2}$).

Once the horizontal heat advection is split into its along-shore and across-shore components, their seasonal variations are evident on both the New Jersey and Delmarva shelves. Off NJ (Fig. 4.9), the along-shore and across-shore heat advection terms have both smaller temporal means and variances during spring and winter when the water column is well mixed than those during summer and fall seasons when the water column is more stratified. Specifically, water stratification enhances the baroclinic horizontal heat advection, which further exhibits large temporal variation due to varying surface wind forcing. The temporal variations in offshore regions are relatively larger than those in inshore regions, indicating the potential impact of shelf break front variability.

Off Delmarva (Fig. 4.10), both the temporal mean and variation of along-shore and across-shore heat advection have larger magnitudes during summer and fall when the water column is mostly stratified than those during the spring and winter seasons when the water column is well mixed. Similar to those on the NJ shelf, the temporal variations of heat advection in the Delmarva offshore region are much larger than those in inshore regions during all seasons.

When along-shore and cross-shore advection is further split into "barotropic" (al_heat_bar , ac_heat_bar) and "baroclinic" (al_heat_var , ac_heat_var) components as described in section 4.2.3, their seasonal variations are also evident on both the NJ and DMV shelves (Fig. 4.11, 4.12). Off NJ (Fig. 4.11), during spring and winter seasons, all along-shore and across-shore heat advection terms are small with magnitudes less than 50 $W \cdot m^{-2}$, especially inshore. During summer and fall, these terms have larger magnitudes, with *al_heat_bar* being mostly negative and *ac_heat_bar*

positive. Term *al_heat_var* is mostly positive during both summer and fall, while *ac_heat_var* is mostly negative during summer and positive or close to zero during fall.

Off DMV, *al_heat_bar* is negative and *ac_heat_bar* positive during spring, summer and fall. Their magnitudes are relatively larger during summer and fall when compared with spring. Terms *al_heat_var* and *ac_heat_var* only have relatively larger magnitudes during summer, with *al_heat_var* being positive inshore and negative offshore, while *ac_heat_var* is just the opposite, being negative inshore and positive offshore. During fall, *al_heat_var* and *ac_heat_var* have relatively larger magnitudes at offshore region, with *al_heat_var* being positive and *ac_heat_var* negative.

4.4 Discussion and interpretation

4.4.1 Surface heat flux

The air-sea net heat flux is a combination of short-wave solar radiation into the ocean, long-wave radiation emission out of the ocean, and sensible and latent air-sea heat flux. The values of mean net surface heat flux on the SNE, GBK, DMV and SVA shelves are found to be relatively larger than those at the NJ and LI shelves (Fig. 4.2, 4.3). The large values of surface net heat flux into the ocean off SNE and GBK are mainly contributed by lower heat loss from sensible and latent heat flux out of ocean (Fig. 4.14).

Significant tidally induced vertical mixing off SNE and GBK is well documented (Butman and Beardsley, 1987; Townsend and Pettigrew, 1997; Wilkin, 2006) which during the summer cools down the ocean surface and warms up the ocean bottom. The weak stratification off SNE and GBK is also evident in this modeling study, again due to

strong vertical mixing, and it is enhanced during summer when most MAB shelf water is stratified yet SNE and GBK water is still well mixed (Fig. 4.13). This mechanism helps to enhance the air-sea temperature difference and reduce the surface sensible and latent heat losses.

A similar mechanism also explains the cooling along the MAB near-coast shelf during the fall season (Fig. 4.7), which is associated with mixing in the water column after the break-down of the MAB shelf thermocline, sinking the cooled surface water and raising the warm bottom water and thus enhancing the surface heat loss. In contrast, on the NJ and LI shelves where the water column is more stratified compared with SNE and GBK (Fig. 4.13), the sensible and latent heat flux and long-wave radiation have larger magnitudes, causing more heat loss from the ocean (Fig. 4.14).

Large values of mean net surface heat flux on the DMV and SVA shelves, at the southern end of the model domain, are mainly due to the large shortwave solar radiation input into the ocean (Fig. 4.14). This emphasizes the obvious importance of solar radiation in affecting the heat in the water column, and underscores an important mechanism through which climate change might affect local water temperature by modulating the surface solar radiation into the ocean. Substantial decadal changes in the surface solar radiation have been well documented (Ohmura, 2009; Wild, 2009). Besides the variation of the earth's axis position relative to the sun that causes the seasonal variation, surface solar radiation is directly related to the transparency of the atmosphere, which is further dependent on cloud cover, aerosols and radioactively active gases (Kim and Ramanathan, 2008). Under the current scenario of global climate change and increasing human effect on the global environment, the changes in these factors and

therefore in the surface solar radiation might be expected. However, long-term change in the global-mean net air–sea heat flux is hard to detect due to large uncertainties in the observational air–sea heat flux data sets (IPCC, 2013).

4.4.2 Horizontal heat advection

Results show that the long-term mean horizontal heat advection is balanced with the surface heat flux while heat diffusion is relatively small, indicating the importance of horizontal heat advection in the heat balance. In this study we have separated the horizontal heat advection into its along-shore and across-shore components, with each component further separated into two parts, one part due to the horizontal depth-averaged flow acting on the horizontal depth-averaged temperature gradient (*al_heat_bar* and *ac_heat_bar*) and another part due to depth-varying currents acting on the depth-varying temperature gradient (*al_heat_var* and *ac_heat_bar*). On the New Jersey and Delmarva shelves, along-shore heat advection (*al_heat_bar* + *al_heat_var*) is negative and across-shore (*ac_heat_bar* + *ac_heat_var*) is positive. The combined horizontal heat advection of both along-shore and across-shore components is negative, mainly contributed by the *al_heat_bar* component.

The significance of *al_heat_bar* in contributing to the negative total horizontal heat advection is consistent with one important feature in the MAB, the “cold pool”, a distinctive, bottom-trapped cold volume of water, advected from SNE along-shore downstream to the NJ and DMV shelves and causing a negative heat flux to the downstream waters. This mechanism is most significant during the spring and summer

seasons, before fall and winter when stronger vertical mixing breaks down the "cold pool" feature (Houghton et al., 1982).

Comparing *al_heat_bar* with the surface heat flux, it is found that the magnitude of *al_heat_bar* is too large to balance the surface heat flux, and the other three terms (*al_heat_var*, *ac_heat_bar*, *ac_heat_var*) are needed to exert a net warming effect to complete the balance. Of these three terms, *ac_heat_bar* is dominantly positive, indicating the across-shore heat convergence is necessary for the heat balance, which is consistent with the result in Lentz (2010) using the OAFlux product as the atmospheric forcing (see section 4.1).

It is worth noting that the atmospheric forcing used in this study, from the National Center for Environmental Prediction (NCEP), yields a different result than that obtained by Lentz (2010) using the same product. The difference might be attributed to the different temporal lengths of NCEP data used and the temporal variation of surface solar radiation. Here, only four years (2006-2009) of NECP data are used while in Lentz (2010) the 50-yr-mean (1948-2000) NCEP data was used. Decadal changes in observed surface solar radiation are substantial (Ohmura, 2009; Wild, 2009). Specifically, a decline of surface solar radiation from widespread measurements in the 1950s until the mid-1980s has been observed by many land-based sites (well known as 'global dimming') (Stanhill and Cohen, 2001; Liepert, 2002), and only a partial recovery from the 1980s onward ('brightening') (Wild et al., 2005). Thus in the 50-yr (1948-2000) NCEP mean data which assimilated the observational data and was used in (Lentz, 2010), the surface solar radiation is expected to have a larger magnitude than that in the 4-yr (2006-2009) NCEP data used in this study. It is therefore possible that in this study the surface air-sea

heat flux is not large enough to balance the horizontal heat advection, while in Lentz (2010) the surface air-sea heat flux from NCEP 50-yr data is large enough to complete the balance.

Looking at the split (barotropic and baroclinic) heat advection terms off NJ and DMV (Fig. 4.6), it was found that the large magnitude of negative *al_heat_bar* mainly contributes to the negative total horizontal heat advection. This is different from what was found off SNE during summer by Fewings and Lentz (2011), that is, the across-shore heat advection is the main part cooling the water column, indicating a small along-shelf heat flux in the heat balance.

That this difference might be attributable to innate regional differences could be tested by directly examining the same region of the SNE shelf as considered by Fewings and Lentz (2011). However oceanic data interpolation from model grid points onto the along/across-shore profiles off SNE would be needed and mass and heat balances are hard to achieve from interpolated data. Besides the regional differences, different time scales might be another factor in causing the above different conclusions. In Fewings and Lentz (2011), the time scale is from weeks to months and the time window is during summer when the wind-induced upwelling is persistently dominant. The upwelling-associated across-shore heat advection due to depth-varying currents acting on the depth-varying temperature gradients (*ac_heat_var*) should be negative with large magnitude during summer, which will be examined more in the next section, and might outweigh the along-shore heat advection. In this study, the conclusion of the importance of along-shore heat advection is based on the longer time scale of four-year (2006-2009).

4.4.3 Wind induced upwelling/downwelling effects

Water stratification not only influences the surface air-sea surface heat flux as introduced in section 4.4.1, but also affects horizontal heat advection. When the water column is stratified, the baroclinic horizontal heat advection components (*al_heat_var* and *ac_heat_var*), begin to play more important roles in transporting heat, especially on time scales of weeks to months, to the inshore direction during coastal upwelling and offshore during downwelling. One example off the NJ near-shore region (<40km across-shore distances) was shown in Figure 4.15, showing inshore (positive value) heat transport during one downwelling event (June 7th of 2006) and offshore (negative value) heat transport during one upwelling event (June 19th of 2006). This mechanism has also been well documented in many studies, and the across-shore heat transport is shown to be highly correlated with the surface wind forcing (Lentz, 1987; Dever and Lentz, 1994; Austin, 1999; Fewings and Lentz, 2011). As illustrated in Figure 4.16, because of the shallowness and relatively less significant stratification in the near-coast region comparing with the mid- and outer-shelves, the *ac_heat_var* term ($\int -\partial(\tilde{u}\tilde{T})/\partial x dz$) is negative during upwelling, and positive during downwelling.

In this study, during summers of the simulation time (2006-2009) when the water column on the NJ and DMV shelves is more stratified, *ac_heat_var* was found to be significantly negatively correlated with the surface along-shore wind stress (Fig. 4.17), especially for more inshore regions within 50 km from the coast. This explains the finding that off NJ and DMV during summer when upwelling-favorable winds prevail,

ac_heat_var is negative, especially for more near-shore regions (Fig. 4.11, 4.12). During the fall and winter seasons when the water column becomes vertically well mixed, *ac_heat_var* becomes small (Fig. 4.11, 4.12). This underscores the previous point about the difference between results in this study and Fewings and Lentz (2011) about the role of along-shore heat advection, and we further speculate that during the summer months off South New England in the Fewings and Lentz (2011) study the negative across-shore heat advection associated with the dominant coastal upwelling circulation might have been large enough to de-emphasize the role of along-shore heat advection.

4.4.4 Implications for the surfclam fishery under global warming

As shown in the previous two chapters, water temperature plays a key role in determining surfclam larval growth rates, larval duration and relative vertical position in the water column, and hence exerts an important control on surfclam larval connectivity. Average water temperature experienced by larvae during the larval stage is found to be proportional to the settlement rates, defined as the percentage of the number of settled larvae with respect to the total number released. Under a global warming scenario, increasing water temperature would be expected to increase the surfclam larval mean settlement rate, potentially helping to boost the surfclam larval settlement. However, the post-settlement process from larval settlement until larval survival into recruitment also plays an important role in determining the surfclam stock recruitment, and is influenced by the surrounding physical environment. For example, Narváez et al. (2014) show in their modeling results that under a global warming scenario surfclam biomass may decline due to high mortality from larval settlement until larval recruitment. The possible

northward range expansion of the adult population might be able to outweigh the influences of high mortality due to high bottom water temperature. However, this expansion might lag behind the range contraction of the south population boundary (Guo et al., 2005; Holt et al., 2005), thus compressing the total population range (Narváez et al., 2014).

A mean along-coast connectivity pattern from the northeast to the southwest among different surfclam subpopulations was shown in Chapters 2 and 3. Simulated surfclam larvae are generally able to drift more than 100 km along the coast southwestward during the larval life span before settlement or mortality, with large temporal and spatial variability. The length of the along-shore larval drift is a result of the combined effects of the mean along-shore current and the duration of larval stage, where larval pelagic duration is an inverse function of larval growth rate as it takes less time for larvae to reach settlement with higher growth rates. Thus the warming water temperature under global warming may be expected to increase the mean surfclam larval growth rates, and indirectly decrease the mean larval span and thereby decrease along-shore drifting distances. This anticipated result is of interest as the current population connectivity pattern might be modified, with the shorter mean along-shore southwest larval drift equivalent to a net northeast shift of surfclam populations, which might potentially serve as a fortuitous adjustment to the warming water temperature for surfclam adults on the bottom (Narváez et al., 2014).

As described in the surfclam larval model and shown in the coupled modeling results, water temperature is an important factor in determining larval vertical swimming behavior and the relative larval vertical position in the water column, thereby affecting

the larval across-shore movement pattern during different coastal across-shore circulation patterns. Under global warming, more surfclam larvae will be expected to stay below thermocline in the stratified water column according to the modeling results in chapter 3. Assuming the summer upwelling-favorable wind pattern remains dominant, surfclam larvae are expected to experience more inshore transport and an increase in the surfclam inshore population.

However, this is directly counter to what is happening – the state fishery is gone, and the inshore abundances, especially in the south, have been declining (NEFSC, 2010). This suggests the need for further research, e.g., Narváez et al. (2014), on the surfclam larval post-settlement processes, since besides larval supply and settlement, post-settlement mortality variability in response to physical environment changes and predator population changes are also potentially important factor in causing surfclam stock recruitment variations. The ocean surface wind patterns are expected to vary under climate changes, but so far the confidence is low in changes of ocean surface wind forcing due to large uncertainties in observation data sets and measures used (IPCC, 2013).

4.5 Summary

Surface air-sea heat flux and horizontal heat advection are the two most important terms in the ocean heat balance on the MAB shelf, generally balancing each other in the long-term state. This indicates that the long-term change in the MAB shelf temperature is either the result from changes in the incoming solar radiation, atmosphere transparency,

etc. which affect the net air-sea surface heat flux, or changes in the mean circulation pattern and water temperature structure which are associated with horizontal heat advection. Horizontal heat diffusion is only evident at shelf break regions with sharp bathymetry changes.

Seasonal variation in water temperature is mainly driven by the seasonally varying surface heat fluxes. Across-shore horizontal heat advection variations associated with different coastal across-shore circulation patterns generally affect water temperature variation on shorter time scales from days to weeks. This is most significant during spring and summer seasons when the MAB water column is more stratified compared with that during fall and winter. The coastal upwelling system transports warm surface water offshore and cold bottom water inshore, creating a negative heat advection flux to the inshore region and positive heat flux to the offshore, while the coastal downwelling system does the opposite.

Fluctuations of the across-shore current system are principally determined by the surface wind forcing, with time scales from days to week, with the seasonal stratification also mediating the significance of coastal across-shore circulation. The long-term variation of water temperature is most likely due to variations in along-shore heat advection, specifically, the along-shore heat advection due to the depth-averaged currents acting on the depth-averaged horizontal temperature gradient. Its importance is also consistent with the Shearman and Lentz (2010) finding that the along-shore transport mechanism associated with the mean coastal current system running from Labrador in the north to Cape Hatteras in the south is the main factor controlling the MAB long-term temperature changes. The well-known “cold pool” feature in the MAB is also important

in affecting the MAB shelf water heat budget, transporting large volume of cold bottom water alongshore southwestward during the spring and summer seasons, causing a significant negative along-shore heat advection as observed in this study.

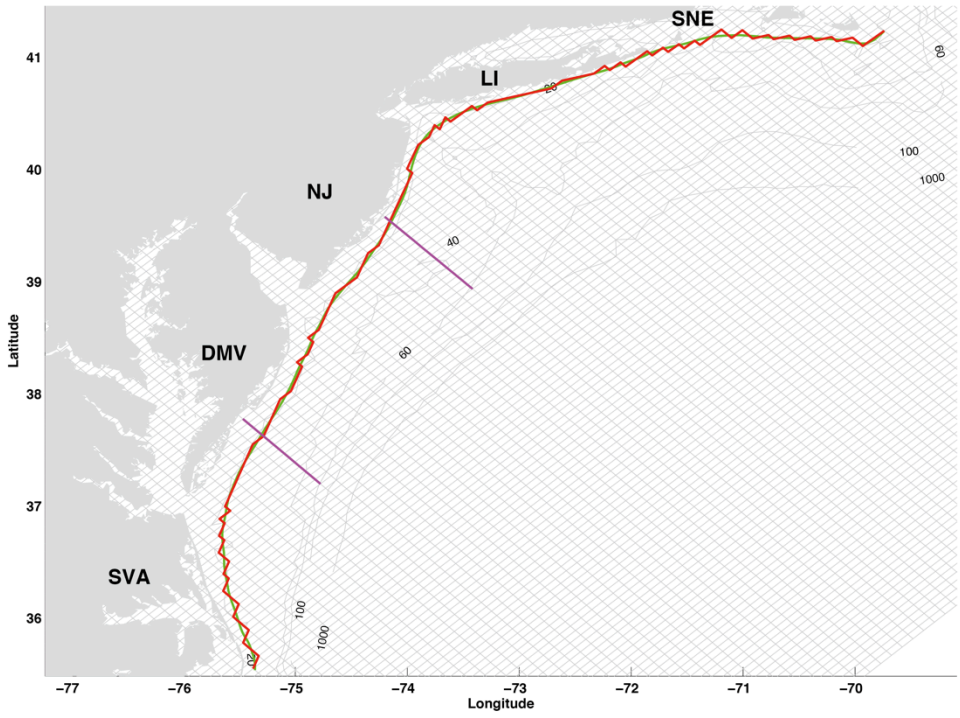

Figure 4.1 The approximate 20-m isobath position (green) and actually selected model grid points closest to the isobaths (red) are plotted in the along-shore direction. Two approximate across-shore transects off the NJ and DMV shelves are plotted in purple lines. The grey rectangles show the ROMS grid boxes, and 20-, 40-, 60-, 100- and 1000m isobaths are also shown.

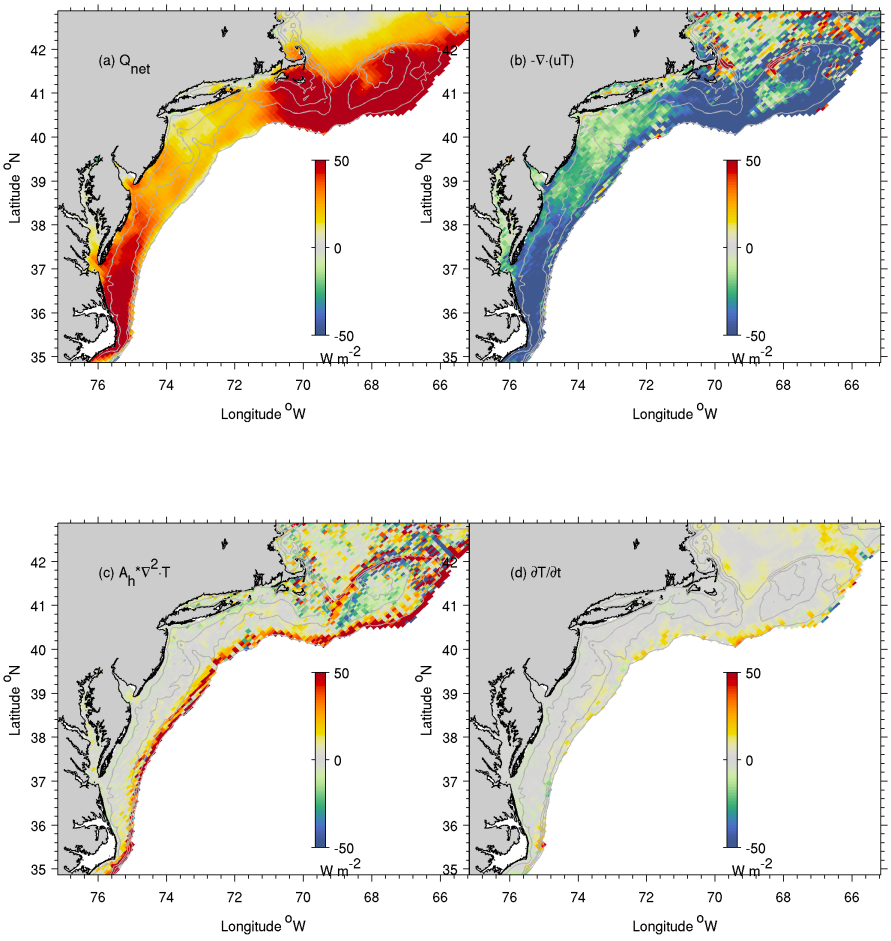

Figure 4.2 Four-year (2006-2009) mean depth integrated heat budget terms in MAB: a) *Q_net*: net heat transfer between air and ocean; b) *temp_hadv*: horizontal advection; c) *temp_hdiff:* horizontal diffusion; d) *dT/dt*: net heat content change rate.

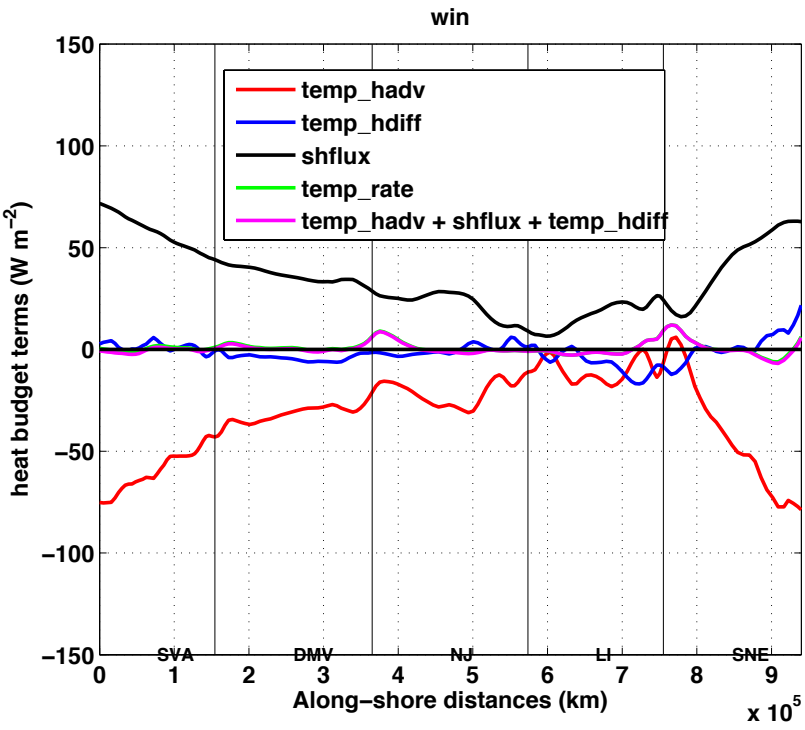

Figure 4.3 Four-year (2006-2009) mean depth-integrated heat budget terms along the 20-m isobath (see Fig. 4.1 for the exact location). Red curve indicate the horizontal heat advection term (temp_hadv), blue curve indicate the horizontal heat diffusion (temp_hdiff), black curve indicate the net surface heat flux (Q_net, or shflux), grenn curve indicate the net heat content change rate in the water column (temp_rate), purple curve indicate the combination of horizontal heat advection, horizontal heat diffusion and net surface heat flux (temp_hadv + temp_hdiff + shflux). The x-axis indicates the along-shore distance from south to the north with different regions separated by grey vertical lines. The y-axis indicates values of different heat budget terms.

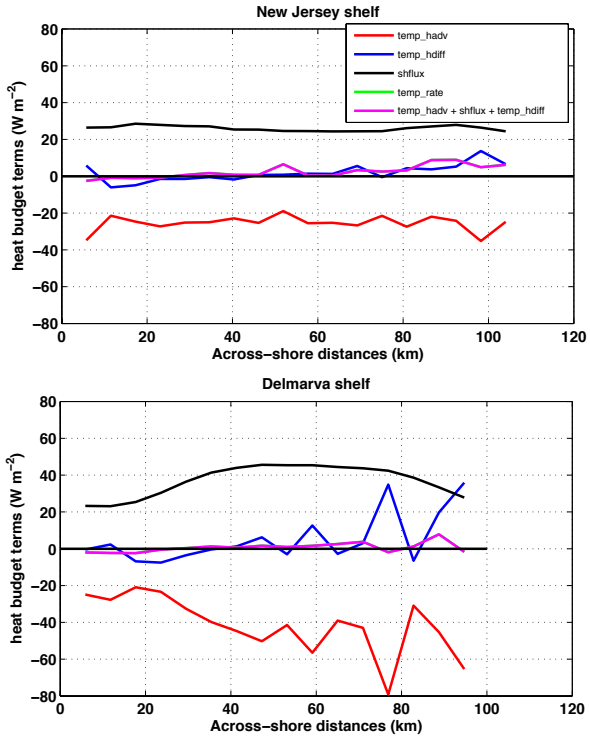

Figure 4.4 Four-year (2006-2009) mean depth-integrated heat budget terms off New Jersey (upper panel) and Delmarva (lower panel) (see Fig. 4.1 for their exact locations). Red curves indicate the horizontal heat advection term (temp_hadv), blue curves indicate the horizontal heat diffusion (temp_hdiff), black curves indicate the net surface heat flux (Q_net, or shflux), green curves indicate the net heat content change rate in the water column (temp_rate), purple curves indicate the combination of horizontal heat advection, horizontal heat diffusion and net surface heat flux (temp_hadv + temp_hdiff + shflux). The x axis indicates the across-shore distances from inshore to offshore, y axis indicates values of different heat budget terms.

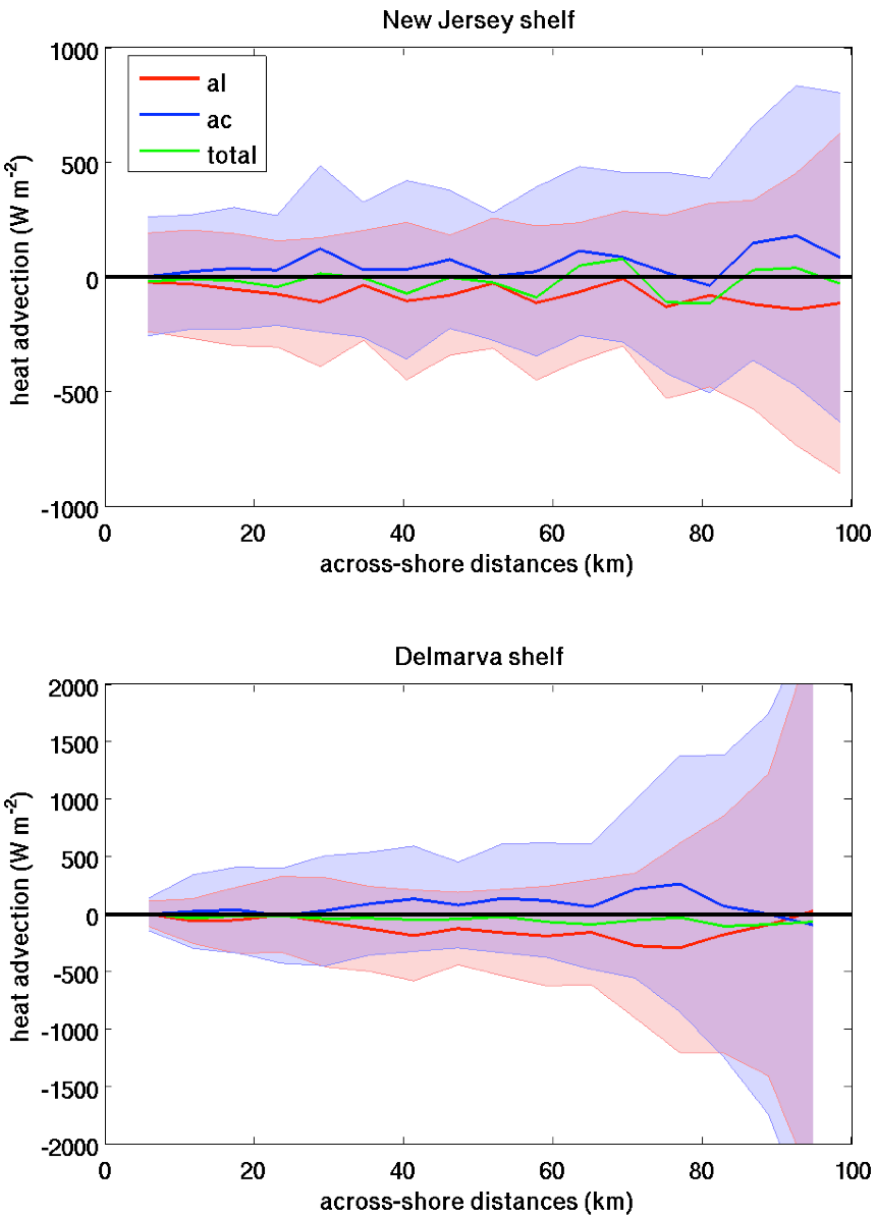

Figure 4.5 Four-year (2006-2009) mean (curves) and variation (shaded region) of along-shore (red, *al*) and across-shore (blue, *ac*) heat advection during all four seasons off New Jersey (upper panel) and Delmarva (lower panel). Their sums are shown in green curves in each panel.

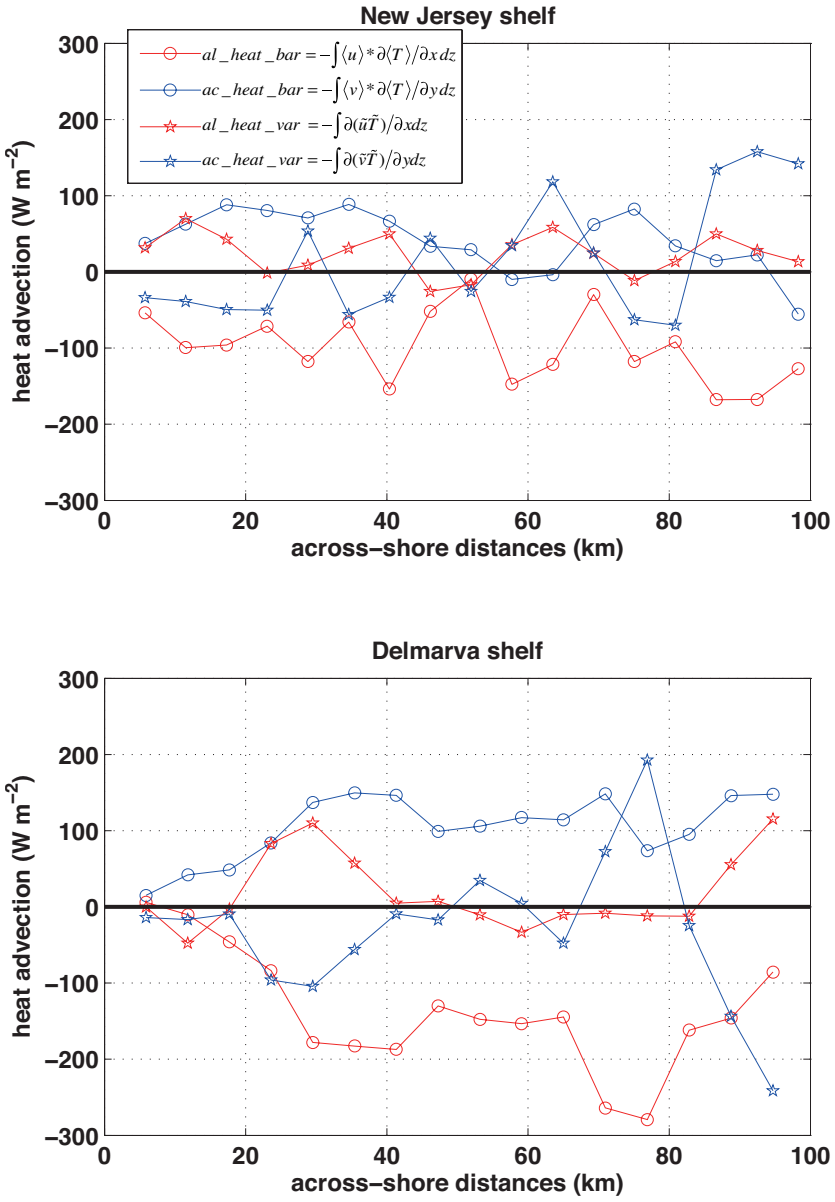

Figure 4.6 Four-year (2006-2009) mean of *al_heat_bar* (red circle, $-\int \langle u \rangle * \partial \langle T \rangle / \partial x \, dz$), *ac_heat_bar* (blue circle, $-\int \langle v \rangle * \partial \langle T \rangle / \partial y \, dz$), *al_heat_var* (red star, $-\int \partial(\tilde{u}\tilde{T}) / \partial x dz$), *ac_heat_var* (blue star, $-\int \partial(\tilde{v}\tilde{T}) / \partial y dz$) off NJ (upper panel) and Delmarva (lower panel).

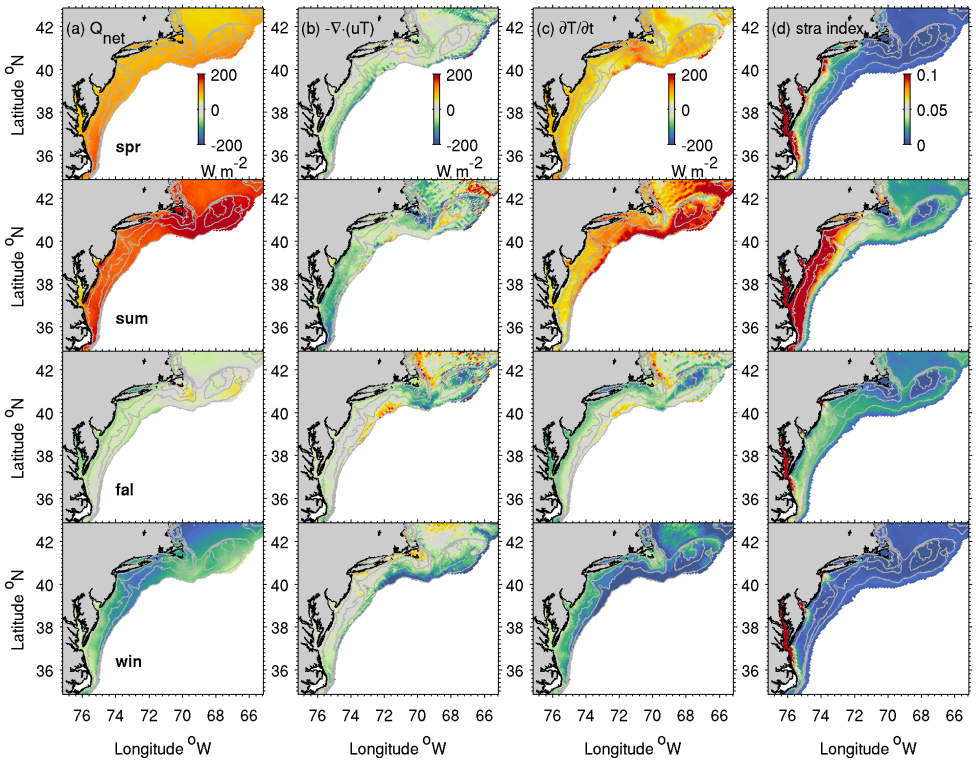

Figure 4.7 Seasonal variations of four-year (2006-2009) averaged heat budget terms (*Q_net*: column a panels; *temp_hadv*: column b panels; *dT/dt*: column c panels) and the stratification index (column d panels). The 1st row indicates those during spring, 2nd row for summer, 3rd row for fall and 4th row for winter.

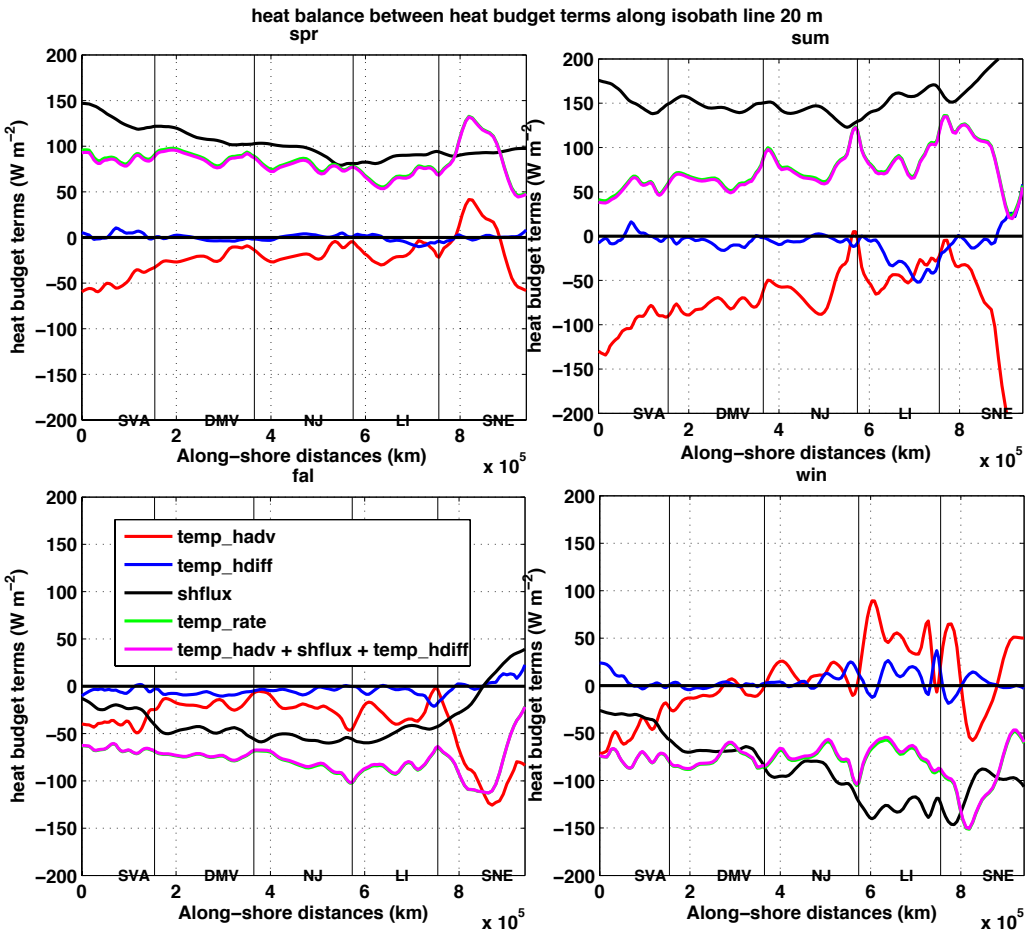

Figure 4.8 Seasonally mean depth-integrated heat budget terms along the 20-m isobaths (see Fig. 4.1 for the exact location). Red curves indicate the horizontal heat advection term (temp_hadv), blue curves indicate the horizontal heat diffusion (temp_hdiff), black curves indicate the net surface heat flux (Q_net, or shflux), grenn curves indicate the net heat content change rate in the water column (temp_rate), purple curves indicate the combination of horizontal heat advection, horizontal heat diffusion and net surface heat flux (temp_hadv + temp_hdiff + shflux). The x-axis indicates the along-shore distance from south to the north with different regions separated by grey vertical lines. The y-axis indicates values of different heat budget terms in $W \cdot m^{-2}$.

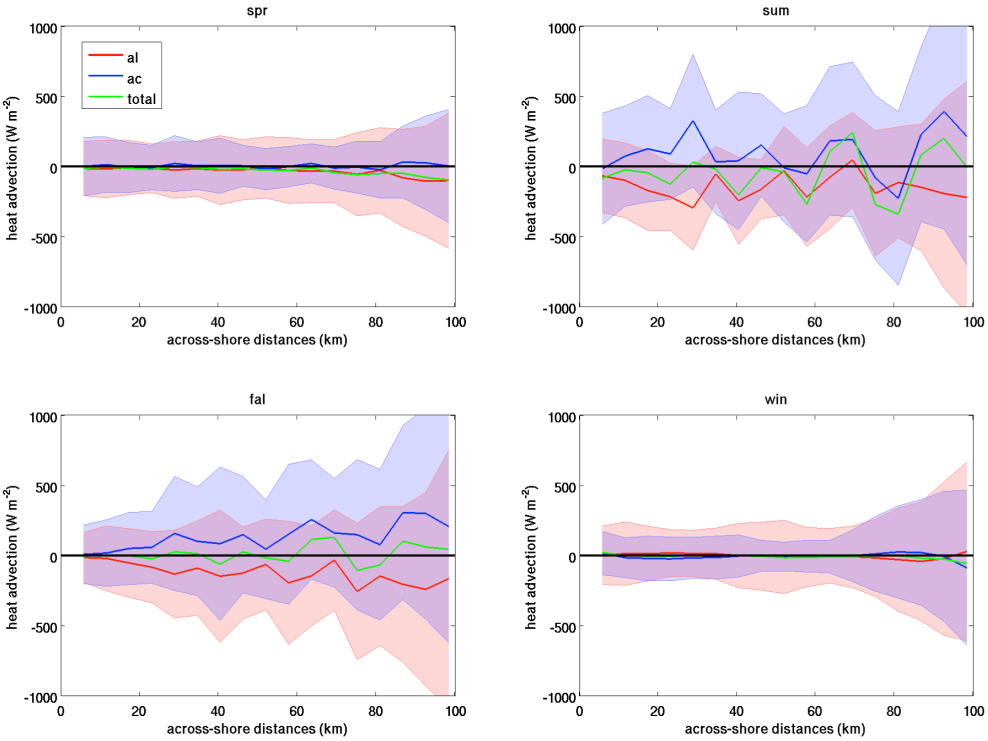

Figure 4.9 Seasonal mean (curves) and variation (shaded region) of along-shore (red, *al*) and across-shore (blue, *ac*) heat advection during all four seasons off New Jersey.

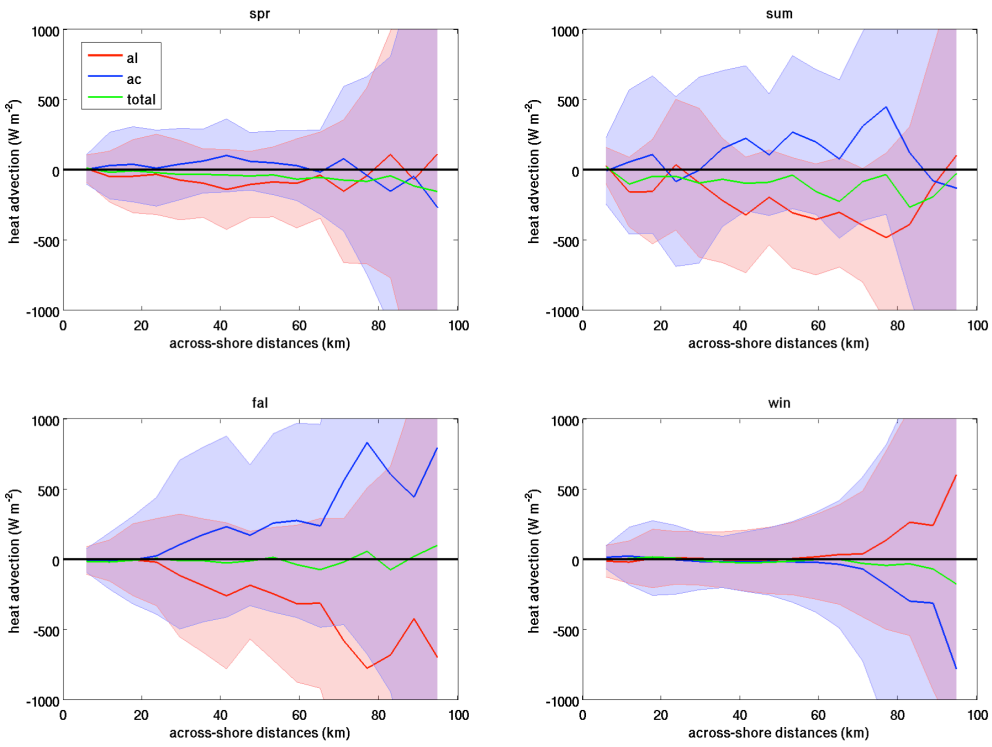

Figure 4.10 Seasonal mean (curves) and variation (shaded region) of along-shore (red, *al*) and across-shore (blue, *ac*) heat advection during all four seasons on the Delmarva shelf.

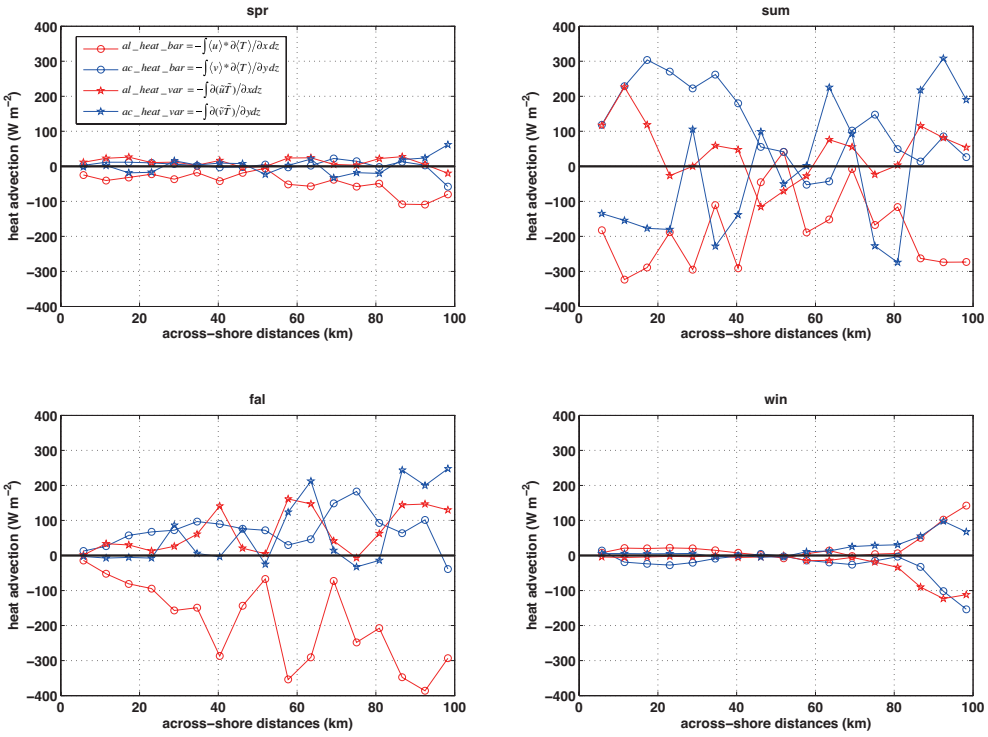

Figure 4.11 Seasonal means of *al_heat_bar* (red circle, $-\int \langle u \rangle * \partial \langle T \rangle / \partial x \, dz$), *ac_heat_bar* (blue circle, $-\int \langle v \rangle * \partial \langle T \rangle / \partial y \, dz$), *al_heat_var* (red star, $-\int \partial (\tilde{u}\tilde{T}) / \partial x dz$), *ac_heat_var* (blue star, $-\int \partial (\tilde{v}\tilde{T}) / \partial y dz$) on the NJ shelf during spring, summer, fall and winter seasons.

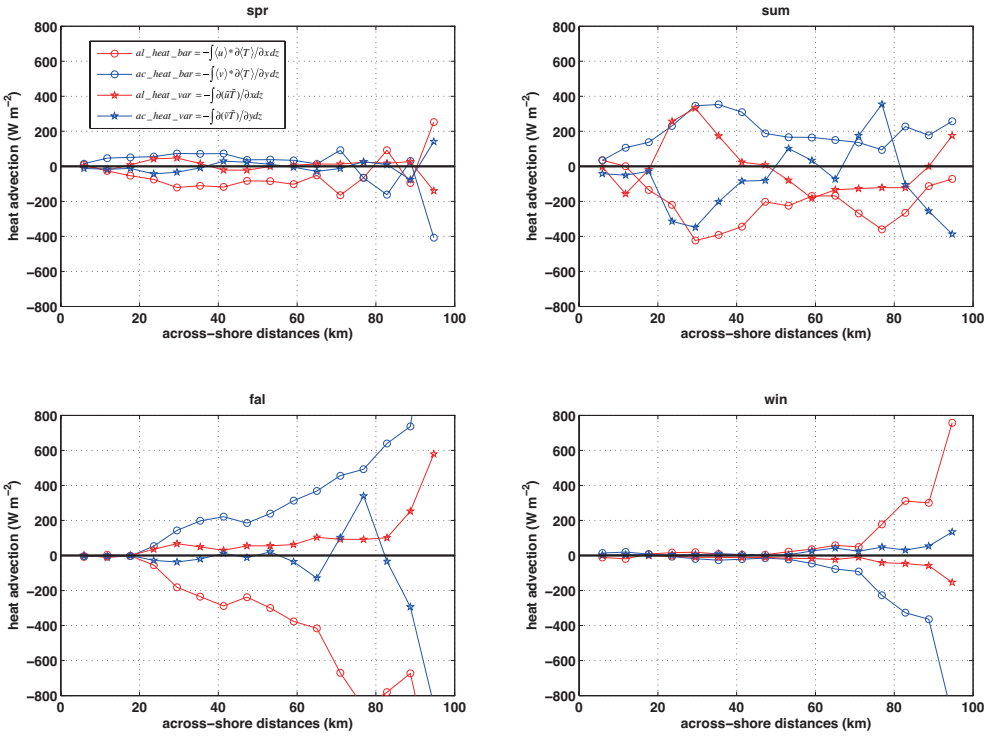

Figure 4.12 Seasonal means of *al_heat_bar* (red circle, $-\int \langle u \rangle * \partial \langle T \rangle / \partial x \, dz$), *ac_heat_bar* (blue circle, $-\int \langle v \rangle * \partial \langle T \rangle / \partial y \, dz$), *al_heat_var* (red star, $-\int \partial (\tilde{u}\tilde{T}) / \partial x dz$), *ac_heat_var* (blue star, $-\int \partial (\tilde{v}\tilde{T}) / \partial y dz$) off DMV during spring, summer, fall and winter seasons.

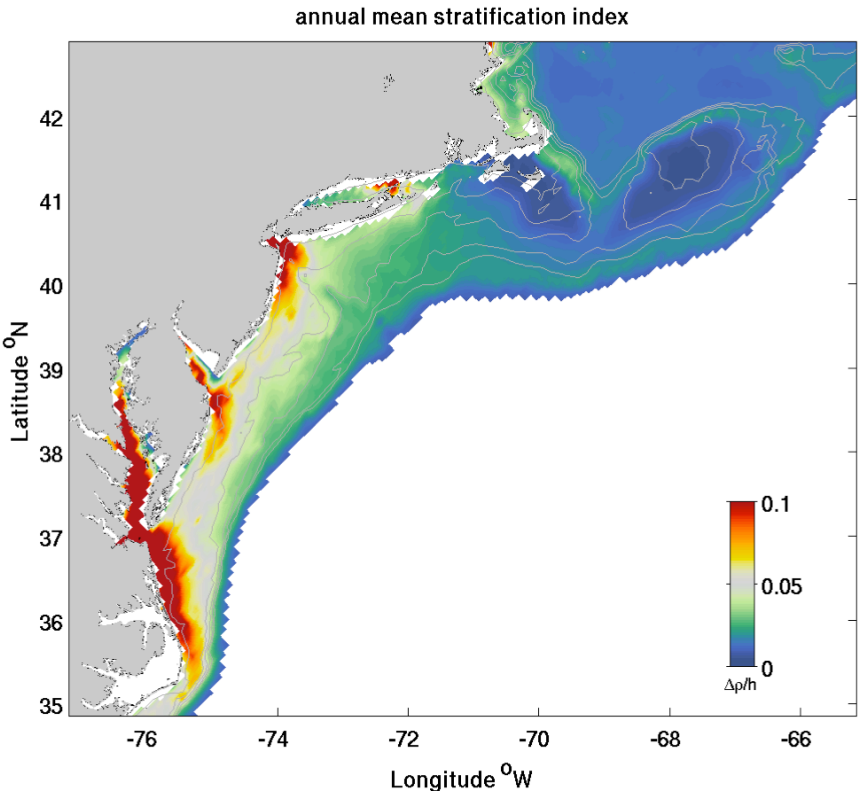

Figure 4.13 Four-year (2006-2009) mean stratification index, calculated by the density differences between the surface and bottom, divided by the water depth, i.e.: $\Delta\rho / h$.

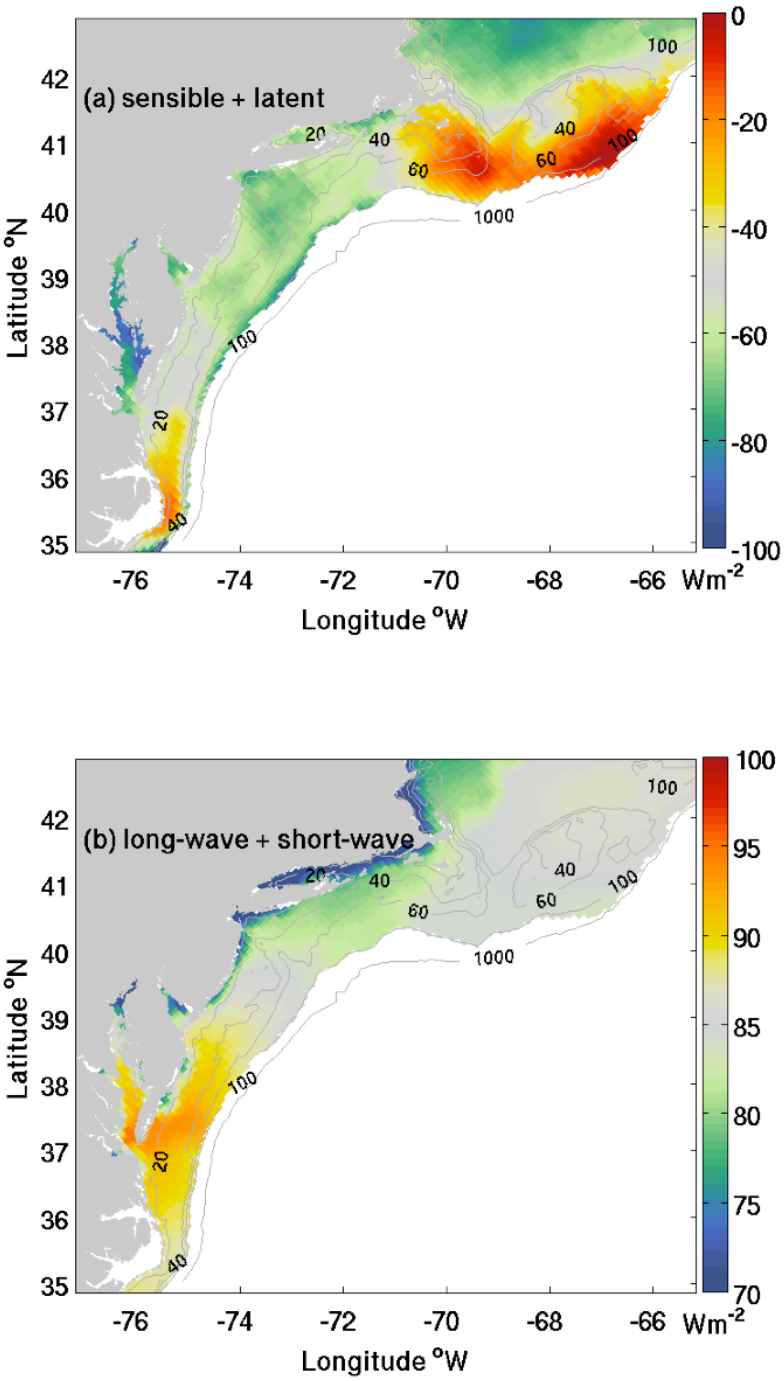

Figure 4.14 Four-year (2006-2009) mean sensible+latent (panel a) and longwave+shortwave radiation (panel b) heat fluxes in $W \cdot m^{-2}$. The 20-, 40-, 60-, 100- and 1000m isobaths are indicated by grey lines.

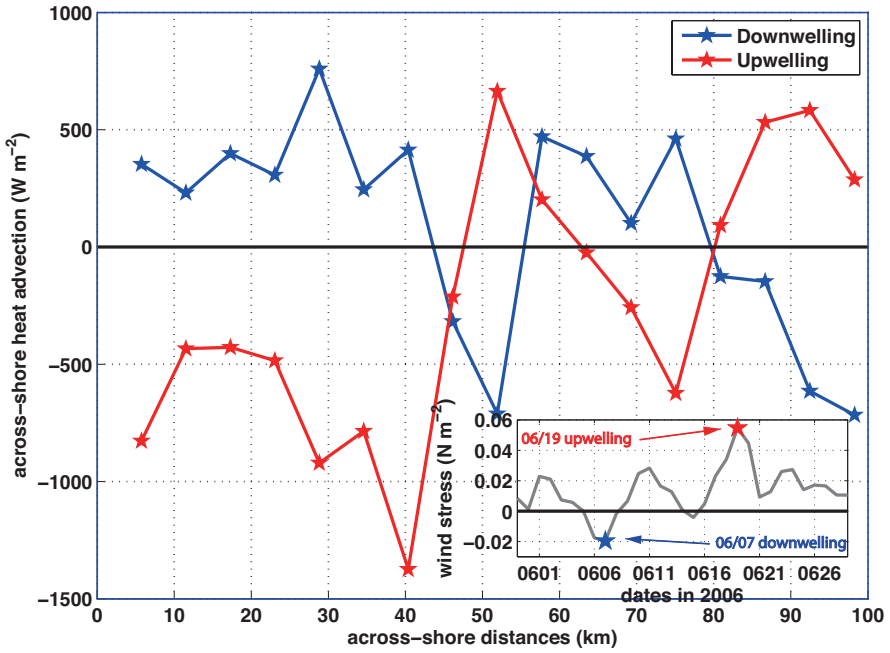

Figure 4.15 New Jersey one-day averaged across-shore heat advection due to the depth-varying currents acting on the depth-varying temperature gradients (*ac_heat_var*) during downwelling (blue star curves, June 7th 2006) and upwelling (red star curves, June 19th 2006) scenarios. X-axis indicates the offshore distances (in kms) from the coast for different across-shore stations. Y-axis indicates the heat advection values in The bottom right inset indicates the along-shore wind stress time series in June 2006 off New Jersey near-coast (See Fig. 4.1 for its position), with the blue and red stars showing the along-shore wind stress on the selected downwelling and upwelling dates (June 7th and June 19th in 2006).

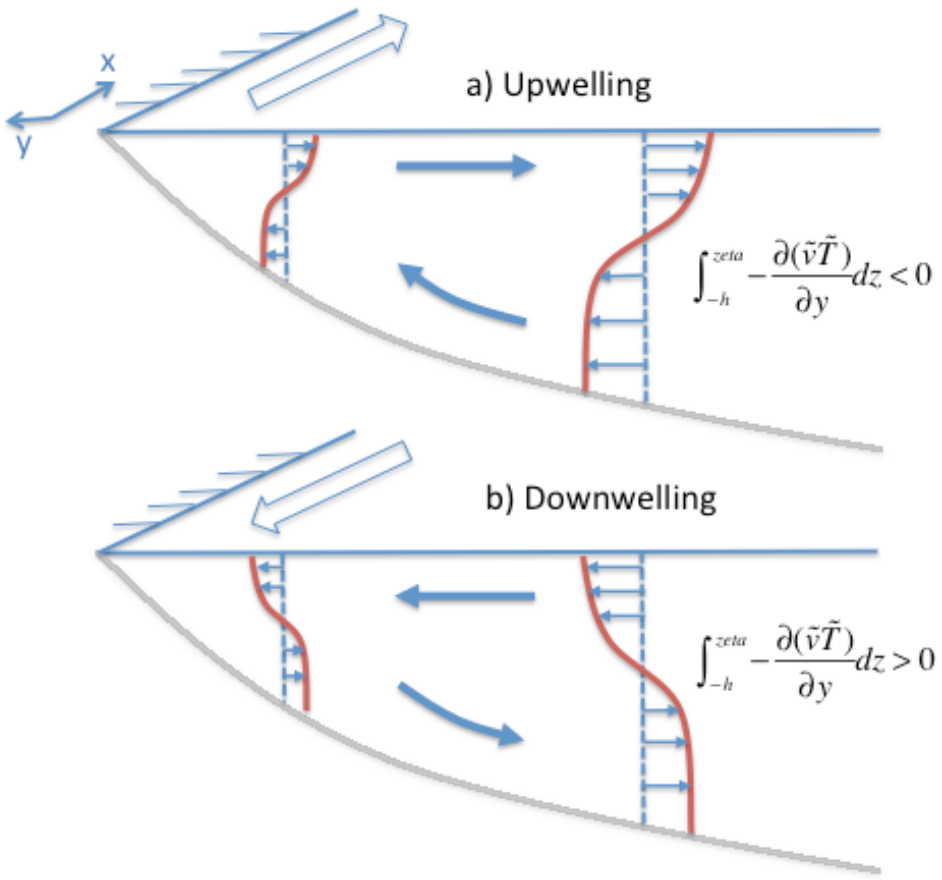

Figure 4.16 Diagram showing the coastal across-shore circulation during upwelling (panel a) and downwelling (panel b) cases off MAB. X-axis indicates the across-shore direction, with inshore being positive, while y-axis indicates the along-shore direction, with upstream northward/northeastward being positive. Red curves indicate the vertical temperature profiles. Blue solid arrows indicate across-shore current directions. Blue box arrows on top of the surface indicate the surface along-shore wind directions. Grey lines on the bottom indicate the ocean bottom.

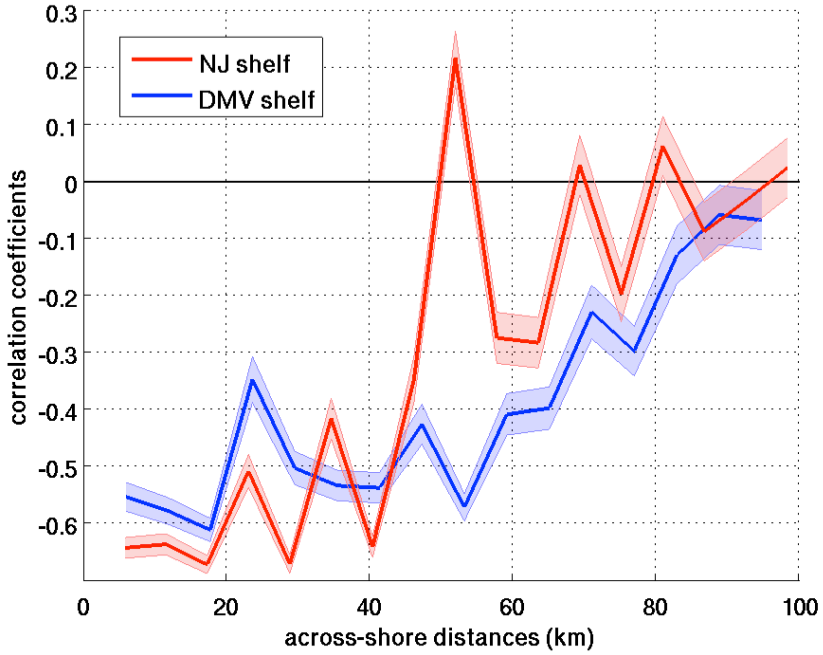

Figure 4.17 Correlation coefficients at across-shore stations of the surface along-shore wind stress with across-shore heat advection due to depth-varying currents acting on depth-varying horizontal temperature gradients (*ac_heat_var*), for New Jersey shelf (red curve) and Delmarva shelf (blue curve). Their positions were indicated in Fig. 4.1. Shaded region indicated one standard deviation from the mean.

CHAPTER 5. CONCLUSIONS

To study the primary larval transport pathways and inter-population connectivity patterns of the Atlantic surfclam, *Spisula solidissima*, a coupled modeling system combining a physical circulation model of the Middle Atlantic Bight (MAB), Georges Bank (GBK) and the Gulf of Maine (GoM), and an individual-based surfclam larval model has been implemented, validated and applied. Model validation shows that the model can reproduce the observed physical circulation patterns and surface and bottom water temperature, and recreates the observed distributions of surfclam larvae during upwelling and downwelling events.

The model results show a typical along-shore connectivity pattern from the northeast to the southwest among the surfclam populations distributed from Georges Bank west and south along the MAB shelf. Continuous surfclam larval transport and settlement into regions off Delmarva (DMV) and New Jersey (NJ) is found in this 2006 to 2009 modeling simulation. Assuming this pattern is unchanged from the 1980's and 1990's, this result suggests that insufficient larval supply is unlikely to be the factor causing the failure of the population to recover after the observed decline of the surfclam populations in DMV and NJ from 1997 to 2005. The GBK surfclam population is relatively more isolated than populations to the west and south in the MAB; model results suggest substantial inter-population connectivity from southern New England to the Delmarva region.

Simulated surfclam larvae generally drift for over one hundred kilometers along the shelf, exhibiting a mean downstream pattern following the mean coastal current from the northeast to the southwest. The distance traveled is highly variable, however, both in space and over time. Surfclam larval transport and settlement intra-annual variations in

2006 were investigated, and also those primary physical mechanisms causing such variations. Most high-frequency (periods of 2~10 days) variations in along-shore larval transport are associated with changes in the along-shore surface wind stress, with seasonal variations speculated to be driven mainly by changes in the across-shelf density gradient.

Larval across-shelf movement is found to be highly correlated with the along-shore surface wind stress mediated by coastal upwelling and downwelling episodes, but the correlation is further dependent on the vertical distribution of the larvae, particularly their position relative to the thermocline. Most surfclam larvae released from the Mid Atlantic shelf stay below the thermocline and experience a net onshore transport during the summer-stratified season when upwelling-favorable wind forcing dominates.

A proposed critical value of water temperature at the thermocline successfully explains the observed patterns of vertical distribution of surfclam larvae and their across-shelf movement on the New Jersey and South Virginia shelves. Specifically, when the water temperature at the thermocline is above the critical value (19.0 ^{o}C in this study), surfclam larvae tend to escape the warm surface layer to concentrate below the thermocline and follow the across-shelf movement of bottom water, and when the water temperature at the thermocline is below this critical value, larvae tend to concentrate close to or above the thermocline and follow the surface water across-shelf movement.

Our results indicate that the highest larval settlement rate, that is the highest percentage of settled larvae with respect to the total number of those released, occurs for those larvae released during July to early October in 2006, corresponding to higher

average temperatures experienced by the larvae (ATEL). This underscores the importance of shelf water temperature in affecting surfclam larval settlement and population connectivity, and suggests that an understanding of the heat budget on the MAB shelf, as well as the underlying physical mechanisms involved, is essential to better predict the effects of (e.g.) future climate change and variability.

Analysis of the four years (2006-2009) of model results shows that surface air-sea heat flux and horizontal heat advection are the two most important terms in the vertically integrated ocean heat balance on the MAB shelf, generally balancing each other in the long-term state. The mean circulation pattern and water temperature structure determining the horizontal heat advection are expected to play important roles in affecting shelf temperature. Horizontal heat diffusion is only evident at shelf break regions with sharp bathymetry changes.

Seasonal variation of water temperature is mainly controlled by the seasonally varying surface heat fluxes. Across-shore horizontal heat advection variations associated with different coastal across-shore circulation patterns generally affect water temperature on shorter time scales from days to weeks. This is most significant during the spring and summer seasons when the MAB water column is more stratified than it is during fall and winter. The coastal upwelling system transports warm surface water offshore and cold bottom water inshore, creating a negative heat advective flux to the inshore region and positive heat flux to the offshore, while the coastal downwelling system does the opposite. Fluctuation in the across-shore current system is mainly determined by the surface wind forcing, and the variation time scales are generally from days to weeks.

The long-term variation of water temperature is most likely due to variations in along-shore heat advection, specifically the component due to the depth-averaged currents acting on the depth-averaged horizontal temperature gradient, which is found to play an important role in the horizontal heat advection and the total heat balance. Its importance is consistent with the finding in Shearman and Lentz (2010) that the along-shore transport mechanism associated with the mean coastal current system running from Labrador in the north to Cape Hatteras in the south is the main factor controlling long-term temperature changes in the MAB. The well-known "cold pool" feature in MAB is also important in affecting the MAB shelf water heat budget, transporting large volumes of cold bottom water alongshore southwestward during spring and summer seasons, causing large negative along-shore heat advection as observed in this study.

All these results provide an important insight into the general mechanism of how physical environmental factors interact with biological behavior of the larvae to influence larval transport, connectivity and population dynamics, and also imply potential large impacts of large-scale climate change on benthic species and coastal ecosystems.

APPENDIX

Appendix A: Larval daily mortality and sensitivity to larval duration

A1. Introduction

In our current surfclam larval model, daily background mortality has not been included. Environmental and ecological factors influencing mortality are undoubtedly complex, and are not understood well enough to incorporate in any simple manner. As an example, larval ontogenic changes in mortality are known to occur in plankton (Johnson and Shanks, 2003; Metaxas and Burdett-Coutts, 2006), yet the details are poorly characterized in the literature (Metaxas and Saunders, 2009) making them hard to adequately parameterize. Therefore, for simplicity, we introduce a 35-day cutoff to the larval life span to permit comparability across regions without introducing a completely unconstrained term into the analysis.

Another implicit mortality effect in the model occurs through larval supply to habitat unsuitable for larval settlement. In particular, larvae transported and settled into regions deeper than 60 m are assumed to die, in accordance with the fact that surfclams are only found on the shelf at depths shallower than 60 m.

Daily larval mortality is indeed likely to be important in determining larval settlement rate and population connectivity. We have therefore performed a sensitivity analysis that explores the consequences of a uniform daily planktonic mortality rate. One of the constraints to inclusion of a planktonic mortality factor is the limited number of larvae released at each time step. (Currently at the DMV and NJ release sites, the total number of larvae released is only 2000 and 1800 respectively at each release time). For

example, applying an assumed daily mortality of Z = 3/35, we will only have about 100~200 larvae left after a period of about 30 days, calculated through the formula: $n = N*exp(-Z*age)$. If we further exclude those larvae that are unable to grow large enough to reach settlement within the larval life span of 35 days or settle into unsuitable habitats deeper than 60 m, there will be very few larvae that eventually reach successful settlement in the model, and the resulting population statistics will be uncertain. One way to work around this issue is to release larger numbers of larvae from each region, but the resulting computational cost is huge. As a compromise, our sensitivity analysis used offline calculations for planktonic mortality.

A2. Method

Herein the larval mortality sensitivity is tested offline, incorporating the "daily mortality" into the calculation by introducing the "survival rate" of each larva, which means the probability that each larva can survive after a certain time period. The survival rate is defined by the following formula: $sur\_rate = exp(-Z*age)$, a function of mortality rate (Z) and larval age, and its value is between [0, 1]. Based on this method, the expected values of the average larval drifting distances, ATEL (averaged temperature experienced by larvae), etc., after applying the daily mortality can be obtained based on a probably distribution function (pdf) defined by the survival rate formula.

Taking the calculation of larval along-shore drifting distance as one example. Let $L = L(t)$, be the modified larval drifting distance. Then we have:

$$E(L) = \int_0^{Age} L(t) * pdf(t)\,dt \tag{A.1}$$

Here:

$$L(t) = v * t \tag{A.2}$$

where t is the time each larva has stayed in the water, and we assume v is the averaged along-shore drifting speed (in km/day). In the current model we obtain the value of v by looking at the net drifting distances (L_{Age}) from release time (t=0) to settlement time (t=Age), i.e.:

$$v = L_{Age} / Age \tag{A.3}$$

Here L_{Age} is the net larval along-shore drifting distance from the release position until the larval settlement position, or the position at the end of larval span of 35 days (*Age*) before applying the larval survival rates.

Let T be the time (in days) each larva can survive after applying the larval survival rates, assuming that larva will die after the time T. Then we will have the following formula for the cumulative distribution function (cdf) with respect to T:

$$F(t) = P(T \le t) = 1 - P(T > t) = 1 - \exp(-Z * t) \tag{A.4}$$

Here Z is the daily mortality value. Therefore:

a) when $t = 0$, $F(t = 0) = 1$, indicating that larva could live for a duration of 0 days for sure, with the probability of 1; and
b) $F(t = \infty) = 0$, indicating that larva will eventually die.

These two limits of the cdf both make obvious physical sense.

In our study, we have assumed that larva only stay in the water column for the duration of larval age (35 days or earlier), and after this larval age, they will either reach settlement or just die. Therefore, the modified cdf becomes:

$$F(t)=\begin{cases}1-\exp(-Z*t),\ 0\le t<Age\\ 1,\ t\ge Age\end{cases} \tag{A.5}$$

From the above cdf we can calculate the probability distribution function (pdf) with respect to t:

$$pdf(t)=F'(t)=\begin{cases}Z*\exp(-Z*t),\ 0\le t<Age\\ \int_{Age}^{\infty}Z*\exp(-Z*t)dt=\exp(-Z*Age),\ t=Age\\ 0,\ t>Age\end{cases} \tag{A.6}$$

Putting (A.6) and (A.2) into (A.1), we get:

$$\begin{aligned}E(L)&=\int_0^{Age}v*t*Z*\exp(-Z*t)dt+L_{Age}*P(t=Age)\\ &=\int_0^{Age}L_{Age}/Age*t*Z*\exp(-Z*t)dt+L_{Age}*\exp(-Z*Age)\\ &=L_{Age}*\{\frac{Z}{Age}*[-\frac{Age}{Z}*\exp(-Z*Age)+\frac{1}{Z^2}-\frac{\exp(-Z*Age)}{Z^2}]\\ &\qquad+\exp(-Z*Age)]\}\\ &=\frac{L_{Age}}{Z*Age}*[1-\exp(-Z*Age)]\end{aligned} \tag{A.7}$$

This is the expected value of larval drifting distance after we have applied daily mortality and survival probability theory.

Looking at the influences before and after this daily mortality has been applied to the larval drifting distance calculation (L_{Age} $v.s$ $E(L)$), we define a ratio between $E(L)$ and L_{Age} as follows:

$$R_{ratio} = \frac{E(L)}{L_{Age}} = \frac{1-\exp(-Z*Age)}{Z*Age} \tag{A.8}$$

A few tests to calculate the value of this ratio when Z=3/35 are shown in Table A1. Applying daily mortality would have a net effect of decreasing larval along-shore drifting distances by 50~70%.

The e-folding time for mortality is 1/Z. So when the larval age exceeds the mortality e-folding time, the exponential term, $\exp(-Z*Age)$, becomes small, and the average larval drifting distance becomes:

$$\begin{aligned} E(L) &= \frac{L_{Age}}{Z*Age} = \frac{v*Age}{Z*Age} = \frac{v}{Z} \\ ratio &= \frac{E(L)}{L_{Age}} = \frac{1}{Z*Age} \end{aligned} \tag{A.9}$$

Furthermore, we can calculate the basic statistical parameters, such as the median, 1st quartile, 3rd quartile, based on the probability profile as shown by (A.5):

$$\begin{aligned} &Let\ F(t = median) = 0.5 \Rightarrow t_{median} = \frac{\log(2)}{Z} \\ &Let\ F(t = 1st\ quartile) = 0.25 \Rightarrow t_{1st} = \frac{\log(4/3)}{Z} \\ &Let\ F(t = 1st\ quartile) = 0.75 \Rightarrow t_{3rd} = \frac{\log(4)}{Z} \end{aligned} \tag{A.10}$$

The corresponding statistics for the larval drifting distances can then be obtained from the following formulae:

$$\begin{aligned} L_{1st} &= v * t_{1st} = \frac{L_{Age}}{Age} * t_{1st} = \frac{\log(2) * L_{Age}}{Z * Age} \\ L_{median} &= v * t_{median} = \frac{L_{Age}}{Age} * t_{median} = \frac{\log(4/3) * L_{Age}}{Z * Age} \\ L_{3rd} &= v * t_{3rd} = \frac{L_{Age}}{Age} * t_{3rd} = \frac{\log(4) * L_{Age}}{Z * Age} \end{aligned} \tag{A.11}$$

So far, the above analysis is based on the assumption of a constant larval drifting speed calculated from the net drifting distance during the larval age, i.e.: $v = L_{Age} / Age$. However, in reality larval drifting speed (v) is not constant, but rather a function varying with time, i.e: $v = v(t)$. So, we can conduct a second analysis based on the new assumption $v = v(t)$:

$$\begin{aligned} L(t) &= \int_0^t v(s)ds \\ L_{Age} &= L(Age) = \int_0^{Age} v(s)ds \end{aligned} \tag{A.12}$$

The larval age, *Age* is independent from its experienced on-time drifting speed, *v(t)*, which is only determined by its local water environment. Therefore:

$$E(L_{Age}) = \int_0^{E(Age)} v(s)ds = \int_0^{E(Age)} v(s)ds \tag{A.13}$$

Also, we know from the previous analysis that:

$$E(Age) = \frac{1 - \exp(-Z * Age)}{Z} \tag{A.14}$$

Therefore:

$$E(L_{Age}) = \int_0^{E(Age)} v(s)ds = \int_0^{\frac{1-\exp(-Z*Age)}{Z}} v(s)ds \tag{A.15}$$

$$R_{ratio} = \frac{E(L_{Age})}{L_{Age}} = \frac{\int_0^{\frac{1-\exp(-Z*Age)}{Z}} v(s)ds}{\int_0^{Age} v(s)ds} \tag{A.16}$$

Since $E(Age) < Age$, then we can also write the ratio as:

$$R_{ratio} = 1 - \frac{\int_0^{Age-\frac{1-\exp(-Z*Age)}{Z}} v(s)ds}{\int_0^{Age} v(s)ds} \tag{A.17}$$

This indicates that it is primarily the ending point of the time period ($Age - \frac{1-\exp(-Z*Age)}{Z}$) that matters most. This formula is also consistent with the previous results with *v* assumed to be constant, in which case:

$$R_{ratio} = \frac{E(L_{Age})}{L_{Age}} = \frac{v * \frac{1-\exp(-Z*Age)}{Z}}{v*Age} = \frac{1-\exp(-Z*Age)}{Z*Age} \tag{A.18}$$

which is exactly (A.8) with *v* assumed to be constant.

A3. Conclusions

We have tested the sensitivity of the dispersal of surfclam larvae to planktonic mortality by introducing a "survival rate" for each larva which indicates the probability of that larva being able to survive after a certain time period. The daily planktonic mortality has been incorporated by the assumption of an exponentially decaying "survival

rate" with respect to larval age, i.e., *sur_rate = exp(-Z*age)*, where Z is the daily mortality rate.

The sensitivity results show that the magnitude of dispersal distances decreases with increasing planktonic mortality. On average, daily mortality has a mean effect of decreasing 50~70% of the larval along-shore drifting distances (e.q. A.8, Table 1). The variation of the current speed each larva experiences during the larval stage determines the magnitude of the impacts of applying larval daily mortality to the mean larval drifting distances (e.q. A.16). For example, if during early larval life, there is a higher probability for larva to experience a stronger current than that during the latter stage, then the ratio of larval drift with daily mortality applied with respect to that without daily mortality applied will be small (e.q. A16), indicating a stronger influence of larval daily mortality on larval drift, and *vice versa*.

This offline method of incorporating daily mortality gives us a general picture of how it affects the mean larval drifting distance. The length of larval drifting distance is further closely related to the larval connectivity pattern among different regions as shown in chapter 2 and chapter 3. The net influence of decreasing larval drifting distance by adding larval daily mortality is expected to decrease the relative magnitude of population connectivity among different regions and increase the relative importance of larval self-supply to each region. However, in order to obtain a more quantitative evaluation of the impacts of applying daily mortality, an alternative in-line method of incorporating daily mortality inside the larval model might be needed, especially considering the large temporal and spatial variations of coastal currents.

Table A.1 Values of ratio of L_{Age} with respect to *E(L)* varying with different larval ages

Age (days)	R_{ratio}	Age (days)	R_{ratio}
20	0.478	28	0.379
21	0.464	29	0.369
22	0.450	30	0.359
23	0.437	31	0.350
24	0.424	32	0.341
25	0.412	33	0.333
26	0.400	34	0.325
27	0.389	35	0.317

Appendix B: Inter-annual variation in larval settlement

As introduced in Chapter 2 (section 2.3), a four-year simulation (2006-2009) of the coupled modeling system was conducted in this study. Surfclam larvae were released each year from those regions with large adult populations within the Middle Atlantic Bight and Georges Bank. The four-year-mean modeling results were described in section 2.4 in Chapter 2, exhibiting a mean along-shore connectivity pattern from the northeast to the southwest among the surfclam populations distributed from Georges Bank west and south along the MAB shelf.

In addition to the time-mean picture, temporal variations -- both inter-annual and intra-annual -- in larval transport, settlement and connectivity are also of interest. The intra-annual variation and the associated underlying physical mechanisms were examined in Chapter 3 based on the year 2006 simulation. In the following, the inter-annual variation of the population connectivity and larval transport is briefly examined for the four years from 2006 to 2009.

From the 2006-2009 simulation results, we have calculated the surfclam larval dispersal kernel with and without mortality enforced at the end of the larval stage (35 days) (Fig. B1, B2). The no-mortality case (NoM case) considers all the settled and non-settled larvae at the end of the larval stage, from which we can study how the coupled physical model and larval IBM together determine larval transport and geographic connectivity. For comparison, the mortality case (M case) incorporates only those larvae which successfully reach settlement within 35 days, and exclude those not large enough

to settle, or those which settle at inappropriate depths deeper than 60 m. The M case gives information about the pattern of larval settlement, defined as the portion of larvae from one region that were both transported and successfully settled in another, while the NoM case shows the overall pattern of larval supply, which is defined as the portion of larvae transported from one region to another.

The connectivity pattern shown in all four years is similar in both cases (NoM and M), indicating an alongshore connection from the northeast to the southwest, but with varying magnitudes. Generally, only two nearby regions have close connections, e.g., the pairs DMV-SVA, NJ-DMV, LI-NJ, SEN-LI and GBK-SNE. In contrast, GBK is a region where most larvae stay on the bank. For example, an average of over 80% of larvae released on GBK still remain on the bank, and 5% successfully settle on the bank, while only 12% are transported into the SNE region and nearly none of them successfully settled.

Among the larvae released from LI and DMV during the four years, most of them are transported and settle into their downstream nearby regions, which are NJ and SVA respectively, while a relatively smaller number stay and settle within their release region (Fig. B1, B2). For those larvae released on the NJ shelf during 2007 and 2008, more larvae remain and settle than those larvae that are transported and successfully settle to the south (i.e., self-seeding exceeds successful connectivity with the adjacent southern regions). In contrast, in 2006 a comparable number of larvae released on the NJ shelf remain and settle compared to those successfully transported to downstream regions. Finally, in 2009 a larger proportion of larvae released from NJ shelf are transported and successfully settle to the southwest DMV region. Year 2007 appears to be an especially

successful self-recruiting year, during which a larger proportion of larvae released from SVA, DMV and NJ are all retained on the original shelves (Fig. B1, B2).

As previously introduced in sections 2.4 and 3.3, larval along-shore and across-shore drifting distances show large temporal variations. The inter-annual variation in the annual-mean along-shore drifting distances, as shown in Figure B3, indicates that years 2007 and 2008 are different from years 2006 and 2009 in that the August larval releases in 2007 and 2008 experience much less along-shore drift than the same month releases in 2006 and 2009. This most likely could explain the previous finding in Figure B1 and B2 that in 2007 and 2008 a larger proportion of larvae released from SVA, DMV and NJ are still retained on the original shelves than those transported downstream. This suggests a relatively weaker along-shore current in August during 2007 and 2008.

Another interesting finding is the much stronger mean along-shore southwestward larval drift during late September and early October in 2009 than those during the other years (Fig. B3), indicating a potentially much different along-shore current pattern in 2009. As introduced in chapter 3, the seasonal variation of along-shore current on the shelf is strongly associated with the seasonal variation of the position of the maximum across-shore density gradient, which is further dependent on the seasonal variation of vertical stratification. The inter-annual variation of the mean along-shore currents simulated here suggests, in turn, significant inter-annual variation in the shelf water structure. Episodic changes in external forcing, -- e.g., the strength of the northern boundary inflow, the influence of Gulf Stream warm core rings, and so on – are also possible causative factors.

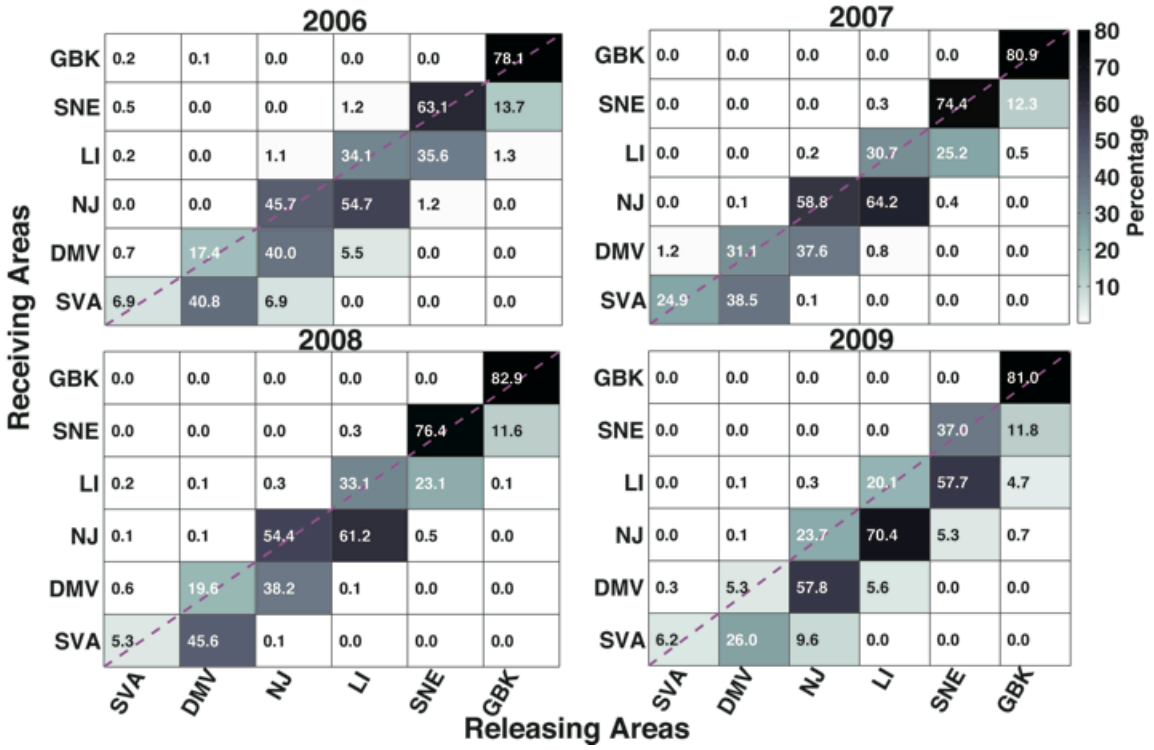

Figure B1. Annual-mean connectivity matrices of surfclam larval transport from 2006 to 2009 without mortality enforced (NoM case) at the end of larval life span (35 days).

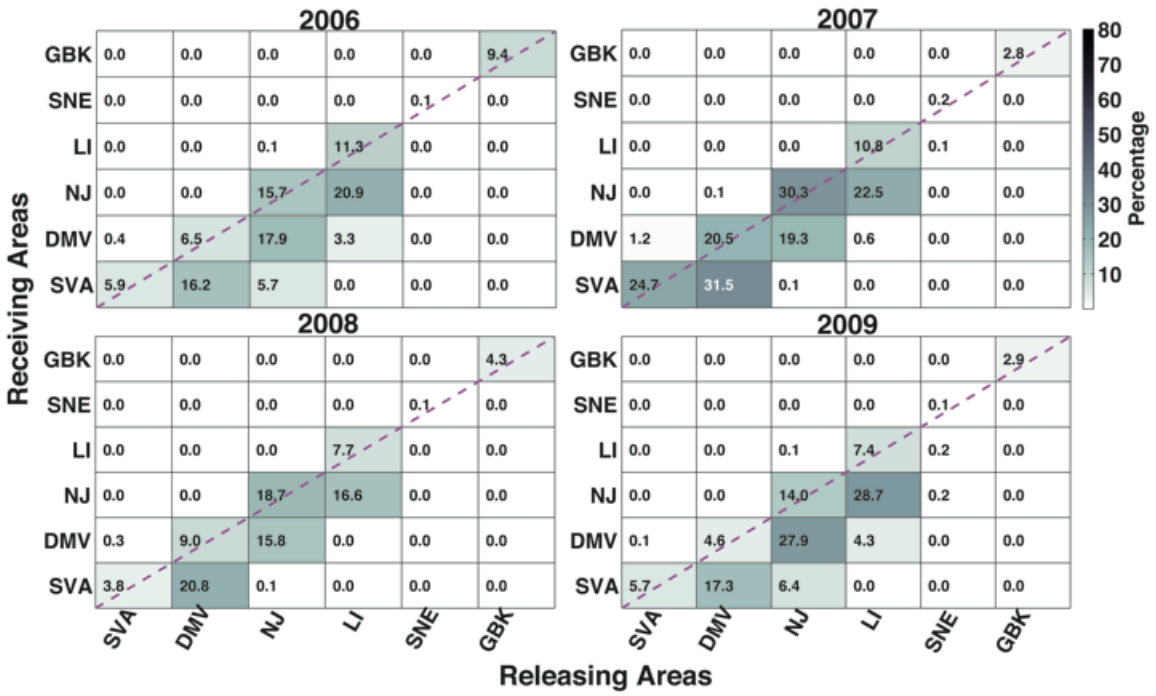

Figure B2. Annual0-mean connectivity matrices of surfclam larval transport from 2006 to 2009 with mortality enforced (M case) at the end of larval life span (35 days), and excluding those larvae that do not reach settlement size or settle into inappropriate habitats deeper than 60 m.

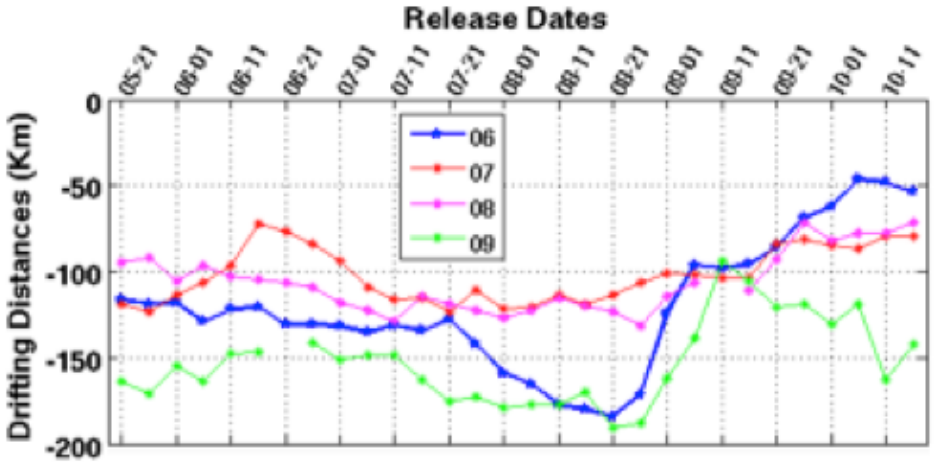

Figure B3. Variation in the mean along-shore larval drifting distances among all larvae released from the SVA, DMV, NJ, LI, SNE and GBK regions for year 2006 (blue), 2007 (red), 2008 (pink) and 2009 (green) respectively. The x-axis indicates different release dates in each year from May 21st until October 11th. The y-axis indicates the mean along-shore drifting distances in km.

Acknowledgement of Previous Publications

Chapter 2 has been submitted and accepted for publication by the scientific journal, *Journal of Estuarine, Coastal and Shelf Science*, as shown below. The larval model development part in this chapter is the teamwork in close collaboration with the other project collaborators, Eric N. Powell, Roger Mann, John Klinck, and Daphne Munroe.

Zhang, X., Haidvogel, D.B., Munroe, D., Powell, E.N., Klinck, J., Mann, R., Castruccio, F., *In press*. Modeling larval connectivity of the Atlantic surfclams within the Middle Atlantic Bight: Model development, larval dispersal and metapopulation connectivity. *Journal of Estuarine, Coastal and Shelf Science*.

Chapter 3 has been submitted for publication in the scientific journal, *Journal of Estuarine, Coastal and Shelf Science*, as shown below.

Zhang, X., Haidvogel, D.B., Munroe, D., Powell, E.N., submitted-b. Modeling larval connectivity of the Atlantic surfclams within the Middle Atlantic Bight: Physical mechanisms underlying larval transport and settlement variations. *Journal of Estuarine, Coastal and Shelf Science*.

REFERENCES

Aikman, F., Posmentier, E.S., 1985. Stratification and shelf-slope interaction in the Middle Atlantic Bight - a numerical study. Journal of Geophysical Research-Oceans 90, 4895-4905.

Aristizabal, M., Chant, R., 2013. A Numerical Study of Salt Fluxes in Delaware Bay Estuary. Journal of Physical Oceanography 43, 1572-1588.

Arnold, W.S., Hitchcock, G.L., Frischer, M.E., Wanninkhof, R., Sheng, Y.P., 2005. Dispersal of an introduced larval cohort in a coastal lagoon. Limnology and Oceanography 50, 587-597.

Austin, J.A., 1999. The role of the alongshore wind stress in the heat budget of the North Carolina inner shelf. Journal of Geophysical Research-Oceans 104, 18187-18203.

Austin, J.A., Lentz, S.J., 1999. The relationship between synoptic weather systems and meteorological forcing on the North Carolina inner shelf. Journal of Geophysical Research-Oceans 104, 18159-18185.

Ayata, S.D., Ellien, C., Dumas, F., Dubois, S., Thiebaut, E., 2009. Modelling larval dispersal and settlement of the reef-building polychaete Sabellaria alveolata: Role of hydroclimatic processes on the sustainability of biogenic reefs. Continental Shelf Research 29, 1605-1623.

Backus, R.H., 1987. Geology, in: Backus, R.H. (Ed.), Georges Bank. MIT Press, Cambridge, MA, pp. 22-24.

Beardsley, R.C., Boicourt, W.C., 1981. On estuarine and continental ‐ shelf circulation in the Middle Atlantic Bight, in: Warren, B.A., Wunsch, C. (Eds.), Evolution of physical oceanography: scientific surveys in honor of Henry Stommel. MIT Press, Cambridge, Mass, pp. 198–235.

Bleck, R., 2002. An Oceanic general circulation model framed in hybrid isopycnic-Cartesian coordinates (vol 4, pg 55, 2002). Ocean Modelling 4, 219-219.

Bos, O.G., Hendriks, I.E., Strasser, M., Dolmer, P., Kamermans, P., 2006. Estimation of food limitation of bivalve larvae in coastal waters of north-western Europe. Journal of Sea Research 55, 191-206.

Botsford, L.W., Hastings, A., Gaines, S.D., 2001. Dependence of sustainability on the configuration of marine reserves and larval dispersal distance. Ecology Letters 4, 144-150.

Broekhuizen, N., Lundquist, C.J., Hadfield, M.G., Brown, S.N., 2011. Dispersal of Oyster (Ostrea Chilensis) Larvae in Tasman Bay Inferred Using a Verified Particle Tracking Model That Incorporates Larval Behavior. Journal of shellfish research 30, 643-658.

Budgell, W.P., 2005. Numerical simulation of ice-ocean variability in the Barents Sea region Towards dynamical downscaling. Ocean Dynamics 55, 370-387.

Butman, B., Beardsley, R.C., 1987. Long-Term Observations on the Southern Flank of Georges Bank .1. A Description of the Seasonal Cycle of Currents, Temperature, Stratification, and Wind Stress. Journal of Physical Oceanography 17, 367-384.

Byers, J.E., Pringle, J.M., 2006. Going against the flow: retention, range limits and invasions in advective environments. Marine Ecology Progress Series 313, 27-41.

Cargnelli, L.M., Griesbach, S.J., Packer, D.B., Weissberger, E., 1999. Atlantic surfclam, Spisula solidissima, life history and habitat characteristics. , Essential fish habitat source document. Northeast Region, Northeast Fisheries Science Center, Woods Hole, Massachusetts.

Castelao, R., Glenn, S., Schofield, O., Chant, R., Wilkin, J., Kohut, J., 2008. Seasonal evolution of hydrographic fields in the central Middle Atlantic Bight from glider observations. Geophysical Research Letters 35.

Chapman, D.C., 1985. Numerical Treatment of Cross-Shelf Open Boundaries in a Barotropic Coastal Ocean Model. Journal of Physical Oceanography 15, 1060-1075.

Chen, K., He, R., Powell, B.S., Gawarkiewicz, G.G., Moore, A.M., Arango, H.G., 2014. Data assimilative modeling investigation of Gulf Stream Warm Core Ring interaction with continental shelf and slope circulation. Journal of Geophysical Research: Oceans, n/a-n/a.

Chen, K., He, R.Y., 2010. Numerical Investigation of the Middle Atlantic Bight Shelfbreak Frontal Circulation Using a High-Resolution Ocean Hindcast Model. Journal of Physical Oceanography 40, 949-964.

Churchill, J.H., Levine, E.R., Connors, D.N., Cornillon, P.C., 1993. Mixing of Shelf, Slope and Gulf-Stream Water over the Continental-Slope of the Middle Atlantic Bight. Deep-Sea Research Part I-Oceanographic Research Papers 40, 1063-1085.

Condie, S.A., Waring, J., Mansbridge, J.V., Cahill, M.L., 2005. Marine connectivity patterns around the Australian continent. Environmental Modelling & Software 20, 1149-1157.

Council, M.A.F.M., 2005. Overview of the surfclam and ocean quahog fisheries and quota considerations for 2006 and 2007, Mid Atlantic Fishery Management Council, Dover, DE.

Cowen, R.K., Gawarkiewic, G., Pineda, J., Thorrold, S.R., Werner, F.E., 2007. Population Connectivity in Marine Systems An Overview. Oceanography 20, 14-21.

Cowen, R.K., Sponaugle, S., 2009. Larval Dispersal and Marine Population Connectivity. Annual Review of Marine Science 1, 443-466.

Csanady, G.T., Magnell, B.A., 1987. Mixing processes, in: Backus, R.H. (Ed.), Georges Bank. . MIT Press, Cambridge, MA, pp. 163-169.

Dekshenieks, M.M., Hofmann, E.E., Klinck, J.M., Powell, E.N., 1996. Modeling the vertical distribution of oyster larvae in response to environmental conditions. Marine Ecology Progress Series 136, 97-110.

Dekshenieks, M.M., Hofmann, E.E., Powell, E.N., 1993. Environmental-Effects on the Growth and Development of Eastern Oyster, Crassostrea-Virginica (Gmelin, 1791), Larvae - a Modeling Study. Journal of shellfish research 12, 241-254.

Dever, E.P., Lentz, S.J., 1994. Heat and Salt Balances over the Northern California Shelf in Winter and Spring. Journal of Geophysical Research-Oceans 99, 16001-16017.

Dzwonkowski, B., Kohut, J.T., Yan, X.H., 2009. Seasonal differences in wind-driven across-shelf forcing and response relationships in the shelf surface layer of the central Mid-Atlantic Bight. Journal of Geophysical Research-Oceans 114.

Edwards, K.P., Hare, J.A., Werner, F.E., Seim, H., 2007. Using 2-dimensional dispersal kernels to identify the dominant influences on larval dispersal on continental shelves. Marine Ecology Progress Series 352, 77-87.

Fairall, C.W., Bradley, E.F., Hare, J.E., Grachev, A.A., Edson, J.B., 2003. Bulk parameterization of air-sea fluxes: Updates and verification for the COARE algorithm. Journal of Climate 16, 571-591.

Fay, C.W., Neves, R.J., Pardue, G.B., 1983. Life Histories and Environmental Requirements of Coastal Fishes and Invertebrates (Mid-Atlantic). Surfclam. Virginia Polytechnic Institute and State University Blacksburg, USA.

Fewings, M.R., Lentz, S.J., 2011. Summertime cooling of the shallow continental shelf. Journal of Geophysical Research-Oceans 116.

Flather, R.A., 1976. A tidal model of the northwest European continental shelf. Memoires Societe Royale des Sciences de Liege, 141-164.

Fleming, N.E., Wilkin, J., 2010. MOCHA: A 3-D Climatology of the Temperature and Salinity of the Middle Atlantic Bight. 91, , . EOs Trans, AGU, Abstract PO35G-08.

Fong, D.A., Geyer, W.R., 2002. The alongshore transport of freshwater in a surface-trapped river plume. Journal of Physical Oceanography 32, 957-972.

Gaines, S.D., Gaylord, B., Largier, J.L., 2003. Avoiding current oversights in marine reserve design. Ecological Applications 13, S32-S46.

Garland, E.D., Zimmer, C.A., 2002. Hourly variations in planktonic larval concentrations on the inner shelf: Emerging patterns and processes. Journal of Marine Research 60, 311-325.

Garland, E.D., Zimmer, C.A., Lentz, S.J., 2002. Larval distributions in inner-shelf waters: The roles of wind-driven cross-shelf currents and diel vertical migrations. Limnology and Oceanography 47, 803-817.

Gawarkiewicz, G., Bahr, F., Beardsley, R.C., Brink, K.H., 2001. Interaction of a slope eddy with the shelfbreak front in the Middle Atlantic Bight. Journal of Physical Oceanography 31, 2783-2796.

Gawarkiewicz, G., Monismith, S., Largier, J., 2007. Observing Larval Transport Processes Affecting Population Connectivity Progress and Challenges. Oceanography 20, 40-53.

Gireesh, R., Gopinathan, C.P., 2008. Effects of microalgal diets on larval growth and survival of Paphia malabarica chemnitz. Aquaculture Research 39, 552-556.

GLOBEC, 1991. Global Ocean Ecosystems Dynamics, Initial Science Plan, Washington, D.C, p. 93.

Goldberg, R., 1989. Biology and Culture of the Surfclam, in: Manzi, J.J., Castagna, M. (Eds.), Clam Mariculture in North America. Elsevier Science Publishers, Amsterdam, pp. 263-276.

Gong, D., Kohut, J.T., Glenn, S.M., 2010. Seasonal climatology of wind-driven circulation on the New Jersey Shelf. Journal of Geophysical Research-Oceans 115.

Guo, Q., Taper, M., Schoenberger, M., Brandle, J., 2005. Spatial-temporal population dynamics across species range: from central to margin. . Oikos, 47-57.

Haase, A.T., Eggleston, D.B., Luettich, R.A., Weaver, R.J., Puckett, B.J., 2012. Estuarine circulation and predicted oyster larval dispersal among a network of reserves. Estuarine Coastal and Shelf Science 101, 33-43.

Hare, J.A., Churchill, J.H., Cowen, R.K., Berger, T.J., Cornillon, P.C., Dragos, P., Glenn, S.M., Govoni, J.J., Lee, T.N., 2002. Routes and rates of larval fish transport from the southeast to the northeast United States continental shelf. Limnology and Oceanography 47, 1774-1789.

Hare, J.A., Cowen, R.K., 1996. Transport mechanisms of larval and pelagic juvenile bluefish (Pomatomus saltatrix) from South Atlantic Bight spawning grounds to Middle Atlantic Bight nursery habitats. Limnology and Oceanography 41, 1264-1280.

Hare, M.P., Weinberg, J., Peterfalvy, O., Davidson, M., 2010. The "Southern" Surfclam (Spisula Solidissima Similis) Found North of Its Reported Range: A

Commercially Harvested Population in Long Island Sound, New York. Journal of shellfish research 29, 799-807.

Hare, M.P., Weinberg, J.R., 2005. Phylogeography of surfclams, Spisula solidissima, in the western North Atlantic based on mitochondrial and nuclear DNA sequences. Marine Biology 146, 707-716.

Harris, C.K., Butman, B., Traykovski, P., 2003. Winter-time circulation and sediment transport in the Hudson Shelf Valley. Continental Shelf Research 23, 801-820.

Hastings, A., Harrison, S., 1994. Metapopulation Dynamics and Genetics. Annual Review of Ecology and Systematics 25, 167-188.

He, R.Y., Wilkin, J.L., 2006. Barotropic tides on the southeast New England shelf: A view from a hybrid data assimilative modeling approach. Journal of Geophysical Research-Oceans 111.

Hickey, B.M., 1979. The California Current system—hypotheses and facts. Progress in Oceanography 8, 191-279.

Hill, A.E., 1991. Vertical migration in tidal currents. Marine Ecology Progress Series 75, 39-54.

Holt, R.D., Keitt, T.H., Lewis, M.A., Maurer, B.A., Taper, M.L., 2005. Theoretical models of species' borders: single species approaches. Oikos, 18-27.

Houghton, R.W., Schlitz, R., Beardsley, R.C., Butman, B., Chamberlin, J.L., 1982. The Middle Atlantic Bight cold pool: Evolution of the temperature structure during summer 1979. Journal of Physical Oceanography 12, 1019-1029.

Hurley, D.H., Walker, R.L., 1996. The effects of larval stocking density on growth, survival, and development of laboratory-reared Spisula solidissima similis (Say, 1822). Journal of shellfish research 15, 715-718.

Hurley, D.H., Walker, R.L., 1997. Effects of temperature and salinity upon larval growth, survival and development in hatchery reared southern Atlantic surfclams Spisula solidissima similis. Journal of the World Aquaculture Society 28, 407-411.

Incze, L., Xue, H.J., Wolff, N., Xu, D., Wilson, C., Steneck, R., Wahle, R., Lawton, P., Pettigrew, N., Chen, Y., 2010. Connectivity of lobster (Homarus americanus) populations in the coastal Gulf of Maine: part II. Coupled biophysical dynamics. Fisheries Oceanography 19, 1-20.

Incze, L.S., Naimie, E., 2000. Modelling the transport of lobster (Homarus americanus) larvae and postlarvae in the Gulf of Maine. Fisheries Oceanography 9, 99-113.

IPCC, 2013. Climate Change 2013, in: Stocker, T.F., Qin, D., Plattner, G.K., Tignor, M.M.B., Allen, S.K., Boschung, J. (Eds.), Chapter 3. Observations:Ocean, Cambridge, United Kingdom and New York, NY, USA, pp. 273-275.

Johnson, K.B., Shanks, A.L., 2003. Low rates of predation on planktonic marine invertebrate larvae. Marine Ecology Progress Series 248, 125-139.

Jones, D.S., 1981. Reproductive cycles of the Atlantic surf clam Spisula solidissima, and the ocean quahog Arctica islandica off New Jersey. Journal of shellfish research 1.

Joyce, T.M., 1987. Meteorology and air-sea interactions., Jones and Bartlett.

Kim, C.K., Park, K., Powers, S.P., Graham, W.M., Bayha, K.M., 2010. Oyster larval transport in coastal Alabama: Dominance of physical transport over biological behavior in a shallow estuary. Journal of Geophysical Research-Oceans 115.

Kim, D.Y., Ramanathan, V., 2008. Solar radiation budget and radiative forcing due to aerosols and clouds. Journal of Geophysical Research-Atmospheres 113.

Kim, Y., Powell, E.N., 2004. Surfclam histopathology survey along the Delmarva mortality line. Journal of shellfish research 23, 429-441.

Kohut, J.T., Glenn, S.M., Chant, R.J., 2004. Seasonal current variability on the New Jersey inner shelf. Journal of Geophysical Research-Oceans 109.

Largier, J.L., 2003. Considerations in estimating larval dispersal distances from oceanographic data. Ecological Applications 13, S71-S89.

Leaman, K.D., Johns, E., Rossby, T., 1989. The average distribution of volume transport and potential vorticity with temperature at three sections across the Gulf Stream. Journal of Physical Oceanography 19, 36-51.

Leis, J.M., Van Herwerden, L., Patterson, H.M., 2011. Estimating Connectivity in Marine Fish Populations: What Works Best? Oceanography and Marine Biology: An Annual Review, Vol 49 49, 193-234.

Lentz, S.J., 1987. A Heat-Budget for the Northern California Shelf during Code-2. Journal of Geophysical Research-Oceans 92, 14491-14509.

Lentz, S.J., 2001. The influence of stratification on the wind-driven cross-shelf circulation over the North Carolina shelf. Journal of Physical Oceanography 31, 2749-2760.

Lentz, S.J., 2008a. Observations and a model of the mean circulation over the Middle Atlantic Bight continental shelf. Journal of Physical Oceanography 38, 1203-1221.

Lentz, S.J., 2008b. Seasonal variations in the circulation over the Middle Atlantic Bight continental shelf. Journal of Physical Oceanography 38, 1486-1500.

Lentz, S.J., 2010. The Mean Along-Isobath Heat and Salt Balances over the Middle Atlantic Bight Continental Shelf. Journal of Physical Oceanography 40, 934-948.

Lentz, S.J., Beardsley, R.C., Irish, J.D., Manning, J., Smith, P.C., Weller, R.A., 2003. Temperature and salt balances on Georges Bank February-August 1995. Journal of Geophysical Research-Oceans 108.

Lentz, S.J., Shearman, R.K., Plueddemann, A.J., 2010. Heat and salt balances over the New England continental shelf, August 1996 to June 1997. Journal of Geophysical Research-Oceans 115.

Levin, L.A., 2006. Recent progress in understanding larval dispersal: new directions and digressions. Integrative and Comparative Biology 46, 282-297.

Liepert, B.G., 2002. Observed reductions of surface solar radiation at sites in the United States and worldwide from 1961 to 1990. Geophysical Research Letters 29.

López, P.C., Carson, H.S., Cook, G.S., Fodrie, F.J., Becker, B.J., DiBacco, C., Levin, L.A., 2012. What Controls Connectivity? An Empirical, Multi-Species Approach. Integrative and Comparative Biology 52, 511-524.

Lough, R.G., Buckley, L.J., Werner, F.E., Quinlan, J.A., Edwards, K.P., 2005. A general biophysical model of larval cod (Gadus morhua) growth applied to populations on Georges Bank. Fisheries Oceanography 14, 241-262.

Lynch, D.R., Holboke, M.J., Naimie, C.E., 1997. The Maine coastal current: Spring climatological circulation. Continental Shelf Research 17, 605-634.

Lynch, D.R., Ip, J.T.C., Naimie, C.E., Werner, F.E., 1996. Comprehensive coastal circulation model with application to the Gulf of Maine. Continental Shelf Research 16, 875-906.

Ma, H.G., 2005. Spatial and temporal variation in surfclam (Spisula solidissima) larval supply and settlement on the New Jersey inner shelf during summer upwelling and downwelling. Estuarine Coastal and Shelf Science 62, 41-53.

Ma, H.G., Grassle, J.P., 2004. Invertebrate larval availability during summer upwelling and downwelling on the inner continental shelf off New Jersey. Journal of Marine Research 62, 837-865.

Ma, H.G., Grassle, J.P., Chant, R.J., 2006a. Vertical distribution of bivalve larvae along a cross-shelf transect during summer upwelling and downwelling. Marine Biology 149, 1123-1138.

Ma, H.G., Grassle, J.P., Rosario, J.M., 2006b. Initial recruitment and growth of surfclams (Spisula solidissima Dillwyn) on the inner continental shelf of New Jersey. Journal of shellfish research 25, 481-489.

Manderson, J.P., 2008. The spatial scale of phase synchrony in winter flounder (Pseudopleuronectes americanus) production increased among southern New England nurseries in the 1990s. Canadian Journal of Fisheries and Aquatic Sciences 65, 340-351.

Mann, R., Campos, B.M., Luckenbach, M.W., 1991. Swimming Rate and Responses of Larvae of 3 Mactrid Bivalves to Salinity Discontinuities. Marine Ecology Progress Series 68, 257-269.

Marra, J., Houghton, R.W., Garside, C., 1990. Phytoplankton Growth at the Shelf-Break Front in the Middle Atlantic Bight. Journal of Marine Research 48, 851-868.

McCay, B.J., Brandt, S., Creed, C.F., 2011. Human dimensions of climate change and fisheries in a coupled system: the Atlantic surfclam case. Ices Journal of Marine Science 68, 1354-1367.

Mellor, G.L., 2003. Users Guide for a Three-Dimensional, Primitive Equation, Numerical Ocean Model, Princeton University, p. 55.

Metaxas, A., Burdett-Coutts, V., 2006. Response of invertebrate larvae to the presence of the ctenophore Bolinopsis infundibulum , a potential predator. . Journal of Experimental Marine Biology and Ecology 334, 187-195.

Metaxas, A., Saunders, M., 2009. Quantifying the “bio-” components in biophysical models of larval transport in marine benthic invertebrates: advances and pitfalls. . The Biological Bulletin 216, 257-272.

Miller, J.L., Lee, T.N., 1995. Gulf-Stream Meanders in the South-Atlantic Bight .1. Scaling and Energetics. Journal of Geophysical Research-Oceans 100, 6687-6704.

Miller, S.H., Morgan, S.G., 2013. Interspecific differences in depth preference: regulation of larval transport in an upwelling system. Marine Ecology Progress Series 476, 301-306.

Miller, T.J., 2007. Contribution of individual-based coupled physical-biological models to understanding recruitment in marine fish populations. Marine Ecology Progress Series 347, 127-138.

Moran, A.L., Manahan, D.T., 2004. Physiological recovery from prolonged 'starvation' in larvae of the Pacific oyster *Crassostrea gigas*. Journal of Experimental Marine Biology and Ecology 306, 17-36.

Mukai, A.Y., Westerink, J.J., Luettich, R.A., D., M., 2002. Eastcoast 2001, a tidal constituent database for the western North Atlantic, Gulf of Mexico, and Caribbean Sea., U.S. Army Corps of Engineers, Engineer Research and Development Center Tech. Rep., p. 196.

Munk, P., Larsson, P.O., Danielsen, D., Moksness, E., 1995. Larval and Small Juvenile Cod Gadus-Morhua Concentrated in the Highly Productive Areas of a Shelf Break Front. Marine Ecology Progress Series 125, 21-30.

Munroe, D.M., Klinck, J.M., Hofmann, E.E., Powell, E.N., 2012. The role of larval dispersal in metapopulation gene flow: Local population dynamics matter. Journal of Marine Research 70, 441-467.

Munroe, D.M., Powell, E.N., Mann, R., Klinck, J.M., Hofmann, E.E., 2013. Underestimation of primary productivity on continental shelves: evidence from maximum size of extant surfclam (Spisula solidissima) populations. Fisheries Oceanography 22, 220-233.

Narváez, D.A., Klinck, J.M., Powell, E.N., Hofmann, E.E., Wilkin, J., Haidvogel, D.B., 2012a. Circulation and behavior controls on dispersal of eastern oyster (Crassostrea virginica) larvae in Delaware Bay. Journal of Marine Research 70, 411-440.

Narváez, D.A., Klinck, J.M., Powell, E.N., Hofmann, E.E., Wilkin, J., Haidvogel, D.B., 2012b. Modeling the dispersal of eastern oyster (Crassostrea virginica) larvae in Delaware Bay. Journal of Marine Research 70, 381-409.

Narváez, D.A., Munroe, D., Hofmann, E.E., Klinck, J., Powell, E.N., Mann, R., Curchitser, E.N., 2014. Long-term dynamics in Atlantic surfclam (Spisula solidissima) populations: The role of bottom water temperature. . Journal of Marine Systems In press.

NEFSC, 2010. 49th Northeast Regional Stock Assessment Workshop (49th SAW) Assessment Report, Northeast Fisheries Science Center Reference Document. United States Department of Commerce, p. 383.

North, E.W., Schlag, Z., Hood, R.R., Li, M., Zhong, L., Gross, T., Kennedy, V.S., 2008. Vertical swimming behavior influences the dispersal of simulated oyster larvae in a coupled particle-tracking and hydrodynamic model of Chesapeake Bay. Marine Ecology Progress Series 359, 99-115.

Nye, J.A., Link, J.S., Hare, J.A., Overholtz, W.J., 2009. Changing spatial distribution of fish stocks in relation to climate and population size on the Northeast United States continental shelf. Marine Ecology Progress Series 393, 111-129.

O'Connor, M.I., Bruno, J.F., Gaines, S.D., Halpern, B.S., Lester, S.E., Kinlan, B.P., Weiss, J.M., 2007. Temperature control of larval dispersal and the implications for marine ecology, evolution, and conservation. Proceedings of the National Academy of Sciences 104, 1266–1271.

O'Reilly, J.E., Evans-Zetlin, C., Busch, D.A., 1987. Primary production, in: Backus, R.H. (Ed.), Georges Bank. MIT Press, Cambridge, MA, pp. 220-223.

Ohmura, A., 2009. Observed decadal variations in surface solar radiation and their causes. Journal of Geophysical Research-Atmospheres 114.

Ólafsson, E.B., Peterson, C.H., Ambrose, W.G., 1994. Does recruitment limitation structure populations and communities of macro-invertebrates in marine soft sediments: the relative significance of presettlement and postsettlement processes. Oceanography and Marine Biology, Vol 32 32, 65-109.

Olson, R.R., Olson, M.H., 1989. Food Limitation of Planktotrophic Marine Invertebrate Larvae - Does It Control Recruitment Success. Annual Review of Ecology and Systematics 20, 225-247.

Peck, M.A., Hufnagl, M., 2012. Can IBMs tell us why most larvae die in the sea? Model sensitivities and scenarios reveal research needs. Journal of Marine Systems 93, 77-93.

Pfeiffer-Hoyt, A.S., McManus, M.A., 2005. Modeling the effects of environmental variability on Balanus glandula larval development. Journal of Plankton Research 27, 1211-1228.

Pineda, J., Hare, J.A., Sponaugle, S., 2007. Larval Transport and Dispersal in the Coastal Ocean and Consequences for Population Connectivity. Oceanography 20, 22-39.

Powell, E.N., Bochenek, E.A., Klinck, J.M., Hofmann, E.E., 2002. Influence of food quality and quantity on the growth and development of Crassostrea gigas larvae: a modeling approach. Aquaculture 210, 89-117.

Przeslawski, R., Webb, A.R., 2009. Natural Variation in Larval Size and Developmental Rate of the Northern Quahog Mercenaria Mercenaria and Associated Effects on Larval and Juvenile Fitness. Journal of shellfish research 28, 505-510.

Quijon, P.A., Grassle, J.P., Rosario, J.M., 2007. Naticid snail predation on early post-settlement surfclams (Spisula solidissima) on the inner continental shelf of New Jersey, USA. Marine Biology 150, 873-882.

Rasmussen, L.L., Gawarkiewicz, G., Owens, W.B., Lozier, M.S., 2005. Slope water, Gulf Stream, and seasonal influences on southern Mid-Atlantic Bight circulation during the fall-winter transition. Journal of Geophysical Research-Oceans 110.

Renaud, S.M., Thinh, L.V., Lambrinidis, G., Parry, D.L., 2002. Effect of temperature on growth, chemical composition and fatty acid composition of tropical Australian microalgae grown in batch cultures. Aquaculture 211, 195-214.

Reynolds, R.W., Smith, T.M., Liu, C., Chelton, D.B., Casey, K.S., Schlax, M.G., 2007. Daily high-resolution-blended analyses for sea surface temperature. Journal of Climate 20, 5473-5496.

Reyns, N.B., Eggleston, D.B., Luettich, R.A., 2006. Secondary dispersal of early juvenile blue crabs within a wind-driven estuary. Limnology and Oceanography 51, 1982-1995.

Reyns, N.B., Eggleston, D.B., Luettich, R.A., 2007. Dispersal dynamics of post-larval blue crabs, Callinectes sapidus, within a wind-driven estuary. Fisheries Oceanography 16, 257-272.

Roosenburg, W.H., Wright, D.A., Castagna, M., 1984. Thermal Tolerance by Embryos and Larvae of the Surf Clam Spisula-Solidissima. Environmental Research 34, 162-169.

Ropes, J.W., 1968. Hermaphroditism in the surf clam, *Spisula solidissima*. Proceedings of the National Shellfisheries Association 58.

Ropes, J.W., 1980. Biological and fisheries data on the Atlantic surf clam, *Spisula solidissima*. Northeast Fisheries Center, National Marine Fisheries Service, National Oceanic and Atmospheric Administration, Woods Hole, Massachusetts.

Rose, G.A., 2005. On distributional responses of North Atlantic fish to climate change. Ices Journal of Marine Science 62, 1360-1374.

Rumrill, S.S., 1990. Natural Mortality of Marine Invertebrate Larvae. Ophelia 32, 163-198.

Savina, M., Menesguen, A., 2008. A deterministic population dynamics model to study the distribution of a benthic bivalve with planktonic larvae (Paphia rhomboides) in the English Channel (NW Europe). Journal of Marine Systems 70, 63-76.

Schofield, O., Kohut, J., Glenn, S., 2008. Evolution of coastal observing networks - Ocean observing, is undergoing dramatic advances that will have immediate benefits to society. Sea Technology 49, 31-+.

Shanks, A.L., 2009. Pelagic Larval Duration and Dispersal Distance Revisited. Biological Bulletin 216, 373-385.

Shanks, A.L., Brink, L., 2005. Upwelling, downwelling, and cross-shelf transport of bivalve larvae: test of a hypothesis. Marine Ecology Progress Series 302, 1-12.

Shanks, A.L., Eckert, G.L., 2005. Population persistence of California Current fishes and benthic crustaceans: A marine drift paradox. Ecological Monographs 75, 505-524.

Shanks, A.L., Largier, J., Brink, L., Brubaker, J., Hooff, R., 2002. Observations on the distribution of meroplankton during a downwelling event and associated intrusion of the Chesapeake Bay estuarine plume. Journal of Plankton Research 24, 391-416.

Shanks, A.L., Largier, J., Brubaker, J., 2003. Observations on the distribution of meroplankton during an upwelling event. Journal of Plankton Research 25, 645-667.

Shchepetkin, A.F., McWilliams, J.C., 1998. Quasi-monotone advection schemes based on explicit locally adaptive dissipation. Monthly Weather Review 126, 1541-1580.

Shchepetkin, A.F., McWilliams, J.C., 2003. A method for computing horizontal pressure-gradient force in an oceanic model with a nonaligned vertical coordinate. Journal of Geophysical Research-Oceans 108.

Shchepetkin, A.F., McWilliams, J.C., 2005. The regional oceanic modeling system (ROMS): a split-explicit, free-surface, topography-following-coordinate oceanic model. Ocean Modelling 9, 347-404.

Shearman, R.K., Lentz, S.J., 2003. Dynamics of mean and subtidal flow on the New England shelf. Journal of Geophysical Research-Oceans 108.

Shearman, R.K., Lentz, S.J., 2010. Long-Term Sea Surface Temperature Variability along the US East Coast. Journal of Physical Oceanography 40, 1004-1017.

Short, J., Metaxas, A., Daigle, R.M., 2013. Predation of larval benthic invertebrates in St George's Bay, Nova Scotia. Journal of the Marine Biological Association of the United Kingdom 93, 591-599.

Smith, W.G., Morse, W.W., 1985. Retention of Larval Haddock Melanogrammus-Aeglefinus in the Georges Bank Region, a Gyre-Influenced Spawning Area. Marine Ecology Progress Series 24, 1-13.

Stanhill, G., Cohen, S., 2001. Global dimming: a review of the evidence for a widespread and significant reduction in global radiation with discussion of its probable causes and possible agricultural consequences. Agricultural and Forest Meteorology 107, 255-278.

Swearer, S.E., Shima, J.S., Hellberg, M.E., Thorrold, S.R., Jones, G.P., Robertson, D.R., Morgan, S.G., Selkoe, K.A., Ruiz, G.M., Warner, R.R., 2002. Evidence of self-recruitment in demersal marine populations. Bulletin of Marine Science 70, 251-271.

Szedlmayer, S.T., Able, K.W., Rountree, R.A., 1992. Growth and Temperature-Induced Mortality of Young-of-the-Year Summer Flounder (Paralichthys-Dentatus) in Southern New-Jersey. Copeia, 120-128.

Thorson, G., 1966. Some factors influencing the recruitment and establishment of marine benthic communities. Netherlands Journal of Sea Research 3, 267-293.

Tian, R.C., Chen, C.S., Stokesbury, K.D.E., Rothschild, B.J., Cowles, G.W., Xu, Q.C., Hu, S., Harris, B.P., Marino, M.C., 2009. Modeling the connectivity between sea

scallop populations in the Middle Atlantic Bight and over Georges Bank. Marine Ecology Progress Series 380, 147-160.

Tilburg, C.E., Seay, J.E., Bishop, T.D., Miller, H.L., Meile, C., 2010. Distribution and retention of Petrolisthes armatus in a coastal plain estuary: The role of vertical movement in larval transport. Estuarine Coastal and Shelf Science 88, 260-266.

Townsend, D.W., Pettigrew, N.R., 1997. Nitrogen limitation of secondary production on Georges Bank. Journal of Plankton Research 19, 221-235.

Ullman, D.S., Codiga, D.L., 2004. Seasonal variation of a coastal jet in the Long Island Sound outflow region based on HF radar and Doppler current observations. Journal of Geophysical Research-Oceans 109.

Underwood, A.J., Keough, M.J., 2001. Supply-side ecology: the nature and consequences of variations in recruitment of intertidal organisms., in: Bertness, M.D., Gaines, S.D., Hay, M.E. (Eds.), Marine Community Ecology. Sinauer Associates, Sunderland, pp. 183-200.

Walker, R.L., Hurley, D.H., Kupfer, R., 1998. Growth and survival of Atlantic surfclam, Spisula solidissima, larvae and juveniles fed various microalga diets. Journal of shellfish research 17, 211-214.

Walker, R.L., OBeirn, F.X., 1996. Embryonic and larval development of Spisula solidissima similis (Say, 1822) (Bivalvia: Mactridae). Veliger 39, 60-64.

Wang, Z., Haidvogel, D.B., Bushek, D., Ford, S.E., Hofmann, E.E., Powell, E.N., Wilkin, J., 2012. Circulation and water properties and their relationship to the oyster disease MSX in Delaware Bay. Journal of Marine Research 70, 279-308.

Warner, J.C., Geyer, W.R., Lerczak, J.A., 2005. Numerical modeling of an estuary: A comprehensive skill assessment. Journal of Geophysical Research-Oceans 110.

Weinberg, J.R., 2005. Bathymetric shift in the distribution of Atlantic surfclams: response to warmer ocean temperature. Ices Journal of Marine Science 62, 1444-1453.

Weinberg, J.R., Dahlgren, T.G., Halanych, K.M., 2002. Influence of rising sea temperature on commercial bivalve species of the U.S. Atlantic coast. , American Fisheries Society Symposium, pp. 131-140.

Werner, F.E., Cowen, R.K., Paris, C.B., 2007. Coupled Biological and Physical Models Present Capabilities and Necessary Developments for Future Studies of Population Connectivity. Oceanography 20, 54-69.

Werner, F.E., Page, F.H., Lynch, D.R., Loder, J.W., Lough, R.G., Perry, R., Greenberg, D.A., Sinclair, M.M., 1993. Influences of mean advection and simple behavior on

the distribution of cod and haddock early life stages on Georges Bank. Fisheries Oceanography 2, 43-64.

Wild, M., 2009. Global dimming and brightening: A review. Journal of Geophysical Research-Atmospheres 114.

Wild, M., Gilgen, H., Roesch, A., Ohmura, A., Long, C.N., Dutton, E.G., Forgan, B., Kallis, A., Russak, V., Tsvetkov, A., 2005. From dimming to brightening: Decadal changes in solar radiation at Earth's surface. Science 308, 847-850.

Wilkin, J.L., 2006. The summertime heat budget and circulation of southeast new England shelf waters. Journal of Physical Oceanography 36, 1997-2011.

Wright, D.A., Kennedy, V.S., Roosenburg, W.H., Castagna, M., Mihursky, J.A., 1983. Temperature Tolerance of Embryos and Larvae of 5 Bivalve Species under Simulated Power-Plant Entrainment Conditions - a Synthesis. Marine Biology 77, 271-278.

Wright, D.A., Roosenburg, W.H., Castagna, M., 1984. Thermal Tolerance in Embryos and Larvae of the Bay Scallop Argopecten-Irradians under Simulated Power-Plant Entrainment Conditions. Marine Ecology Progress Series 14, 269-273.

Xue, H.J., Incze, L., Xu, D., Wolff, N., Pettigrew, N., 2008. Connectivity of lobster populations in the coastal Gulf of Maine - Part I: Circulation and larval transport potential. Ecological Modelling 210, 193-211.

Zhang, W.G.F., Wilkin, J.L., Chant, R.J., 2009. Modeling the Pathways and Mean Dynamics of River Plume Dispersal in the New York Bight. Journal of Physical Oceanography 39, 1167-1183.